Parametric Estimation of Non-minimum Phase Switch Mode Power Converters

Ruisheng Li

B.Eng., M.Sc.

A thesis submitted for the degree of

Doctor of Philosophy

February 2020

School of Electrical, Electronic and

Computer Engineering

Newcastle University

United Kingdom

DEDICATION

To my loving family

ACKNOWLEDGEMENT

I would like to take this opportunity to thank everyone who is involved in my PhD life in Newcastle city. The work could not be finished without their kind support.

First of all, I would like to express my deep sincere thanks to my supervisor Dr. Matthew Armstrong. He is not only a tutor of my PhD study but also a mentor in my life. Thanks for his support, guidance and kind understanding especially during my depression period. Also, I extend my thanks for his scholarship offer towards my financial support. This couldn't have been be achieved without his amicable helps all the time.

My acknowledgements also go to my friends and colleagues at the UG lab. I would like to thank Dr. Chen Wang for his continuous help and for sharing his knowledge with me throughout my PhD study. In addition, I would like to thank Dr. Maher Algreer for sharing his research experiences of system identification and experimental platform setup. Also, my deep thanks go to Darren Mackie for his kindly help and guidance with my PCB design. Finally, I would like to thank my dear friend and colleagues Mr. Jiankai Ma and Mr. Weichi Zhang for their accompanying and support throughout the 4 years.

In the end, my deepest appreciation goes to my father and my mother. Their love and supports never stops through my entire life. I don't know how to express my thanks to them as they are beyond any beautiful words to me. What I only want to do now is to pray for them for an everlasting healthy and happy life. Last but most important, to say thanks to my wife, Nanmao Dang. You are such a thoughtful lady who always gives me understanding and power to overcome anything. I know that you also face a lot of stress in your work. But nothing seems to stop you from caring about the family all the time. Finally, you have given me such a gift in the last year, which is our lovely daughter Liana. The love and cares I received from you are continuously providing the encouragement to me for now and forever.

ABSTRACT

Nowadays, switching mode power converters (SMPCs) are widely used in many applications. The advanced control technique for converters, such as adaptive control is also spread-used in many converter control scheme designs. System identification as a tool for estimating the converter operating conditions, and providing the information to the controller is a key technique for these applications; and parametric estimation, which is part of the system identification technique, is an advanced identification technique which can allow on-line system identification and adaptive control design. However, most of the research over the past decades has only covered parametric estimation of buck converters and there is barely anything about boost converters or other non-minimum phase converters. The reason behind this is that the parametric estimation results of non-minimum phase converters are not fitted to the calculated model weights, especially for the numerator weights of the model transfer function. Thus, the controller gains cannot be determined correctly by the wrong estimated model weights. It has been a big problem in the application of parametric estimation for decades. In this research, a modelling method which is based on trailing-edge PWM off-time sampling (TEOS) is introduced in order to address this problem.

The objective of this research is to develop an approach to resolve the existing accuracy problems of non-minimum phase SMPC parametric estimation. The problem, which has existed for decades, is that commonly used state-space averaged model numerator weights are not fitted to the non-minimum phase SMPC parametric estimation results. There are several possible ways to address this problem, including modification of converter modelling, modification of parametric estimation mechanism, or with the help of compensators. In this research, the TEOS modelling method has been verified by both simulation and practical experiment to provide the best-fit model weights for the parametric estimation of buck converters and boost converters; and it has also been verified, by simulation, to be used for buck-boost converter parametric estimation, which has opened up great possibilities for its use on other non-minimum phase converters. The experimental results have shown that the proposed modelling approach has improved the accuracy of parametric estimation for boost converters by more than 20% compared with the commonly used state-space averaged modelling approach.

In addition, the TEOS model will also present a thorough inspection of the relationships between system parameters (load resistance, capacitance and inductance) and the model transfer function parameters, which can then realise the sensor-less on-line system parameters estimation or monitoring. This function is also a novel approach to the area of system component monitoring.

In this thesis, the reason behind the problem of non-minimum phase converter parametric estimation is analysed for the first time. The system parametric estimation of three converters (buck, boost and buck-boost) were tested with on-line simulation and off-line experimental tests for both the averaged model and the proposed model. Then, system parameters estimation was also tested for the buck converter and boost converter in the simulation and practical experiment. In addition, the platform setup, the interface build between the Matlab Simulink and the Code Composer Studio (CCS), the settings of the Digital Signal Processor (DSP) TMS320F28335, the parameters design of boost SMPC, and the design of the Printed Circuit Board (PCB) schematics and layout are also presented in this thesis. The outcome of the research should be able to further benefit many applications of advanced control systems, fault detection, and system component monitoring.

TABLE OF CONTENTS

LIST OF FIGURES

LIST OF TABLES

LIST OF ACRONYMS

A/D	Analogue to Digital
AC	Adaptive Control
ADC	Analogue to Digital Controller
AP	Affine Projection
ARMA	Auto-Regressive Moving Average
CCM	Continuous Conduction Mode
CCS	Code Composer Studio
DCM	Discontinuous Conduction Mode
DMA	Direct Access Memory
DPWM	Duty Cycle to PWM
DSP	Digital Signal Processor
ESR	Equivalent Series Resistance
FAP	Fast Affine Projection
IDE	Integrated Development Environment
ITOC	Improved Time Optimal Control
LE	Leading Edge
LHP	Left Half Plane
LMS	Least Mean Squares
MOSFET	Metal–Oxide–Semiconductor Field-Effect Transistor
MRAS	Model Reference Adaptive Systems

M-Sequence	Maximal Length Sequence
OCF	Open Circuit Fault
PCB	Printed Circuit Board
PE	Percentage of Estimation Error
PRBS	Pseudo Random Binary Sequence
PWM	Pulse Width Modulation
RHP	Right Half Plane
RLS	Recursive Least Square
RTW	Real-Time Workshop
SCF	Short Circuit Fault
SI	System Identification
SISO	Single Input Single Output
SMPC	Switch Mode Power Converter
SSA	State-Space Averaged
TE	Trailing Edge
TEOS	Trailing-Edge PWM Off-Time Sampling
TSP	Target Support Package
WT	Weda's Theorem

LIST OF SYMBOL

V_o	Output Voltage
V_{in}	Input Voltage
d	Duty Cycle
L	Inductance
C	Capacitance
T_s	Sampling Time
T_{sw}	Switch Instance
T_{on}	Switch-On Time
T_{off}	Switch-Off Time
i_L	Inductor Current
I_{Lave}	Averaged Inductor Current
V_L	Inductor Voltage
R_L	Inductor Impedance
i_C	Capacitor Current
v_C	Capacitor Voltage
R_C	Capacitor Impedance
I_o	Output Current
R_o	Load Resistance
w_z	Zero Frequency

Q	Quality Factor
w_0	Corner Frequency
f_{sw}	Switching Frequency
δ	Damping Factor
M_p	Percent of Overshoot
X_i	Steady-State of the Converter States
d_o	The Complementary of Duty Cycle
u	Input Data
y	Output Data
w	Transfer Function Weights
$\hat{w}$	Estimated Weights
$\hat{y}(n)$	Estimated Output
e	Estimation Error
$R(i)$	Autocorrelation Matrix
$\beta(i)$	Cross-Correlation Vector
$d(n)$	Desired Signal
λ	Forgetting Factor
μ	Step Size
$\mathbf{M}$	Fisher Information Matrix
V_d	Forward Voltage of the Diode

CHAPTER 1 RESEARCH INTRODUCTION AND THE STRUCTURE OF THE THESIS

1.1 Research Introduction

Nowadays, when talking about switching mode power supplies, there are three popular topics that cannot be ignored, namely advanced adaptive control, fault detection and system monitoring. Within these three topics, there is also a technique which is also unavoidable, namely system identification. This technique has been introduced in many papers. However, for its application on non-minimum phase systems, it is rare to find a paper that is discussing it, as the technique does not seem to work on the non-minimum phase system. Therefore, this research is focused on analysing this problem and proposing a way to address the problem using experimentation to verify the approach.

This research has arisen as a result of several reasons. The first reason concerns SMPCs. Nowadays, due to the many advantages of SMPCs, such as less power consumption and heat dissipation; their small size and weight; and also the development of the DSP, SMPCs are becoming more popular in many applications [1, 2]. The second reason is about system identification technique. System identification technique is used in many areas, and it is treated as a tool for system characteristics estimation for many different purposes. In addition, it always plays an important role in power electronics applications [3, 4]. However, there is still the existing problem of SMPCs system identification, which is also the third reason for this research. As system identification of non-minimum phase converters has been an acknowledged problem for decades, the parametric estimation of a non-minimum phase converter, such as a boost converter, always estimates a set of wrong-model parameters of transfer function [5]. In this research, attempts have been made to explore the reasons behind this problem and to finally come up with a solution to address this problem. In addition, based on the solution method, there are some new findings, namely that system parameters of load resistance, capacitance and inductance can also be monitored via their relationships with model parameters.

As discussed above, this research will be conducted through several steps, including SMPC modelling, problem analysis and system identification technique. Finally, this method will be tested in both simulations and practical experiments for verification.

The final corrected identification method of non-minimum phase converters should benefit many applications, such as advanced control design and system monitoring of power electronics. In the next few sections, the development and review of system identification technique in those three applications will be presented.

1.2 System Identification Technique Development and Review

System identification technique is an advanced technique for estimating a system's model structure, dynamic characteristics, frequency response or the mathematical model parameters. This technique has been developed a lot in recent decades. It can be applied in many areas including electric systems, aerospace vehicles, nuclear reactors, chemical processes, biomedical systems, socioeconomic systems, and environmental and ecological systems [6, 7]. Therefore, system identification as a technique tool can be a separate research area. Its application in electronics and its combination with control theory have led to some well-known techniques such as adaptive control, fault detection, system supervision, etc. In particular, system identification is a vital branch of control theory; as modern control theory consists of three main parts, namely system identification, state estimation and control theory [8]. Since system identification is conducted from the experimental data to determine the system model, it should be able to provide an effective way to build up a mathematical model for any system.

The earliest definition of system identification was given by Zadeh in 1962 [9]. He claimed that system identification is about selecting an equivalent model from a given set of models based on the system's input and output information. In 1974, Eykhoff [10] added that system identification is about finding and utilising a model to describe the essential characteristics of a system. Then Ljung pointed out in 1978 [11] that system identification is comprised of three main parts, namely data, model classification and principle. Among these three parts, data is the basis, principle is the gist, and the model classification is the range of system identification. System identification is aimed at selecting a model from the model classifications that can perfectly match the obtained data from the system.

In order to conduct a system identification of a system, it is important to know the aim of the final model in advance, which will have an impact when choosing the correct type of model (model structure), input signal and equivalent principles. There are usually six aims when conducting a system identification.

(1) System design and control. In an engineering control design, it is necessary to understand the characteristics of the system. Thus, building up a mathematical model can help in studying the relationships between each part of the system.

(2) System analysis. With the knowledge of the mathematical model, it is convenient to analyse the behaviour of the system to help with controller design etc.

(3) System simulation. For some dangerous or complicated systems, it is better to use an equivalent mathematical model in order to indirectly analyse the system.

(4) System estimation. From a model of the system, the natural law of the system can be found to estimate the state variables of the model. This estimation can provide a future vision of system operation.

(5) Fault diagnosis. For some complicated systems such as aerospace, nuclear, missile, large chemical and power plants, etc., system identification can help to supervise and test system faults before they become a problem.

(6) Theory and mechanism verification. A mathematical model can improve the understanding of input and output signals and can help verify system theory and the corresponding mechanisms. It is also useful for understanding the dynamic response of a system.

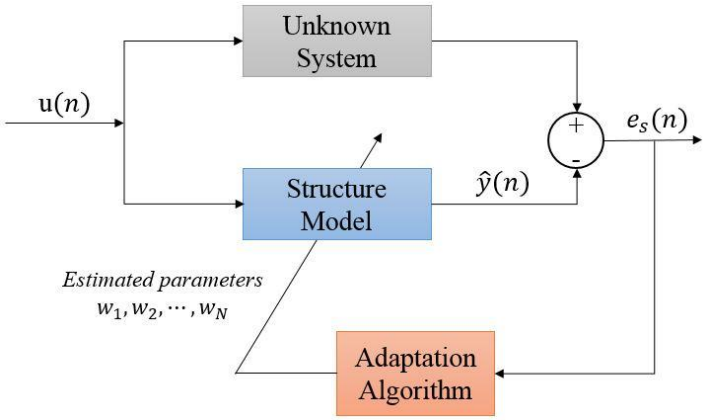

Figure 1.1 The Schematics of Parametric Identification

Figure 1.1 shows the general principles of a parametric system identification process. The difference between parametric estimation and non-parametric estimation will be introduced in detail in Chapter 3. In Figure 1.1, a model structure is selected to represent the unknown system that needs to be identified. Measurements are taken from the input and output of the unknown system, and the parameters (tap weights) of the model are estimated via the use of a real-time estimation algorithm, e.g. recursive least squares (RLS). However, in SMPC applications, a review of the literature reveals that most system identification research is focused on the buck

converter, and rarely on the synchronous boost converter. The reason for this will be discussed in this thesis, which will point out that the buck converter has two left half-plane (LHP) poles and one LHP zero, which makes it a minimum-phase system. However, the boost converter has two LHP poles and one right half-plane (RHP) zero, which makes it as a non-minimum phase system [12, 13]. The existence of the RHP-zero in the boost converter causes an initial voltage drop, which leads to a wrong direction for the change of output voltage at the beginning instance of the response. In addition, an RHP-zero is equivalent to a delay component. This "confuses" the system identification algorithm into implementing an erroneous initial set of output data. As a result, when applying system identification techniques to determine the parameters of the corresponding transfer function, the accuracy of the numerator parameters is often significantly less accurate than the corresponding parameters in the denominator. In the following chapters, this problem will be shown clearly along with its solution.

1.3 System Identification Technique Development and Review in Adaptive Control Applications

The field of adaptive control and adaptive systems has been a very popular topic worldwide for researchers over the last 40 years and can be dated back to the 1950s. The first application was in aeronautics, the air force of the military, which tried to design an advanced controller that could deal with stochastic disturbances while adjusting its performance under uncertain conditions. During this period, the development of adaptive systems progressed rapidly and obtained a great achievement. From the very simple analogue techniques (MIT algorithms) to more complicated algorithms, the unavailability of computer techniques eventually became a limit to real-world applications at the time [14, 15]. During the 1960s, the area of adaptive systems diverged in two different directions. The first direction was Model Reference Adaptive Systems (MRAS), whereby the controller can modify itself to achieve the required performance [16-18]. The other direction was self-tuning controllers, in which an identification technique was applied due to the use of matrix inversion lemma [19, 20]. With the estimated parameters, the controller could then adapt itself to the required behaviour. During the 1970s, with the increased use of modern computers, many of the latest theories and methods were finally able to be used in real-world applications. The research in adaptive systems mainly includes the use of algebraic approaches in control design, the parameterisation of controllers, the use of rational fraction functions and the digitalisation of signals and models [21, 22]. During the 1980s, the

adaptive system area was developed further. As microprocessor technology became more widely used, digitalisation became more attractive than analogue equipment for real-time use. Auto-tuning systems began to appear. Conferences of specifically adaptive systems have been held and several monographs and papers were published. During the 1990s, more attempts were concentrated on applying new methods to adaptive system areas such as artificial intelligence, neuron networks and fuzzy techniques [23-25]. Since 2000s, research has been focused more and more on improving the quality of the control performance, and applying adaptive systems to different applications such as a popular application for adaptive control of switching mode power DC-DC converters.

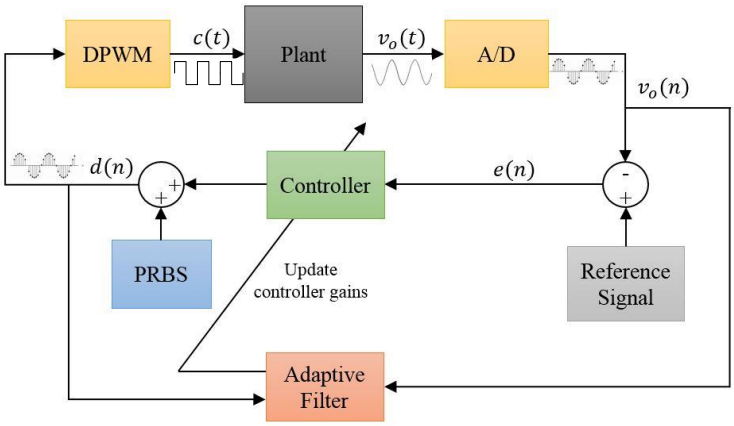

Figure 1.2 Adaptive Control Mechanism

In recent years, SMPCs have been extensively used in many low-cost, low-power electronic applications. However, high-quality output voltage regulation is also considered a strict requirement for these applications. With the rapid development of DSPs, many researchers use efficient and novel control methods instead of topology modification to achieve improved voltage regulation. However, influenced by many internal and external disturbances, undesirable time-varying system parameters significantly limit the capabilities of conventional fixed-gain controllers [26]. For this reason, state-of-the-art adaptive control systems, often based on parametric system identification techniques, are becoming increasingly popular, and often result in superior system performance. Figure 1.2 above shows the typical structure of such an adaptive control system [27]. The output of the plant $v_0(t)$ is converted and sampled to $v_0(n)$ via the analogue to digital converter (A/D). A reference signal is compared with the sampled digital signal $v_0(n)$ to generate an error signal $e(n)$ which is processed by the controller. Digital signal $d(n)$ will is calculated and forwarded to the digital PWM (DPWM)

block to produce a PWM signal to control the plant to the reference voltage. In parallel with the closed-loop control structure, an adaptive filter is added to estimate a best-fit set of controller gains by processing the digital output and desired signals via an adaptive algorithm. The Pseudo Random Binary Sequence (PRBS) signal is a rich-frequency signal to enhance the system dynamics to help with parametric estimation process [98, 99]. In many uncertain situations, the system is likely to be influenced, which could possibly cause degradation or even a catastrophic system failure. Physically speaking, the factors that can cause a failure include ageing, high voltage stress, insulation failures, interconnection failures, mechanical wear, vibrations, shocks, manufacturing defects and harsh environmental conditions (e.g. temperature and humidity) [28-31]. System disturbances and inaccuracies remain an issue in many applications that are related to the quality of power supply output. Much research has been directed at improving the quality of the power supply's waveform. Designing an efficient control scheme is an effective way to resolve the problems, which are also a popular focus for DC-DC SMPCs. To design a proper controller for converters, there are four aspects that can be improved upon [32]:

(1) Dynamic response: to have a good transient response to ensure a smaller oscillation of the output voltage.
(2) Stability: to obtain a relatively small steady-state error and keep the system response stable.
(3) Robustness: the controller should be robust against the uncertainties of the system. Particularly, for the occurrence of large signal disturbance (load change or input change), the output voltage should be able to converge to its desired value.
(4) Following ability: for some cases, it requires that the amplitude of output voltage can change along with the time as the value pre-set by the controller.

In order to achieve robust control performance, with the ability to respond to system uncertainty, an adaptive control technique is preferred to adjust, in real time, the controller gains to optimally control the system. Adaptive Control (AC) is a popular advanced control technique in many modern state-of-the-art electrical systems that is likely to be used in many industrial devices where the parameters of the systems are unknown, or possibly can be dynamically influenced, such as; component variations, unpredictable load changes or large signal disturbances, etc. [26], which would affect the performance of the controller over time. Adaptive control systems can be applied to resolve these time-varying uncertainties, which also can learn and track the characteristic behaviour to achieve optimal control performance. An adaptive controller is comprised of a controller and an adaptive filter that can estimate the dynamics response and

adjust the controller gains in real time. Designing an adaptive controller consists of the following steps.

- Characterise the dynamics behaviour of the closed-loop system.
- Determine a suitable control law with adjustable controller gains.
- Create a system identification strategy design for obtaining the information inside a system.
- Combine control law with system identification technique for real-time control design [26].

Before adjusting the adaptive controller to its optimal point, it is important to apply real-time System Identification (SI) to identify the system parameters. This involves sampling the input and output signals, before applying an appropriate algorithm to estimate the parameters of the system. After the parameters have been determined, an appropriate decision-making process can be applied to the adaptive controller [27]. Therefore, the first step is aimed at modelling the control system with a mathematical model that can correctly display its dynamic characteristics. The second step is aimed at designing an effective controller with adjustable parameters for the plant. The third step is to implement a suitable SI-method for on-line obtaining of the information of the system in order to help the designed controller. The final step is to apply the complete control scheme to the plant and test its validity.

1.4 System Identification Technique Development and Literature Review of Fault Detection Applications

SMPCs based on Pulse-Width Modulation (PWM) as a supply link are present within almost every modern electronic circuit. Therefore, its operating performance is crucial for a system's reliability. Any occurrence of a fault in the circuit would possibly cause a big, perhaps even catastrophic failure to the system [33-35]. Building a supervisory system to monitor the system parameters is therefore necessary. In the specific case of a converter circuit, there are several important components: the inductor, capacitor, semiconductor devices and the load resistor. Two well-known approaches in the scientific literature exist: model-based and signal processing-based. The first approach compares the value between the expected value and the sensor reading value. The second approach is done from the neural network or from some mathematical, statistical and algebraic operations from where it is possible to extract

information concerning the fault's existence. In [36], a set-membership methodology to detect and isolate faults is proposed via model-based fault detection. As presented in [3], a generalised gradient-descent algorithm to detect the parameter changes is compared to a pre-defined acceptable range of parameter values. The authors in [37] has used a Kalman Filter to monitor the parameters' variations in model-based fault diagnosis of DC-DC boost converters. In [35], a method which is based on a multi-layered was proposed, multivalued neuron-neural network with complex QR decomposition to train and validate the data on the SapwinPE simulator platform. This shows a good estimation result and demonstrates the superior performance of the SapwinPE platform. As semiconductor devices are ranked among the weakest components [38], researchers are showing interest in this component. There are several common faults of switch, which are Short-Circuit Fault (SCF) and Open-Circuit Fault (OCF). The research in [39-42] is aimed at detecting faults of the switch MOSFET by measuring the drain-to-source voltage or gate-to-source voltage, and comparing it with a pre-defined suitable voltage. The switch failure can also be detected based on the inductor slope as in [43], whose theory is also utilised by many other researchers [44-47].

From observations of some of the works in the literature review, both fault detection and system monitoring are mainly based on model-based, pre-defined values comparison, neural networks, or mathematical, statistical and algebraic operations. There is no fault detection or system-monitoring method derived from exploring the relationships between transfer function weights and the system parameters and using parametric estimation technique. In this thesis, a new system monitoring approach that stems directly from the derivation of system parameter relationships based on parametric SI is introduced. This approach is expected to clearly show the relationships between the model parameters and the system parameters of load resistance, capacitance and inductance, in order to help the operator to monitor the system parameters simply by applying parametric SI techniques to the system, with no need to calculate a pre-defined threshold value, or to apply a complex neural network.

1.5 The Objective and Contribution of the Thesis

The research objective stems from the literature review of power electronics SI. As mentioned in Section 1.2, it is rare to find a paper about the parametric estimation of non-minimum phase converters. Since SMPCs play a vital role in almost every modern electronic circuit, it is important to have SI technique validity for any kind of topology. Therefore, the first objective

of the research is to explore and analyse the reasons behind this. The second objective is to find a proper method for addressing the problem of parametric SI of non-minimum phase converters, specifically on a traditional boost converter circuit. The third objective is to verify the theories through both simulation and experimental tests. The final objective is to analyse the advantages and disadvantages of the method based on the obtained results. Apart from the four main objectives, there is another finding based on the solution method, which is the on-line system parameters monitoring via the exploitation from the modelling method. Although it is not the main objective of the research, its importance in fault detection and system monitoring needs to be considered.

The contributions of the research can be summarised in the following points:

a). The proposed TEOS modelling method has addressed the existing estimation accuracy problem of non-minimum phase SMPCs SI, which is likely to benefit many applications in the field of adaptive control and fault detection. Until now, most of the publications only consider the buck converter to avoid dealing with this issue as parametric estimation of non-minimum phase converters is still a problem with no solution.

b). This proposed modelling method has been verified to have the ability to be used in the SI of buck converters, boost converters and buck-boost converters by the simulation results and the experimental results of buck converters and boost converters.

c). This research has proposed a new way for the application of fault detection and system parameters monitoring by exploiting the transfer function weights and system parameters relationships inside the proposed modelling method, without calculating a pre-defined threshold value in advance, or applying any complex neural networks.

d). The reasons behind the non-minimum phase converters parametric estimation problem have, for the first time been analysed in detail throughout this thesis. This work has not been presented or discussed in any papers.

1.6 Publications Arising from this Research

Published Papers

1- **R. Li**, M. Armstrong, S. Gadoue, and C. Wang, "On-line parameter estimation of non-minimum phase switch mode power DC-DC boost converters," in *Proc. IET International Conf.* on *Power Electron., Machines and Drives, PEMD* 2016, vol. 2016, Glasgow, United Kingdom.

1.7 The Structure of the Thesis

As this research is mainly focused on SMPC modelling, SI and system parameters monitoring, Chapter 2 introduces two modelling methods: the commonly used State-Space Averaged (SSA) model and the proposed solution modelling method, the TEOS model. The proper simplification steps of the TEOS model and the system parameters derivation steps are presented at the end of the chapter. In Chapter 3, the methodology of SI is introduced, and the definitions, categories and schematics of the technique demonstrated. The two identification algorithms, which have been applied for the SI test, are also presented along with their derivations. In Chapter 4, several sets of simulation results are demonstrated and discussed, including the comparison between the two identification algorithms, the comparison between the performance of the SSA model and TEOS model parametric estimation, and system parameters monitoring on buck circuits and the boost circuit. In addition, the buck-boost converter circuit, as a non-minimum phase converter, is also tested with the two modelling methods – the performance of which also strengthens the validity of the proposed modelling method to be a solution to non-minimum phase SMPC system identification. Chapter 5 describes the setup of the platform, including boost PCB design, interface-building and DSP implementation; while the experimental results will be presented in Chapter 6, comprising of the parametric estimation and system parameters monitoring results based on the two modelling methods, respectively. Finally, the conclusions and future research recommendations are presented in Chapter 7.

CHAPTER 2 SWITCH MODE POWER CONVERTER TOPOLOGIES MODELLING

2.1 SMPCs Modelling Methods Review and Existing Problem Introduction

SMPCs can be used to transfer, control and adjust the output voltage. In recent years, SMPCs have replaced the standard linear regulators in many applications due to their many advantages, such as less power consumption and heat dissipation, and their small size and weight. Their major advantage is their high level of efficiency. Briefly speaking, the passive components (inductor and capacitor) can provide a high effective power conversion when analysing under ideal conditions. The ideal condition is assumed that no power is consumed when switching between the two instances, fully ON (current flows with no voltage) and fully OFF (has voltage without current flow). In addition, with the same level of power, increasing the switching frequency means decreasing the switching period, which further means that the required energy storage in passive components becomes less. Finally, this can help reduce the size and weight of the passive components. The analysis leads to a conclusion of a high-switching frequency requirement.

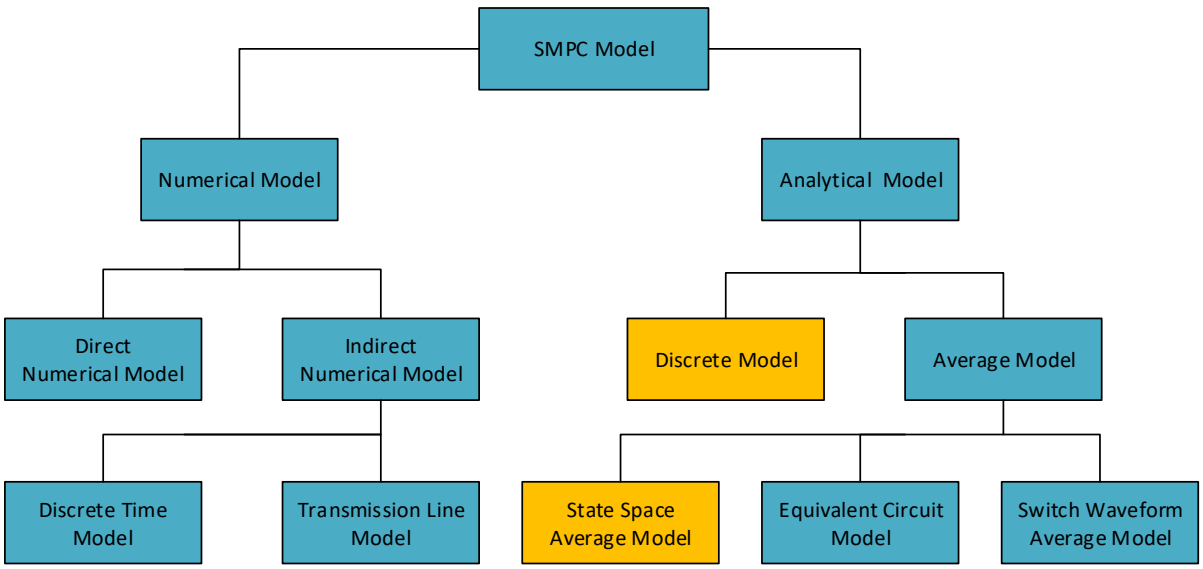

Figure 2.1 SMPC Modelling Methods

The SMPC modelling methods presented in literature are generally summarised in Figure 2.1 [48-52]. They can be generally separated into two categories. One is the numerical modelling method (direct numerical model and indirect numerical model), while the other one is the

analytical modelling method. The numerical method is based on calculations by different chosen algorithms in order to achieve a numerical result which can describe the characteristics of the analysing system. This method is good for system analysing numerically, but it is not good for understanding and the design of a physical system. This research will apply the analytical modelling method, in which two of the major categories are the discrete modelling method and the SSA modelling method. Over a long period of time, the SSA model is widely used due to its ability of linearity characteristics of SMPC, such as SI, control design, etc. Particularly for the buck converter SI, many researchers use SSA as the modelling method. Furthermore, it is rare to find a paper about parametric estimation methods of non-minimum phase converters. In this research, a small-signal discrete model has been tested to resolve the problem of minimum-phase SMPC system identification. In this chapter, these two modelling methods will be explained in detail: the discrete model and the SSA model. The discrete model used in the research is termed as a TEOS small-signal discrete model, which has been highlighted in Figure 2.1.

Converters can also be classified into two categories due to their frequency-phase response: the minimum phase converter and the non-minimum phase converter. For a non-minimum phase system, the zeros of the continuous-time system are in the right-hand side of the complex plane; while in the discrete z-plane there is one or more than one zero out of the unit circle. In contrast to a closed-loop system, if all the poles and zeros of a continuous transfer function are negative, the system is called a minimum phase system. Boost converter and buck-boost converter with a RHP-zero on their transfer functions belong to the group of non-minimum phase converters. A buck converter is a classic minimum phase converter. In bode plot, for a minimum phase system, there is a certain relationship between its magnitude-frequency characteristic and its phase-frequency characteristic. If one of them can be decided, the other one can also be deduced from the decided one. However, this cannot be applied to a non-minimum phase system. There is no certain relationship between two characteristics for a non-minimum phase system. There are two classic situations that contribute to a non-minimum phase system, one consists of non-minimum phase components, meaning that the feedback loop has an unstable section, while the other situation is because of the time lag system. A big phase lag in a non-minimum phase system will slow down the response of the output signal; and by using Laplace Transform, the phase lag can also be deduced as a RHP-zero. Furthermore, due to the reason for the uncertain relationship, the SI of a system will identify a set of wrong numerator parameters because of the phase lag, and a set of correct denominator parameters which represent the system's stability.

The difference between the minimum phase system and the non-minimum phase system is shown in Table 2.1.

Categories	**Type**	**Transfer Function**	**Characteristics**
Minimum phase	Buck Converter	No RHP-zero	1. Certain relationship between magnitude and phase response. 2. No phase lag exists
Non-minimum phase	Boost Converter	RHP-zero	1. Small phase margin 2. No certain relationship between magnitude and phase response 3. Phase lag exists
	Buck-boost Converter		

Table 2.1 Minimum phase and Non-minimum phase

In this research, buck converters, boost converters, and buck-boost converters were all tested on parametric estimation with the proposed modelling method, and then compared with their SSA model performance. Each converter has been modelled by the two modelling methods. Among them, two classic converters of buck converter and boost converter are chosen to be tested in the practical experiments covered in Chapter 6. Buck converters can produce a DC voltage lower than the input voltage, while a boost converter can generate a higher DC voltage than the input. Thirdly, a buck-boost converter is configured to produce two kinds of output voltage with a higher or lower output voltage [53]. These three topologies are depicted in Figure 2.2. Usually for different applications, the chosen topology is based on the different final desired levels of regulated voltage. In the research, buck converter and boost converter are chosen as representative of widely used minimum-phase converters and non-minimum phase converters, respectively. For the state-of-the-art research, most parametric estimation techniques are based on DC-DC synchronous buck converters due to its validity and accuracy compared to any non-minimum phase topologies. However, in the later sections, the proposed TEOS model will show the possibility that non-minimum phase converter parametric estimation can also be accurate; and from the TEOS model, there is also a possibility to monitor the system parameters on-line by exploiting the parameter relationships inside. Although this

is not the main objective of the research, it still needs to be consdiered as an important finding, which could benefit the area of fault detection and system monitoring.

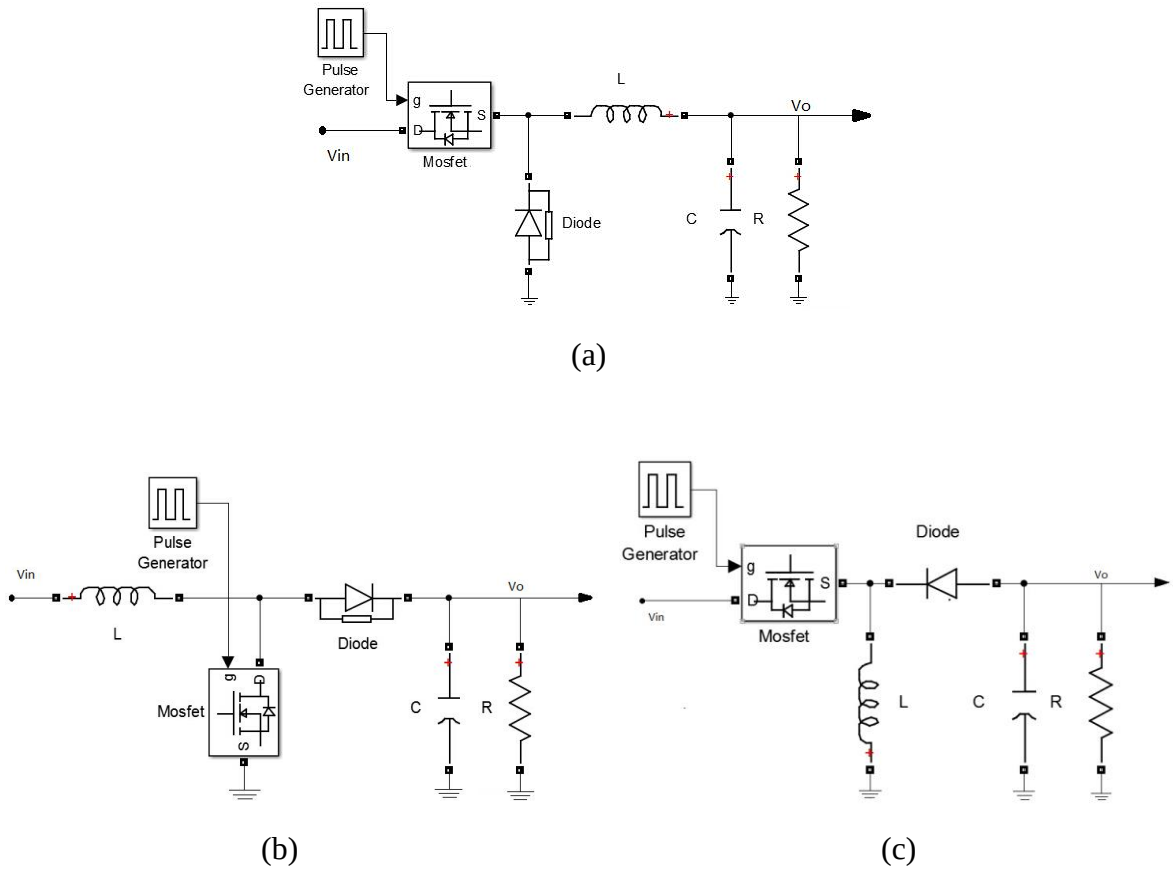

Figure 2.2 Topologies: (a): buck converter, (b): boost converter, (c): buck-boost converter

In [54], the authors assumed the same template model for a buck and boost converter; but then includes a compensation term to the numerator for the model of the boost converter [55] to facilitate improved SI. However, despite better accuracy, the SI results are not accurate enough to estimate the passive components. In this thesis, the reason has been found and clearly discussed, which is RHP-zero, for why an accurate identification results of boost converter cannot be achieved. Thus, it can be assumed that the identification results could be accurate if the problem of RHP-zero can be addressed. In [13], it is pointed out that for an analogue voltage-mode control, leading edge (LE) PWM can lead to minimum-phase responses in non-minimum phase converters (boost and flyback converters).

Following on from this, in [56, 57] the discrete-time model and digital control is considered, which takes into account the effects of A/D sampling and delays in the digital control loop. Off-time sampling with trailing edge (TE) digital pulse-width modulator (DPWM) is shown to offer

improved performance and can result in desirable minimum-phase responses that can overcome the wrong-direction effect on SI. In this research, the discrete-time model is applied and is shown to successfully overcome the RHP-zero effects and to achieve correct estimation results. This will offer benefits to many non-minimum phase adaptive control issues utilising parametric estimation.

2.2 DC-DC Buck SMPC Modelling

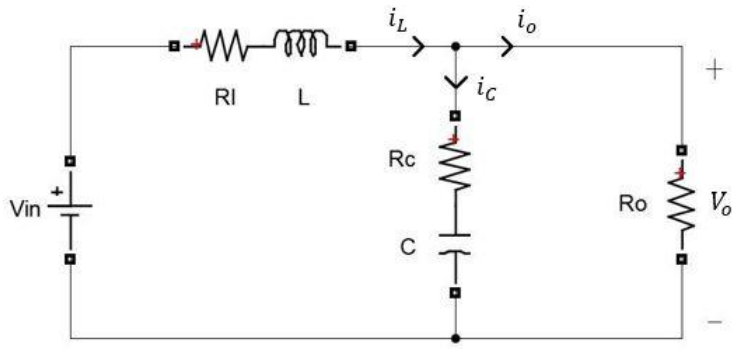

(a)

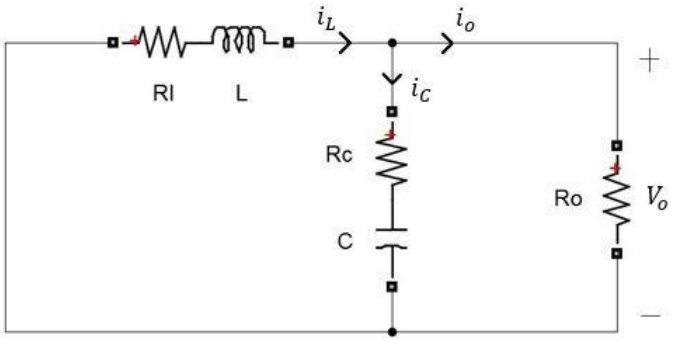

(b)

Figure 2.3 Two operation modes – buck converter, (a): On state, (b): Off state

The DC-DC buck converter circuit is composed of inductor (L), capacitor (C), power MOSFET switch, power diode and load resistor (R_o).The power switch is assumed to be a lossless component in the following calculations to simplify the final derived transfer function. In the practical experiments, the diode is replaced with the same MOSFET as the power switch, and the resistance of the switch is 1.1mΩ. A buck converter is used to step down the input voltage

(V_{in}) by controlling the duty cycle (d) of the power switch (e.g. MOSFET). The relationship between output voltage (V_o) and V_{in} can be described as equation (2.1) [53].

$$V_o = dV_i \tag{2.1}$$

As shown in Figure 2.3, a buck converter has two operating instances during one switching period. One is the 'ON state' when the power switch is turned on and the power diode is off, while the other is the 'OFF state' when the power switch is off and the power diode is on. During the 'ON state', the inductor and capacitor begin to store energy from the input voltage, and in the 'OFF state', the two components will discharge the stored energy through the diode loop. In a buck converter, the capacitor is used for filtering and stabilising the output voltage and the inductor is used to store and transfer the energy; and the converters have two operating modes. If the inductor current does not reduce to zero, the situation is described as a Continuous Conduction Mode (CCM). If during a response loop the inductor current drops to zero for a period, it is called a Discontinuous Conduction Mode (DCM). As a result, there is a possibility that the inductor current drops to zero and remains at zero; in which situation, both the power diode and the power switch are off. [53] In this research, power converters are assumed to be working under CCM at all times.

The switching period is defined as the sum of two intervals, as presented in equation (2.2).

$$T_{sw} = T_{on} + T_{off} \tag{2.2}$$

The percentage of T_{on} to the whole switching period is duty cycle $D = T_{on}/T_{sw}$. In addition, the PWM signal is utilised to control the duty ratio D in order to control the output voltage as expressed in equation (2.1). For the ON-state operation, as shown in Figure 2.3 (a), it can be depicted as a set of differential equations:

$$V_{in} = i_L R_L + L\frac{di_L}{dt} + V_c + C\frac{dV_C}{dt}R_c \tag{2.3}$$

$$i_L = C\frac{dV_C}{dt} + \frac{V_o}{R_o} \tag{2.4}$$

$$V_o = C\frac{dV_C}{dt}R_c + Vc \tag{2.5}$$

For OFF-state operations, as shown in Figure 2.3 (b), only equation (2.3) is different and can be re-written as:

$$0 = i_L R_L + L\frac{di_L}{dt} + Vc + C\frac{dV_C}{dt}Rc \tag{2.6}$$

2.2.1 Averaged Modelling

Generally, DC-DC converters can be described by state-space models. The formal expression of state-space is shown in equation (2.7) [56]:

$$\dot{\boldsymbol{x}} = \boldsymbol{A_i x} + \boldsymbol{B_i} V_{in}$$

$$y = \boldsymbol{C_i x} + \boldsymbol{D_i} V_{in} \tag{2.7}$$

A, B, C, and *D* are the system matrices. The indicator *i* represents two operating states, *i=1* stands for ON state and *i = 2* stands for OFF state. *y* is the output. *x* is the state variables comprised by inductor current and capacitor voltage as they are the energy storage components: $\boldsymbol{x} = [i_L \;\; v_C]^T$.

By rearranging the equations of (2.3) – (2.5) the buck converter can be described in the form of (2.7), where matrices A_1, B_1, C_1 and D_1 can be derived:

$$\boldsymbol{A_1} = \begin{bmatrix} \frac{R_O R_C - R_L R_O - R_L R_C}{L(R_O + R_C)} & \frac{-R_O}{L(R_O + R_C)} \\ \frac{R_O}{C(R_O + R_C)} & \frac{-1}{C(R_O + R_C)} \end{bmatrix}, \qquad \boldsymbol{B_1} = \begin{bmatrix} \frac{1}{L} \\ 0 \end{bmatrix}$$

$$\boldsymbol{C_1} = \begin{bmatrix} \frac{R_O R_C}{R_O + R_C} & \frac{R_O}{R_O + R_C} \end{bmatrix}, \boldsymbol{D_1} = 0 \tag{2.8}$$

By solving equations (2.4) – (2.6), A_2, B_2, C_2 and D_2 can be achieved. As for the results presented in equation (2.9), only B_2 differs from B_1:

$$\boldsymbol{A_1} = \boldsymbol{A_2}, \quad \boldsymbol{B_1} = \begin{bmatrix} \frac{1}{L} \\ 0 \end{bmatrix}, \quad \boldsymbol{B_2} = 0, \quad \boldsymbol{C_1} = \boldsymbol{C_2}, \quad \boldsymbol{D_1} = \boldsymbol{D_2} \tag{2.9}$$

The SMPCs are non-linear systems due to the existence of the power switches. A linear time invariant system of the DC-DC converters can be achieved using an SSA model. The principle is to average the converter's waveforms ($i_L \;\; v_C$) for one switching period in order to establish an equivalent state-space model. Therefore, due to the average process, the ripples of the two states' responses will be nearly cancelled out [53, 58]. The SSA model of the buck converter is

derived by multiplying the ON-state period by d and the OFF-state period by $(1-d)$. d is the duty cycle. Thus, the averaged model is [53]:

$$\dot{\boldsymbol{x}} = \boldsymbol{A_{av}}\boldsymbol{x} + \boldsymbol{B_{av}}V_{in}$$

$$y = \boldsymbol{C_{av}}\boldsymbol{x} + \boldsymbol{D_{av}}V_{in} \tag{2.10}$$

The coefficient of the state variable x and input V_{in} in equation (2.10) are the averaged metrices A_{av} and B_{av} respectively. where

$$\boldsymbol{A_{av}} = \begin{bmatrix} \frac{R_O R_C - R_L R_O - R_L R_C}{L(R_O + R_C)} & \frac{-R_O}{L(R_O + R_C)} \\ \frac{R_O}{C(R_O + R_C)} & \frac{-1}{C(R_O + R_C)} \end{bmatrix}, \quad \boldsymbol{B_{av}} = \begin{bmatrix} \frac{d}{L} \\ 0 \end{bmatrix}$$

$$\boldsymbol{C_{av}} = \begin{bmatrix} \frac{R_O R_C}{R_O + R_C} & \frac{R_O}{R_O + R_C} \end{bmatrix}, \boldsymbol{D_{av}} = 0 \tag{2.11}$$

After getting the system metrics results of the SSA model of the buck converter, a Laplace Transform analysis will need to be performed to obtain its continuous transfer function and solve it with respect to output voltage over duty ratio, namely control-to-output transfer function. The frequency domain transfer function is important in analysing the system and is also important in further SI implementation and linear feedback control design. Control-to-output transfer function is essential to many digital control researches [59, 60] due to its simplified form and its ability to describe system characteristics. The continuous transfer function can then be transformed to z-domain/discrete transfer function by different z-transformation methods, which can give a set of digital system transfer function parameters. For SMPCs control design, duty cycle is the target which can be controlled for any state-variable control design. However, with the help of matrices resulting from equation (2.11) and the equation $G_{vd}(s) = \boldsymbol{C_{av}}(s\boldsymbol{I} - \boldsymbol{A_{av}})^{-1}\boldsymbol{B_{av}}$, d can be extracted out. Therefore, the final control-to-output voltage transfer function can be derived as equation (2.12).

$$G_{vd}(s) = \frac{V_o(s)}{d(s)} = \frac{V_{in}(CR_C s + 1)}{\frac{CL(R_o + R_C)}{R_o + R_L}s^2 + \left(\frac{L}{R_o + R_L} + \frac{CR_L R_o}{R_o + R_L} + CR_C\right)s + 1} \tag{2.12}$$

The transfer function shown in equation (2.12) will be applied for the SI in the subsequent analysis. Apart from the modelling method above, there is also a general form of control-to-

output continuous transfer function for CCM buck converters, which can be found in the book [53]. The form is expressed as equation (2.13):

$$G_{vd}(s) = G_{d0}\frac{1+\frac{s}{w_z}}{1+\frac{s}{Qw_0}+\left(\frac{s}{w_0}\right)^2} \tag{2.13}$$

In equation (2.13), w_z is zero frequency, Q is quality factor, G_{d0} is the dc gain, and w_o is corner frequency, which should be considered carefully. The corner frequency (also known as cut-off frequency or break frequency) w_o is a boundary of energy transferring as the expression in (2.14) [53]:

$$w_0 = \frac{1}{\sqrt{LC}} \tag{2.14}$$

The selection of corner frequency should be lower than the switching frequency (f_{sw}) to ensure the efficient energy transfer. The four parameters in (2.13) can be calculated, as shown in (2.15) [61]:

$$G_{do} = V_{in} = \frac{V_o}{D}$$

$$w_o = \sqrt{\frac{R_O + R_L}{LC(R_O + R_C)}}, \quad \xi = \frac{L + C\left(R_O R_C + R_L(R_O + R_C)\right)}{2\sqrt{LC(R_O + R_C)(R_O + R_L)}}$$

$$w_z = \frac{1}{CR_C} \qquad Q = \frac{1}{2\xi} \tag{2.15}$$

Equation (2.13) clearly shows that the transfer function has two poles and one zero. The two poles influence the dynamic behaviour of the SMPC. These are quality factor (Q) and corner frequency (w_0) in the denominator contributing to the two poles. Another point to mention is that it is the zero frequency (w_z) which produces one zero to the transfer function, as shown in (2.13). w_z is affected by the resistance of output capacitor which should be considered, especially in practical situations. Therefore, when designing the controller for the converter, two zeros of controller are required in order to cancel out the two poles in equation (2.13) and one pole of the controller can be set as the zero of the transfer function, which cancels out the effect of zero.

The quality factor is also related to the amount of overshoot M_P [62]:

$$M_P \approx e^{\frac{-\frac{\pi}{2Q}}{\sqrt{1-\frac{1}{4Q^2}}}} \quad (2.16)$$

After substituting the parameters in equation (2.15) for equation (2.13), it can be found that the final continuous transfer function is the same as the equation of the averaged model, as shown in equation (2.12).

2.2.2 Trailing Edge PWM during Off-time Sampling Modelling

There are three ways to obtain a discrete transfer function: z-transformation from continuous transfer function by a variety of z-transformation methods, difference equation, and small-signal derivation [63-66]. The first method is difficult to achieve using only pen and paper, but it can be calculated easily by coding in Matlab®. However, only the numerical values of transfer function parameter can be found without showing the relationships between each of the system parameters. Difference equation as the Auto-Regressive Moving Average (ARMA) model shown in (2.17) is often achieved by the sampling data building up a regression matrix. To calculate the parameters of $[a_n, b_n]^T$, a proper algorithm which is the main tool for SI will be applied. Thus, discrete transfer function can only be obtained after SI process, which cannot show the component relationships inside its function either. In this research, we are deriving the discrete transfer function from the small-signal model, which will clearly show the relationships between each system parameter in the final equation. Another potential advantage for this proposed modelling approach is that we can choose to model a specific set of output sampling points to adapt to different requirements.

$$y(k) + a_1 y(k-1) + \cdots + a_n y(k-n) = b_0 u(k) + b_1 u(k-1) + \cdots + b_n u(k-n) \quad (2.17)$$

Figure 2.4 [6, 9] describes how perturbations of a state-variable propagate over a switching period where t_s is the A/D converter sampling time. The voltage error signal is assumed to be processed by a digital compensator *Gc(z)*. Then the output of the compensator controls the switch duty cycle via a DPWM, which can be regarded as a D/A converter including a sample-and-hold and followed by signal sampling at the modulated edge [67]. There are two samplers

in the feedback loop. One is the A/D sampling of the voltage error signal, and the other is the modulator sampling. Therefore, there is a delay time t_d between the small-signal perturbations of the voltage error signal and a step increase of the duty cycle $\hat{d}[n]$, which is the time between t_s and modulator sampling at t_p. Thus, for the delay time t_d, it includes the A/D conversion time, the computation delay (i.e., the time for the duty-cycle control signal $u[n]$ computation), and the modulator delay time (the time between the update of u[n] and the switch transition from State 1 to State 2) [63]. The small-signal discrete-time model of OFF-time sampling is shown as equation (2.18).

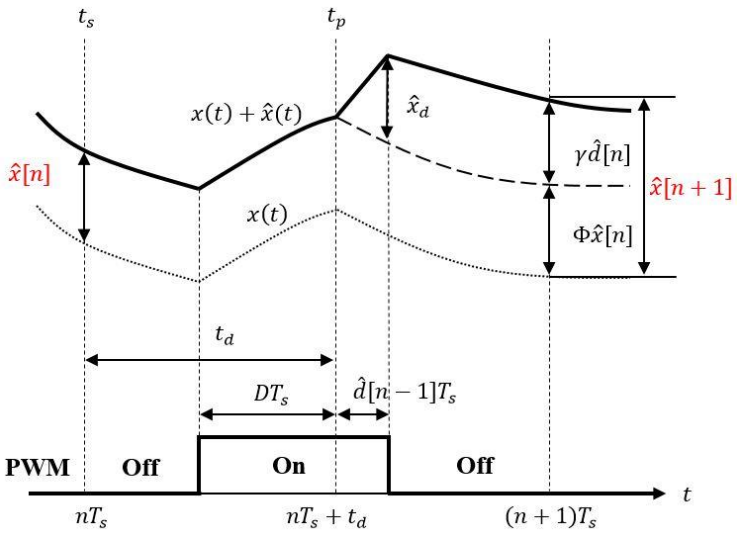

Figure 2.4 Switching Instance when Sampling during Switch-Off Interval

$$\hat{\boldsymbol{x}}[n] = \boldsymbol{\phi}\hat{\boldsymbol{x}}[n-1] + \boldsymbol{\gamma}\hat{\boldsymbol{d}}[n-1]$$

$$\hat{v}_o[n] = \boldsymbol{C_2}\hat{\boldsymbol{x}}[n] = \begin{bmatrix} \dfrac{R_o R_c}{R_o + R_c} & \dfrac{R_o}{R_o + R_c} \end{bmatrix} \begin{bmatrix} \hat{v}_c \\ \hat{\imath}_L \end{bmatrix} \tag{2.18}$$

where R_o is load resistance, and R_c is the equivalent resistance of the capacitor. ϕ and γ represent the propagation period of previous state vectors, and the change of current signal caused by the control signal, respectively. Here, C_2 is used because it is known that the sampling occurs during switch-off time. Thus, the parameters are calculated as shown below:

$$\boldsymbol{\phi} = e^{\boldsymbol{A_2}(T_s - t_d)} e^{\boldsymbol{A_1} DT_s} e^{\boldsymbol{A_2}(t_d - DT_s)} \tag{2.19}$$

$$\boldsymbol{\gamma} = e^{\boldsymbol{A_2}(T_s - t_d)}\boldsymbol{\alpha} T_s \tag{2.20}$$

$$\boldsymbol{\alpha} = (\boldsymbol{A_1} - \boldsymbol{A_2})X_i + (\boldsymbol{B_1} - \boldsymbol{B_2})V_{in} \tag{2.21}$$

Where $\boldsymbol{X_i}$ are the steady-state of the converter states at the end of switch-on time, which can be approximated to be the steady-state of average state-space vector $\overline{\boldsymbol{X}}$. Therefore $\overline{\boldsymbol{X}}$ can be achieved from equation (2.22) [65]. In equation (2.20) and (2.21), the matrix exponentials can be approximated to a closed-form analytical discrete-time model using the approximation $e^{\boldsymbol{A}T_s} \approx \boldsymbol{I} + \boldsymbol{A}T_s$ [68]. The final discrete-time control-to-output transfer function of the buck converter (2.24) for the OFF-time sampling can be calculated by (2.23):

$$\boldsymbol{X_i} \approx \overline{\boldsymbol{X}} = \frac{-\boldsymbol{B_{av}} V_{in}}{\boldsymbol{A_{av}}} \tag{2.22}$$

$$G(z) = \boldsymbol{C_1}(z\boldsymbol{I} - \boldsymbol{\phi})^{-1}\boldsymbol{\gamma} \tag{2.23}$$

$$\frac{V(z)}{D(z)} = \frac{\frac{V_{in}T_s}{LC}(T_s - t_d + CR_c)\left\{z + \frac{T_s}{T_s - t_d + CR_c}\left(\frac{R_c}{R_o} - \frac{CR_c}{T_s} - \frac{(T_s - t_d)R_c}{L} + \frac{t_d}{T_s}\right)\right\}}{1 - \left(2 - \frac{T_s}{R_oC}\right)z^{-1} + \left(1 - \frac{T_s}{R_oC} + \frac{{T_s}^2}{LC}\right)z^{-2}} \tag{2.24}$$

Equation (2.24) has been arranged into its simplest form. If one assumes that R_c and R_L can be ignored, then this is a fair assumption as in many practical applications. R_c and R_L are small enough (typically of order 10^{-3}) that it will not influence the parameters' estimation results to any significant degree. However, in the following simplification steps, R_C will be remained as it is the main cause of the voltage drop as will be discussed in the figure 2.7.

$$\frac{V(z)}{D(z)} = \frac{\frac{V_{in}T_s}{LC}(T_s - t_d)\left\{z^{-1} + \frac{t_d}{T_s - t_d}z^{-2}\right\}}{1 - \left(2 - \frac{T_s}{R_oC}\right)z^{-1} + \left(1 - \frac{T_s}{R_oC} + \frac{{T_s}^2}{LC}\right)z^{-2}} \tag{2.25}$$

Simplification of the transfer function is a very important step for the accuracy of system parameter estimation. Theoretically, the proposed modelling method on SI is likely to be adapted to different SMPC systems, which can also be further verified by the flexibility from the simplification procedure. This will be further discussed in detail in Sub-section 2.5.

2.3 DC-DC Boost SMPC Modelling

A boost converter can step-up the input voltage for a higher output voltage. The two operation modes of boost converter are depicted in Figure 2.5. When the switch is on, as shown in Figure 2.5 (a), the effective circuit consists of two half circuits. In this circumstance, the left half circuit is equivalent to a first-order system, which is only composed of input power supply (V_{in}), inductor (L) and inductor resistance (R_L); and for the right half of the circuit it is constructed by the load resistor (R_O), capacitor (C) and capacitor equivalent series resistance (R_C), which is also equivalent to a first-order system. The inductor is being charged, and the capacitor is being discharged during this time instance. Therefore, the differential equations when the switch is on are:

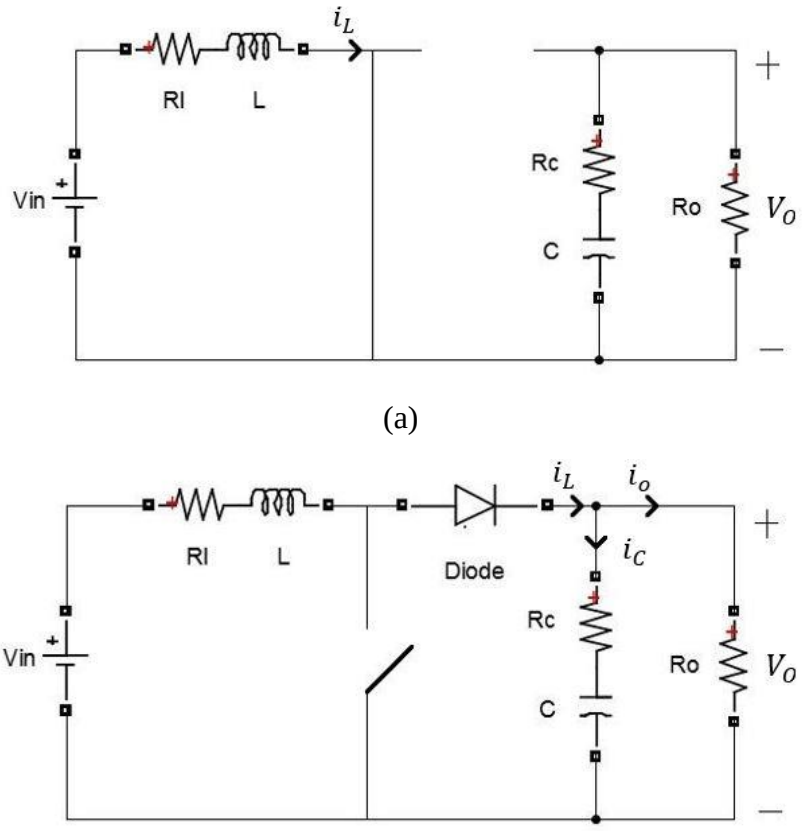

Figure 2.5 Two operation modes – boost converter, a: ON state, b: OFF state

$$V_{in} = \mathrm{L}\frac{di_L}{dt} + i_L R_L \tag{2.26}$$

$$V_O = C\frac{dV_C}{dt}R_C + V_C \tag{2.27}$$

$$\frac{dV_C}{dt} = \frac{-V_O}{R_O C} \tag{2.28}$$

When the switch is off, as shown in Figure 2.5 (b), the energy will be transferred through the diode from the input power supply (V_{in}) to the output load (R_o). During this time interval, the inductor is being discharged and the capacitor is being charged; and the circuit is a second-order system.

If Kirchhoff's law is applied, the differential equations of this OFF period are:

$$i_L = \frac{V_O}{R_O} + C\frac{dV_C}{dt} \tag{2.29}$$

$$C\frac{dV_C}{dt}R_C + V_C = V_O = V_{in} - \mathrm{L}\frac{di_L}{dt} - i_L R_L \tag{2.30}$$

2.3.1 Averaged Modelling

The average state-space model is commonly used for modelling many DC-DC converters for the control application, etc., because this can linearize the non-linearity caused by switching action by taking the average value of the ON and OFF state, as per the method shown in Section 2.2.1. Firstly, system matrices need to be calculated from equation (2.29) and (2.30). The system matrices $\boldsymbol{A_i}$, $\boldsymbol{B_i}$, $\boldsymbol{C_i}$ and $\boldsymbol{D_i}$ of a boost converter are:

For the ON state:

$$\boldsymbol{A_1} = \begin{bmatrix} 0 & 0 \\ 0 & \dfrac{-1}{C(R_o + R_c)} \end{bmatrix}, \qquad \boldsymbol{B_1} = \begin{bmatrix} \dfrac{1}{L} \\ 0 \end{bmatrix}$$

$$\boldsymbol{C_1} = \begin{bmatrix} 0 & \dfrac{R_o}{R_o + R_c} \end{bmatrix}, \qquad \boldsymbol{D_1} = 0 \tag{2.31}$$

For the OFF state:

$$\boldsymbol{A_2} = \begin{bmatrix} \frac{-(R_o R_c)}{L(R_o + R_c)} & \frac{-R_o}{L(R_o + R_c)} \\ \frac{R_o}{C(R_c + R_c)} & \frac{-1}{C(R_o + R_c)} \end{bmatrix}, \qquad \boldsymbol{B_2} = \begin{bmatrix} \frac{1}{L} \\ 0 \end{bmatrix}$$

$$\boldsymbol{C_2} = \begin{bmatrix} \frac{R_o R_c}{R_o + R_c} & \frac{R_o}{R_o + R_c} \end{bmatrix}, \qquad \boldsymbol{D_2} = 0 \tag{2.32}$$

For the next step, substitute equations (2.31) and (2.32) for equation (2.10) and the SSA model matrices can be calculated as:

$$\boldsymbol{A_{av}} = \begin{bmatrix} \frac{d_o R_o R_c}{L(R_o + R_c)} & \frac{-d_o R_o}{L(R_o + R_c)} \\ \frac{d_o R_o}{C(R_o + R_c)} & \frac{-1}{C(R_o + R_c)} \end{bmatrix}, \qquad \boldsymbol{B_{av}} = \begin{bmatrix} \frac{1}{L} \\ 0 \end{bmatrix}$$

$$\boldsymbol{C_{av}} = \begin{bmatrix} \frac{d_o R_o R_c}{R_o + R_c} & \frac{R_o}{R_o + R_c} \end{bmatrix}, \boldsymbol{D_{av}} = 0 \tag{2.33}$$

Where $d_o = (1 - d)$. To simplify the analysis, it can be approximated as shown in (2.34) below.

$$\frac{R_o R_c}{R_o + R_c} \approx R_c, \qquad \frac{R_o}{R_o + R_c} \approx 1, \tag{2.34}$$

Therefore, the state-space matrices can be simplified, as in (2.35):

$$\boldsymbol{A_{av}} = \begin{bmatrix} \frac{d_o R_c}{L} & \frac{-d_o}{L} \\ \frac{d_o}{C} & \frac{-1}{C R_o} \end{bmatrix}, \qquad \boldsymbol{B_{av}} = \begin{bmatrix} \frac{1}{L} \\ 0 \end{bmatrix}$$

$$\boldsymbol{C_{av}} = [d_o R_c \quad 1], \qquad \boldsymbol{D_{av}} = 0 \tag{2.35}$$

Thus, the continuous transfer function of boost converters can be achieved by transformation from state-space matrices. The result is shown in equation (2.36).

$$\frac{V_o(s)}{D(s)} = \frac{V_{in}}{d_o L_e C} \frac{\left(1 - \frac{sL_e}{R_o}\right)(sR_c C + R_c/R_o + 1)}{s^2 + s\left[\frac{(R_l/d_o^2) + (R_c/d_o)}{L_e} + \frac{1}{CR_o}\right] + \frac{(R_l/d_o^2) + (R_c/d_o)}{L_e C R_o} + \frac{1}{L_e C}} \tag{2.36}$$

Where $L_e = L/(1\text{-}d)^2$. From equation (2.36), it is clearly shown that the boost converter has an RHP-zero ($\frac{R_o}{L_e} > 0$) in the numerator of the transfer function. The RHP-zero in continuous-domain leads to a zero outside of the unit circle in the discrete-domain equivalent transfer function. Equation (2.36) can be transformed to a simplified version when R_c equals to zero if R_c is ignored.

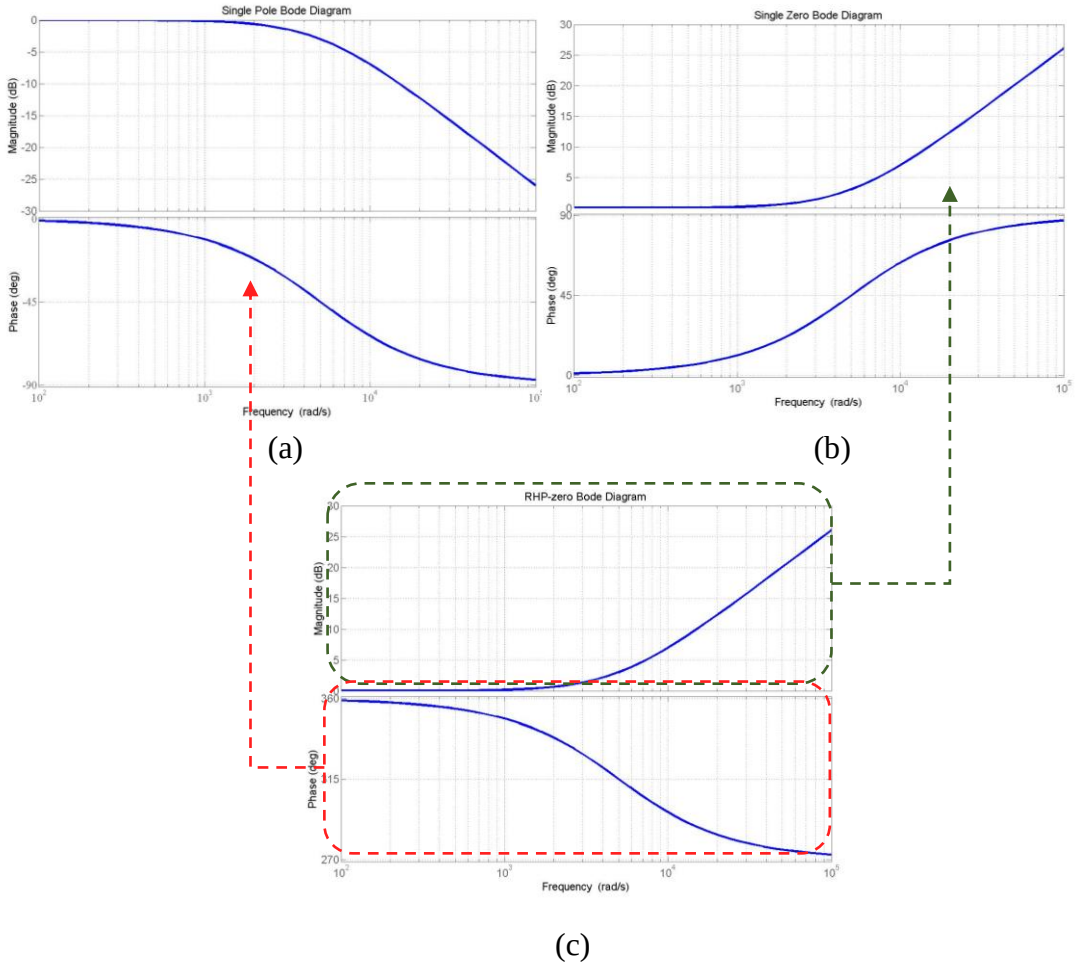

Figure 2.6 Bode Plots Responses: (a) Single Pole, (b) Single zero, (c) RHP-zero

Figure 2.6 shows the bode plots of three situations with the same resistance and capacitor values (single pole response, single zero response and RHP-zero response), the transfer functions of which are $(\frac{1}{s+1}), (s+1)$ and $(s-1)$ respectively. It is clearly shown that the RHP-zero exhibits the magnitude response of the LHP zero, but the phase response of the single pole. As for the minimum phase system, it has a certain relationship between its magnitude response and phase response; but for a non-minimum phase system with an RHP-zero, there is no certain relationship between the two responses. The RHP-zero is mainly caused by a time-lag term.

This characteristic of the RHP-zero makes it hard for the SI process to distinguish a RHP-zero from a LHP zero [13, 53]. In turn, this makes it very difficult for a boost converter to estimate the transfer function accurately. Physically speaking, when the duty cycle is increased for a boost converter, the output voltage should also increase. However, in non-minimum phase systems (e.g. boost and buck-boost converters), a step increase in the duty cycle also increases the duration of capacitor hold-up time for the output voltage. This leads to an initial drop for the change of output voltage in the first place. Consequently, for this situation, it will lead to a wrong direction of SI until the capacitor is recharged by the inductor current and the output voltage begins to increase, as shown in Figure 2.7. The average value of output voltage (shown as the red line) which has been commonly used for SI for decades, obviously there has an initial drop effect on its response. The delay time between the first drop and voltage recovery is inversely proportional to the RHP-zero [57].

In the literature, most works are limited to analysing parametric estimation of the buck converter only, as buck converter is a minimum-phase system which doesn't have the mis-leading effect by the RHP-zero. However, in this research, we have pointed out and explained that the main issue for non-minimum phase converters SI is due to the existence of RHP-zero for the first time and provided a solution. This should help further studies on parametric estimation of non-minimum phase converters.

2.3.2 Trailing Edge PWM during Off-time Sampling Modelling

An equivalent discrete transfer function is necessary for SI in digitally controlled systems. In addition, an appropriate discrete transfer function provides prior knowledge to the order and reference model for the SI. However, the SI results are not correctly fitted to averaged state-space transfer functions for boost converters. The proposed discrete-time modelling method is introduced here, which is mainly introduced for boost converter SI that can address this identification problem. Figure 2.7 is the output response of a boost converter after a step increase of duty cycle. The voltage drop between switch on and off instance is due to the existence of R_C. The upper dashed line is the sampled points, which occurs during the transistor OFF-time. The lower trace line is the sampled point during transistor ON-time. It is apparent that the RHP-zero effect exists on both the lower trace line and the average trace line. The RHP-zero effect can lead to a wrong direction after a step increase of the duty cycle value. The reason for the wrong direction is that during a step increase of the duty cycle, the output voltage should

increase as well, instead the output voltage of boost converter dropping initially for a small period, which is a wrong response direction. This time lag can contribute to errors in SI. However, for the upper trace line, the RHP-zero effect cannot be observed and its response, after an increment of duty cycle, is in the correct direction. Therefore, if we can model the boost converter from the upper trace line it can theoretically avoid the unstable effect caused by the RHP-zero.

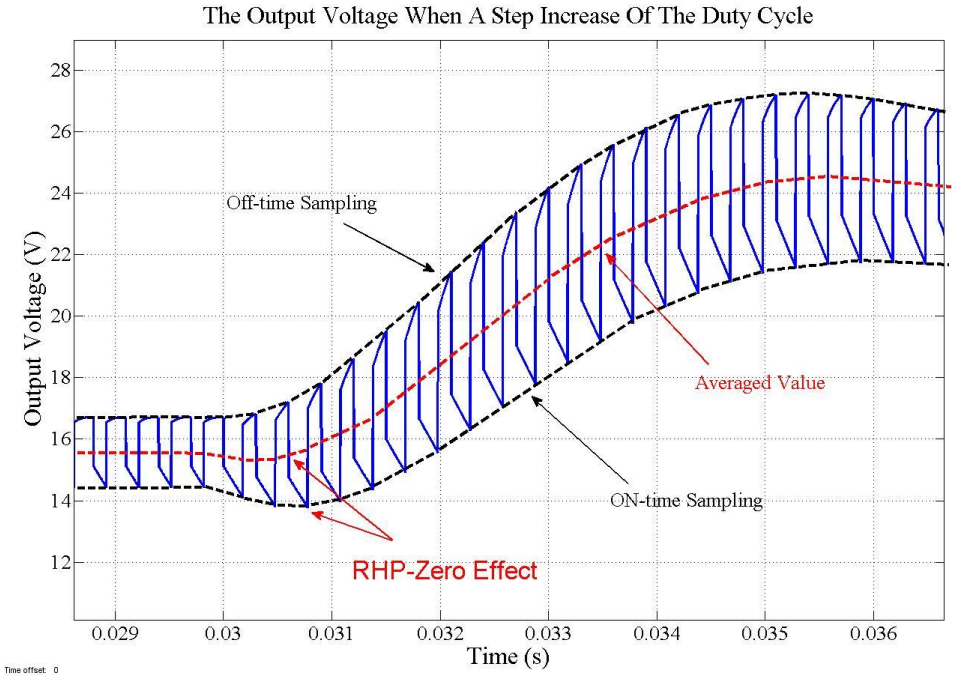

Figure 2.7 Output Voltage Response of Boost Converter during a Step Increase of the Duty Cycle

This modelling method was introduced in Section 2.2.2. With the help from equation (2.18 – 2.31) and the equations (2.31 – 2.33), the TEOS model of boost converter can be derived as shown in equation (2.37).

$$\frac{V(z)}{D(z)} = \frac{V_{in}T_s\left\{\left(\frac{T_s}{LC} - \frac{1}{d_o^2 R_o C}\right)z^{-1} + \frac{1}{d_o^2 R_o C}z^{-2}\right\}}{1 - \left(2 - \frac{T_s}{R_o C}\right)z^{-1} + \left(1 - \frac{T_s}{R_o C} + \frac{(d_o T_s)^2}{LC}\right)z^{-2}} \tag{2.37}$$

The final discrete-domain equation is very long, with more than 30 terms in this mathematical formula. Thus, in Equation (2.37) several terms which have a small value and have much less influence on the result has been removed in order to simplify it. Here, it also shows the importance of the simplification step. In the next section, the simplification steps will be shown

in detail in order to produce a good level of accuracy. From equation (2.17) and the knowledge of the converter system order (a second-order system), a general form is shown in equation (2.38) to correspond to the equation (2.37).

$$H(z) = \frac{b_1 z^{-1} + b_2 z^{-2}}{1 + a_1 z^{-1} + a_2 z^{-2}} \tag{2.38}$$

(a_1, a_2, b_1, b_2) are the four parameters corresponding to the co-efficient of z in the denominator and numerator of equation (2.37), which, consequently, needs to be estimated by the SI technique.

2.4 DC-DC Buck-Boost SMPC TEOS Modelling

As the proposed modelling method has the possibility to address the SI problem of any non-minimum phase systems, thus the buck-boost converter, as another classical non-minimum phase converter, will also be tested with the proposed method. The buck-boost circuit is shown in Figure 2.2. The averaged model and proposed discrete model of the buck-boost converter are both introduced. The way to achieve the final discrete transfer function is the same as the steps in Section 2.2.2. Some of the important procedures shown below.

The state-space matrices of buck-boost converter ON-time are presented in equation (2.39) [69]:

$$\boldsymbol{A_1} = \begin{bmatrix} \dfrac{-1}{C(R_o + R_c)} & 0 \\ 0 & \dfrac{-R_l}{L} \end{bmatrix}, \qquad \boldsymbol{B_1} = \begin{bmatrix} 0 \\ \dfrac{1}{L} \end{bmatrix}$$

$$\boldsymbol{C_1} = \begin{bmatrix} \dfrac{R_o}{R_o + R_c} & 0 \end{bmatrix}, \qquad \boldsymbol{D_1} = 0 \tag{2.39}$$

For the OFF state:

$$\boldsymbol{A_2} = \begin{bmatrix} \dfrac{-1}{C(R_o + R_c)} & \dfrac{R_o}{C(R_c + R_c)} \\ \dfrac{-R_o}{L(R_o + R_c)} & \dfrac{-(R_o R_c)}{L(R_o + R_c)} \end{bmatrix}, \qquad \boldsymbol{B_2} = 0$$

$$\boldsymbol{C_2} = \begin{bmatrix} \dfrac{R_o}{R_o + R_c} & \dfrac{R_o R_c}{R_o + R_c} \end{bmatrix}, \qquad \boldsymbol{D_2} = 0 \tag{2.40}$$

Thus, the final state-space matrices averaged model for the buck-boost converter is:

$$\boldsymbol{A_{av}} = \begin{bmatrix} \dfrac{-1}{C(R_o + R_c)} & \dfrac{d_o R_o}{C(R_o + R_c)} \\ \dfrac{-d_o R_o}{L(R_o + R_c)} & \dfrac{-(d_o R_o R_c)}{L(R_o + R_c)} \end{bmatrix}, \qquad \boldsymbol{B_{av}} = \begin{bmatrix} 0 \\ \dfrac{d}{L} \end{bmatrix}$$

$$\boldsymbol{C_{av}} = \begin{bmatrix} \dfrac{R_o}{R_o + R_c} & \dfrac{d_o R_o R_c}{R_o + R_c} \end{bmatrix}, \boldsymbol{D_{av}} = 0 \tag{2.41}$$

The rules of equation (2.10) can also be applied, and after simplifying the rules in equation (2.34) the averaged state-space model is shown in equation (2.42):

$$\boldsymbol{A_{av}} = \begin{bmatrix} \dfrac{-1}{CR_o} & \dfrac{d_o}{C} \\ \dfrac{-d_o}{L} & \dfrac{-d_o R_c}{L} \end{bmatrix}, \qquad \boldsymbol{B_{av}} = \begin{bmatrix} 0 \\ \dfrac{d}{L} \end{bmatrix}$$

$$\boldsymbol{C_{av}} = [1 \quad d_o R_c], \qquad \boldsymbol{D_{av}} = 0 \tag{2.42}$$

Then, as the same calculation from equation (2.19) to equation (2.23), the final discrete transfer function of buck-boost converter can be achieved by:

$$\begin{aligned} \frac{V(z)}{D(z)} = & \frac{\frac{V_{in} T_s}{(R_c + d_o R_o)} \left(\frac{R_c R_o}{L} + \frac{T_s R_o d_o}{LC} + \frac{1}{C} + \frac{2T_s R_c}{CL} - \frac{1}{C d_o} \right) z^{-1}}{1 - \left(2 - \frac{T_s}{R_o C} \right) z^{-1} + \left(1 - \frac{T_s}{R_o C} + \frac{(d_o T_s)^2}{LC} \right) z^{-2}} \\ & - \frac{\left(\frac{R_c R_o}{L} + \frac{2 d_o R_c^2 T_s^2}{CL^2} + \frac{d_o R_c^3 T_s^2}{CL^2 R_o} + \frac{d_o^2 T_s^2}{C^2 L} \right) z^{-2}}{1 - \left(2 - \frac{T_s}{R_o C} \right) z^{-1} + \left(1 - \frac{T_s}{R_o C} + \frac{(d_o T_s)^2}{LC} \right) z^{-2}} \end{aligned} \tag{2.43}$$

So far, for the modelling methods above, all the topologies used in the simulation and experiment have been introduced – namely the averaged model and proposed discrete model, for the buck converter, the boost converter and the buck-boost converter. In the next part, the simplification steps about the proposed discrete model of buck converter and the boost converter will be discussed in detail in order to give an in-depth look at the relationships between the transfer function parameters and the system parameters.

2.5 Model Simplification and System Parameters Calculation

The proposed modelling method will give a very complicated discrete transfer function, which possibly consists of more than 20 terms inside an equation, especially on the boost converter. Therefore, the simplification step is quite important for ensuring the model accuracy and the feasibility of the system parameters (*R & C*) calculation. As the buck converter and boost converter have been tested in the practical experiment, the simplification procedures and parameter relationships of both converters will be presented in the following parts.

2.5.1 Buck TEOS Model Simplification

From equation (2.24) to equation (2.25), the model of the buck converter has already been simplified. From equation (2.25), the relationship between the parameters of the transfer function and the system parameters (R_o & C) is obvious. The transfer function's parameters can be achieved by the SI approach, and with the identified parameters it is possible to calculate the system parameters from the relationship equations.

As an observation from the simplified equation (2.25), t_d only exists in the numerator part. The value of t_d can only be an approximated value in the experiment, as we cannot give a specific delay time for the controller calculation time and control signal updated time. In addition, system parameter C exists on both the numerator side and the denominator side. However, for the numerator part, R_o only exists on the b_1 side. So therefore, C is better to be estimated from b_1 side as only C is in this equation, and then substitute it into the b_2 equation to calculate R_o. However, for this fact, to ensure a higher model accuracy and to make sure both equations (i.e., a_1 and a_2) can be used to calculate system parameters *Ro & C*, hence, it is better to estimate from the denominator side.

From equation (2.24) and the ARMA model in equation (2.17), we can come up with four equations:

$$b_1 = \frac{V_{in}T_s}{LC}(T_s - t_d);$$

$$b_2 = \frac{V_{in}T_s^2 t_d}{LC}\left(\frac{d}{CR_C} - \frac{1}{R_o} - \frac{C}{T_s} - \frac{d_o T_s}{L}\right) \tag{2.44}$$

$$a_1 = -\left(2 - \frac{T_s}{R_o C}\right)$$

$$a_2 = 1 - \frac{T_s}{R_o C} + \frac{{T_s}^2}{LC} \tag{2.45}$$

As shown in (2.44) and (2.45), R_O and C are a function of a_1 and a_2 and b_1 and b_2. therefore, by accurate estimation of both parameters one can easily monitor the changes of R_O and C in real time and detect any failure or fault in the converter circuit. From equation (2.44), the R_O and C are obtained as equation (2.46).

$$C = \frac{V_{in} T_s (T_s - t_d)}{(b_1 L - V_{in} T_s R_c)}$$

$$R_o = \frac{-1}{\frac{LCb_2}{V_{in} T_s^2 R_c} + \frac{C}{T_s} + \frac{d_o T_s}{L} - \frac{d}{C R_c}} \tag{2.46}$$

It is noted that R_c is not ignored here due to two reasons: Firstly, the model of buck converter is not complicated as that of boost converter containing over 30 items. It doesn't need to ignore R_c for simplification. Secondly, R_c plays a big role when calculating R_o from the observation of equation (2.46). The value of R_c is from the specifications in table 4.1. From equation (2.45), R_o and C can be cancelled out respectively to get two equations:

$$C = \frac{T_s^3}{\{(a_1 + 2) - L T_s (1 - a_2)\}}$$

$$R_o = \frac{L(a_1 + a_2 + 1)}{T_s (a_1 + 2)} \tag{2.47}$$

Therefore, if the system parameter of inductance can be known in advance, and with the help of the estimated transfer function parameters (a_1 & a_2), we can monitor the change in system parameters (R_o & C). If any of the system parameters (R_o & C) can be known in advance, then the inductance can be calculated as well. In the next part, system parameters calculation about boost converter is presented.

2.5.2 Boost TEOS Model Simplification

Before getting the equation (2.38), the whole transfer function after discretisation is displayed in equation (2.48).

$$\frac{V(z)}{D(z)} = \frac{\frac{V_{in}T_s}{d_oC^2L^2R_o(R_c+d_oR_o)}z^{-1}(\mathbf{I}) + \frac{V_{in}T_s}{d_oC^2L^2R_o(R_c+d_oR_o)}z^{-2}(\mathbf{II})}{1-\left(2-\frac{T_s}{R_oC}\right)z^{-1}+\left(1-\frac{T_s}{R_oC}+\frac{(d_oT_s)^2}{LC}\right)z^{-2}} \tag{2.48}$$

Where Ⅰ is composed of eight terms and Ⅱ is composed of 12 terms, as shown in Table 3. From equation (2.48), it is obvious that there are two ways for doing system parameter calculations (numerator part or denominator part). As there are far fewer terms on the denominator part, it seems to be much easier to do estimation based on the transfer function denominator parameters. However, both sides will be tested for system parameters estimation. The transfer function has more complexity for boost converters. t_d can be a specific value in the simulation, which can be assumed to be dT_s, where A/D conversion delay, and computation delay time are assumed to be zero, as they were in the simulation. In order to simplify the equation mathematically, the higher orders of magnitude terms will be selected, and the lower orders of magnitude terms will be removed. The final simplified transfer function can be any form depending on different system specifications and selections of the terms. Therefore, here it is given a set of specifications of a boost converter, as listed in Table 2.2, which is also the practical experimental boost converter design. The parameters design of the boost converter will be shown in the chapter 5.

Sampling Time (T_s)	$50\mu s$
Input Voltage (V_{in})	$12V$
Output Voltage (V_o)	$20V$
Load Resistor (R_o)	6Ω
Capacitor (C)	$180\mu F$
Capacitor Equivalent Resistance (R_c)	$14m\Omega$
Inductor (L)	$680\mu H$

Inductor Equivalent Resistance (R_L)	11 $m\Omega$

Table 2.2 Boost converter specifications

As the final discretised transfer function in equation (2.48), the final obtained terms of Ⅰ and Ⅱ with the calculation results from Table 2.2 are clearly shown in Table 2.3 with their orders of magnitude. The values of each term can have a large difference.

No.	Ⅰ	Order of Magnitude	Ⅱ	Order of Magnitude
1	$-d_o^2T_sC^2R_o^2R_c^2$	-10^{-5}	$d_o^2T_sC^2R_o^2R_c^2$	10^{-5}
2	$d_oC^2LR_o^2R_c$	10^{-2}	$-d_oC^2LR_o^2R_c$	-10^{-2}
3	$-d_oT_sC^2R_oR_c^3$	-10^{-8}	$d_oT_sC^2R_oR_c^3$	10^{-8}
4	$C^2LR_oR_c^2$	10^{-5}	$-C^2LR_oR_c^2$	-10^{-5}
5	$d_o^2T_sCLR_o^2$	10^{-1}	$-d_o^3T_s^2CR_o^2R_c$	-10^{-4}
6	$2d_oT_sCLR_oR_c$	10^{-4}	$-2d_o^2T_s^2CR_oR_c^2$	-10^{-7}
7	$-CL^2R_o$	-10^{-1}	$-d_oT_s^2CR_c^3$	-10^{-10}
8	$d_oT_sL^2$	10^{-2}	CL^2R_o	10^{-1}
9			$T_sCLR_c^2$	10^{-7}
10			$d_o^2T_s^2LR_o$	10^{-3}
11			$-d_oT_sL^2$	-10^{-2}

Table 2.3 Boost transfer function numerator terms and the order of magnitude

From Table 2.3, it can be observed that each term has a big difference which could be $10^1 \sim 10^7$ in their order of magnitude. Analysing these data, it can be found that the absolute value of the biggest order of magnitude for Ⅰ and Ⅱ is 10^{-1}. And to ensure the accuracy of the calculation, it is better to keep another two decimals. Thus, we remain with the terms, which are within the order of magnitude range of 10^3. With the help of the ARMA model in equation (2.17), the two parameters of (b_1 & b_2) are structured as equation (2.48).

$$b_1 = \frac{V_{in}T_s\left(CR_oR_c + d_oT_sR_o - \frac{L}{d_o} + \frac{T_s}{L}\right)}{CL(R_c + d_oR_o)}$$

$$b_2 = \frac{V_{in}T_s\left(-CR_oR_c + \frac{L}{d_o} + \frac{d_oT_s^2}{C} - \frac{T_sL}{C}\right)}{CL(R_c + d_oR_o)} \tag{2.49}$$

Once b_1 and b_2 have been got, the next task is to extract R_o and C out respectively. When calculating the system parameter C from b_2, the equation is a quadratic equation. Therefore, we apply Weda's Theorem (WT) and the root formula in equation (2.50) [70], where x is the unknown variable, and a, b, and c are the co-efficient of the equation. After re-arrangements, the co-efficient in equation (2.50) can be calculated as the equation in (2.51).

$$x = \frac{-b \pm \sqrt{b^2 - 4ac}}{2a} \tag{2.50}$$

$$a = \frac{b_2d_oR_o}{V_{in}T_s} + \frac{R_oR_c}{L} + \frac{b_2R_c}{V_{in}T_s}$$

$$b = -\frac{1}{d_o}$$

$$c = T_s - \frac{d_oT_s^2}{L} \tag{2.51}$$

After simplification steps to re-arrange the terms and with the help of WT, the equation of estimating R_o & C based on numerator part can be written as equation (2.52) and equation (2.53), respectively.

$$R_{o(1)} = \frac{\frac{T_s}{CL^2} - \frac{1}{Cd_o} - \frac{b_1R_c}{V_{in}T_s}}{\frac{b_1d_o}{V_{in}T_s} - \frac{R_c}{L} - \frac{d_oT_s}{CL}}$$

$$R_{o(2)} = \frac{\frac{1}{Cd_o} + \frac{d_o T_s^2}{C^2 L} - \frac{T_s}{C^2} - \frac{b_2 R_c}{V_{in} T_s}}{\frac{b_2 d_o}{V_{in} T_s} + \frac{R_c}{L}} \tag{2.52}$$

$$C_{(1)} = \frac{\frac{d_o T_s R_o}{L} + \frac{T_s}{L^2} - \frac{1}{d_o}}{\frac{b_1 d_o R_o}{V_{in} T_s} - \frac{R_o R_c}{L} + \frac{b_1 R_c}{V_{in} T_s}}$$

$$C_{(2)} = \left| \frac{\frac{1}{d_o} \pm \sqrt{\frac{1}{d_o^2} - 4\left(\frac{b_2 d_o R_o}{V_{in} T_s} + \frac{R_o R_c}{L} + \frac{b_2 R_c}{V_{in} T_s}\right)\left(T_s - \frac{d_o T_s^2}{L}\right)}}{2\left(\frac{b_2 d_o R_o}{V_{in} T_s} + \frac{R_o R_c}{L} + \frac{b_2 R_c}{V_{in} T_s}\right)} \right| \tag{2.53}$$

It is possible to calculate the R_o from each equation of (2.52) and the C from equation (2.53). However, in order to minimise the estimation error as much as possible, it is better to calculate the averaged value of $R_{o(1)}$ and $R_{o(2)}$, and $C_{(1)}$ and $C_{(2)}$, as shown in equation (2.54).

$$R_{o(ave)} = \left(R_{o(1)} + R_{o(2)}\right)/2$$

$$C_{(ave)} = \left(C_{(1)} + C_{(2)}\right)/2 \tag{2.54}$$

If calculating from the denominator side, the equations are much easier as they have fewer terms. Again, with the help of the ARMA model in equation (2.17), the system parameters of R_o & C can be calculated as below.

$$C = \frac{(d_o T_s)^2}{L(a_1 + a_2 + 1)} \tag{2.55}$$

$$R_o = \frac{L(a_1 + a_2 + 1)}{d_o^2 T_s (a_1 + 2)} \tag{2.56}$$

As the simplification steps are based on choosing different terms, it can be any other form if given a different set of specifications. From equations (2.52) to (2.56), it is clearly shown that the system parameters R_o & C of boost converter can be estimated by the parametric estimation results of the boost converter transfer function. The simulation estimation results will be presented in detail in the System Identification section; and the practical results will be shown in the Experimental Results and Discussions section.

2.6 Chapter Summary

In this chapter, the popularly used SSA modelling method and the TE OFF-time sampling modelling method are introduced for three kinds of SMPCs. In addition, the simplification steps of the TEOS model for the buck converter and the boost converter are also presented. After simplification of the model, the relationship between the model parameters and the system parameters become much clearer, and this has provided a possible way to estimate or monitor the system parameters when estimating the model parameters. From the derivation steps, it is apparent that the TEOS model is more complex when compared to the averaged model.

The SSA model is derived from state-space equations, whose final format is a continuous transfer function in the s-domain. It is calculated by averaging the two operating states by duty cycle, while the TEOS model is derived from OFF-time state by small-signal equations with z-transformation to achieve a discrete transfer function format. Therefore, in the practical experiment, the sampling strategy is different, which relies on the settings of the ePWM block. In addition, due to the characteristics of the discrete transfer function for the TEOS model, it is more suitable for the implementation into digital systems; and as the TEOS model is calculated from small-signal equations, it is feasible to modelling a system from different points of a signal. Particularly, for the application of non-minimum phase converters, if we only do sampling during the switch-off time, then this can avoid the RHP zero effect as much as possible in order to help the parametric estimation to be more accurate since, in this case, SI of a system will not be misled by an initial ‘wrong’ response direction caused by the RHP-zero. Another advantage for the TEOS model is that it can show a clear relationship between the model parameters and the system parameters. Based on the relationship, it becomes possible to monitor the system parameters while doing parametric estimation, which will be a novel approach to fault detection and components monitoring.

In this chapter, the problem of non-minimum phase converters SI is introduced and analysed with a proposed solution, and TEOS model has been obtained and shown its potential merits in non-minimum phase converters SI and providing a novel method of system parameters estimation for the first time in the literature.

CHAPTER 3 METHODOLOGY OF SYSTEM IDENTIFICATION

3.1 Introduction

SI is one of the three problems identified in dynamics and control. An operating system has three kinds of information as depicted in Figure 3.1: input u(t), output y(t) and system (S). As shown in Table 3.1, if u(t) and system S can be known in advance, then we need to find y(t), which is a simulation problem. If given y(t) and S, then we must find u(t), which is a control problem. And if we know u(t) and y(t), we can determine what the system looks like, which is a SI problem. SI is the focus of this section.

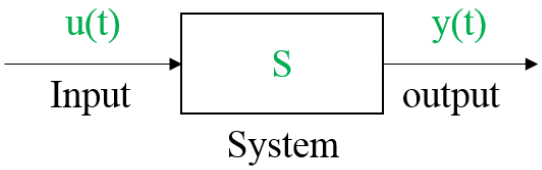

Figure 3.1 System Operation

	Simulation Problem	Control Problem	SI Problem
Given	u(t) & S	y(t) & S	u(t) & y(t)
Find	y(t)	u(t)	S

Table 3.1 Dynamics and Control Problems

SI is important in many research areas. It can be treated as an advanced technique for the purpose of the mathematical model or model parameter identification. In any situation that a mathematical equation of a plant exists, SI can be applied to the system in order to estimate each parameter of its mathematical model based on sampled data without knowing any information (e.g. component values) in advance [71]. For power electronics applications, the SI technique is also popular in the area of signal processing, fault detection and adaptive control, which are required to estimate their model parameters to understand and analyse the dynamic behaviour of the system [71-75]. Finally, an accurate estimated mathematical model will be constructed by the estimation results based on SI as shown by the operation in Figure 1.1.

3.2 Black-Box and White-Box Estimation

Before doing SI of a system, we need to know exactly what the system is. There are two general categories of SI based on two kinds of systems: black-box and white-box estimation [76-78], as depicted in Figure 3.2. For a black-box estimation, no information for the system can be known in advance. A rich-frequency input signal will be applied to the black-box system to obtain the frequency response, before estimating the system from its frequency response analysis. For a white-box estimation, it means having a light in the box, so that the information (components and connections) of the system can be known in advance. Then we can write its differential equations and transfer function and the order of the system can also be known. A rich-frequency input signal will then be applied to the system to determine its model parameters. In this research, the converters are designed specifically so that the system can be modelled accurately in advance. It is just required to apply SI technique to estimate the model parameters. Thus, the situation belongs to the white-box estimation group.

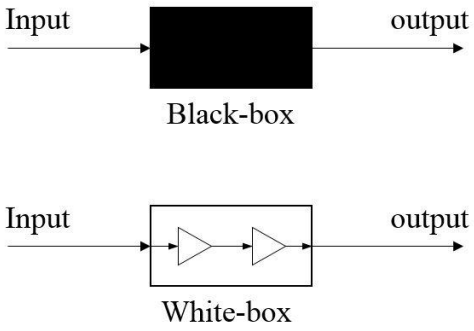

Figure 3.2 Black-box and White-box

3.3 On-line and Off-line Identification

The operation of SI has two types, which are on-line SI and off-line [26, 27]. The difference is whether the plant is working or not when the system is doing sampling and SI operation. Thus, for on-line system identification, the SI process is at each sampling data acquisition instance. On-line estimation is based on the pre-known model structure and order, which means it is based on a white-box estimation. An on-line approach does not need to store all of the sampled data but needs to use the new data to recursively fix the model parameters. The processor is required to do a computational task at each sampling instance to update a new set of model parameters by a selected adaptive algorithm. The chosen adaptive algorithm needs to have a

good convergence speed. In addition, for an on-line adaptive control scheme, the controller gains can be updated to their optimal values during each sampling instance in order to achieve a good control performance [61, 62]. Off-line SI is based on utilising a batch of data which has been stored in the memory. The stored data will be processed when the plant is not working. This method, which is also known as batch estimation [27], is suitable for designing an optimal controller for a complicated system [79]. An off-line approach is also usually used for black-box estimation. Most of the time, the off-line approach can be more accurate, as it has more immunity to signal noise. The disadvantage of off-line estimation is that a large amount of data should be stored. In this research, both on-line system and off-line SIs have been done in order to verify the system parameters estimation approach.

3.4 Parametric and Non-Parametric Estimation

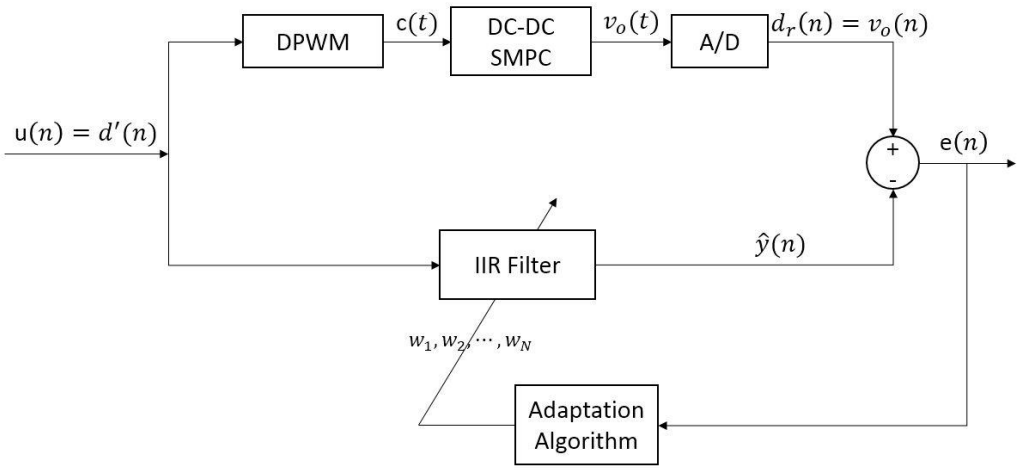

Figure 3.3 Adaptive System Identification Structure

Based on different identification processes, there are two kinds of system identification methods: the non-parametric SI technique, and the parametric estimation techniques [80]. By sampling the input and output signals of a system, the parameters of the system can be estimated by non-parametric estimation techniques or parametric estimation techniques [81]. However, the estimation processes are different. For non-parametric estimation, it is based on the frequency analysis or the impulse response of the system; and this method does not demand a reference model before identification [27, 82-84], which can be classified as black-box estimation. However, non-parametric estimation has to operate off-line after storing a lot of data. This research utilises parametric estimation techniques as shown in Figure 1.1 in the first chapter

[26]. Parametric estimation identifies the parameters of a given reference system model. This approach does not need to store a lot of data for building up a frequency response, so it can be used for on-line applications. In addition, due to the characteristics of on-line operations, this method can also be implemented into closed-loop circuits for adaptive control design, and can be further implemented into DSP for digital control design applications [81]. Due to knowledge of the system structure in advance, parametric estimation is always classified as white-box estimation.

There is a concern, which needs to be considered carefully for the DSP implementation. When a system has a higher order, particularly higher than the second-order, more parameters need to be identified (i.e. the parameters are the coefficient of the transfer function). In this case, additional computational burden is required, and careful consideration of the processor's computational ability is needed. In this research, as the power converters are all second-order systems, this will not be a problem. Figure 3.4 is a flowchart showing parametric estimation [27], while the parametric estimation of a DC-DC converter block diagram is shown in Figure 3.3.

Parametric identification contains four key steps. Before sampling the input and output data, it is important that a rich-frequency signal (e.g. white noise, coloured noise and PRBS) should be injected into the system as an input signal. PRBS, which is preferred for use in digital control systems, is chosen to be combined with the input (D) of the plant. The target of the second step is called 'signal pre-processing', which means filtering the input and output signal in order to remove unwanted noise. A proper filter or mean value calculation of the sampling data can help reduce the noise signal. The third step is to define the system structure and the order of the system. After the structure and order determination, we can figure out the dimensions of the weight vector and the regression vector. The fourth step is to select an adaptive algorithm and implement it to estimate the parameters of the model. The algorithm takes the sampled data to calculate a set of best-fit parameters to the actual model. If the error between measured data and the estimated output data is in an acceptable range, a best-fit estimated model will be constructed [27], which should be able to accurately describe the system dynamics response.

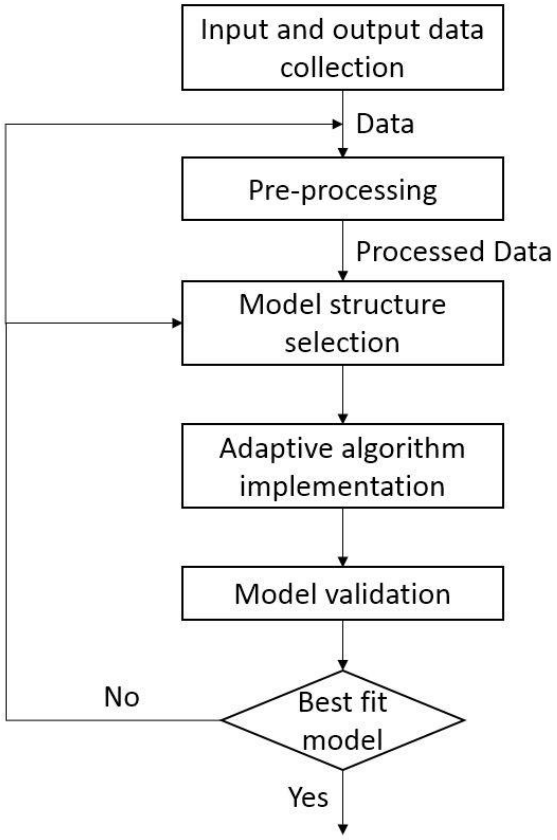

Figure 3.4 Flowchart of Parametric Estimation

3.5 System Identification Algorithms

When researching SI, the selection of algorithms is also very important. There are many adaptive algorithms which can be used for SI purpose (e.g. least mean squares, RLS, affine projections and Kalman filters) [26, 27, 85-89]. There are also some improved algorithms based on their conventional algorithms, such as the improved RLS algorithm of de-coupling RLS or exponential RLS. Many algorithms on power-converter SI applications are developed from signal processing adaptive filtering knowledge. There are some differences between each algorithm in several aspects, such as converging speed, accuracy and computational complexity. For adaptive control applications, each algorithm can contribute to a good control performance due to different required control approaches, such as improvement of system dynamics response or system stability [90, 91]. In this section, two algorithms will be presented: RLS and Fast Affine Projection. Also, in the simulation and practical experiment, two algorithms will also be used to realise the SI process.

From Figure 3.3, $d'(n)$ is a combination of the desired signal $d(n)$ and an excitation signal. Then it is injected to the operating system. The IIR Filter is updated at every time instance by the adaptation algorithm. The filter yields an estimated output with the same input data. Finally, the difference (error) will be reduced by the algorithm at every instance. This is the goal for the adaptive algorithm: trying to reduce the error closed to zero (or to an acceptable range). $d_r(n)$ is the desired signal, which is also the sampled output voltage $v_o(n)$. Then it comes out with the equations [92]:

$$\hat{y}(n) = \sum_{k=0}^{N} w_k u(n-k) = w^T u \tag{3.1}$$

$$\mathrm{w(n)} = [w_0 \quad w_1 \quad \cdots \quad w_N]^T \tag{3.2}$$

$$\mathrm{u(n)} = [u(n) \quad u(n-1) \quad \cdots \quad u(n-N)]^T \tag{3.3}$$

where, u(n) is the input data matrices sampled at each time instance. The filter weights w(n) will be updated by each sampled input data. An optimal set of parameters will be produced when w(n) tends to be stable. $\hat{y}(n)$ is the estimated output of the adaptive filter. Most algorithms are based on the same principle to reduce the prediction error, which is defined as [92]:

$$e_p(n) = d_r(n) - \hat{y}(n) = d_r(n) - \sum_{k=0}^{N} w_k u(n-k) = d_r(n) - w^T u\,(n) \tag{3.4}$$

In order to reduce the difference ($e_p(n)$) between desired value and estimated value, the SI algorithm needs to resolve a set of linear equations to estimate every new set of filter weight. The two algorithms, RLS and FAP, adopted in this experiment will be introduced in the next section.

3.5.1 Recursive Lease Squares (RLS) Algorithm

RLS is widely used due to its three good features, which are a fast convergence rate, good estimation accuracy and fast tracking ability [80]. However, besides its good quality of estimation, it also has a problem of a heavy computational burden (caused by matrix inversion operation-division operation). To reduce the computational complexity, the author in [93] suggests an approximation method for the matrix inversion operation. Generally, a matrix

inversion lemma algorithm will be used to remove this operation [92]. At every calculation, the adaptive algorithm sets out to solve the normal equations:

$$\boldsymbol{R}(i)\boldsymbol{w}(i) = \boldsymbol{\beta}(i) \tag{3.5}$$

Where $R(i)$ is the autocorrelation matrix and $\beta(i)$ is the cross-correlation vector:

$$\boldsymbol{R}(n) = \boldsymbol{R}(n-1) + \boldsymbol{u^T}(n)\boldsymbol{u}(n) \tag{3.6}$$

$$\boldsymbol{\beta}(n) = \boldsymbol{\beta}(n-1) + d(n)\boldsymbol{u}(n) \tag{3.7}$$

If solving equation (3.5) in a direct way, the complexity is found to be $\mathrm{O}(N^3)$ [94]. A classical way to address the problem is with the matrix inversion lemma algorithm, which is shown in Table 3.2. Where $\boldsymbol{P}(n) = \boldsymbol{R^{-1}}(n)$. $P(n)$ can be calculated in a recursive way with $\mathrm{O}(N^2)$ complexity [85]. λ is the forgetting factor. A large value of λ assigns greater importance to the most recent data. For conventional RLS, $\lambda = 1$.

Step	Equation
	Initialisation: $\widehat{\boldsymbol{w}} = 0,\ \boldsymbol{P}(0) = \frac{1}{\delta}\boldsymbol{I}_N$
	For n=1, 2, …
1	$\boldsymbol{S}(n) = \boldsymbol{P}(n-1)\boldsymbol{u}(n)$
2	$\boldsymbol{k}(n) = \dfrac{\boldsymbol{S}(n)}{\lambda + \boldsymbol{u^T}(\mathrm{n})\boldsymbol{S}(n)}$
3	$\boldsymbol{e}(n) = \boldsymbol{d_r}(n) - \boldsymbol{w^T}(n-1)\boldsymbol{u}(n)$
4	$\widehat{\boldsymbol{w}}(n) = \widehat{\boldsymbol{w}}(n-1) + \boldsymbol{k}(n)\boldsymbol{e}(n)$
5	$\boldsymbol{P}(n) = \dfrac{1}{\lambda}[\boldsymbol{P}(n-1) - \boldsymbol{k}(n)\boldsymbol{u}^T(\mathrm{n})\boldsymbol{P}(n-1)]$

Table 3.2 Matrix Inversion Lemma RLS Algorithm [95]

An alternative way to solve the normal equation (3.5), is to transform it into a series of auxiliary normal equations, which are shown in Table 3.3. The focus is transferred from solving the normal equation (3.5) to finding a solution $\Delta\widehat{w}(n)$ for the auxiliary equations by applying iterative techniques [87].

Step	Equation
	Initialisation: $\mathbf{r}(-1) = 0$, $\boldsymbol{\beta}(-1) = 0$, $\widehat{\boldsymbol{w}}(-1) = 0$
	For n=1, 2, …
1	Find $\Delta\boldsymbol{R}(n)$ and $\Delta\boldsymbol{\beta}(n)$
2	$\boldsymbol{\beta_0}(n) = \boldsymbol{r}(n-1) + \Delta\boldsymbol{\beta}(n) - \Delta\boldsymbol{R}(n)\widehat{\boldsymbol{w}}(n-1)$
3	Solve $\boldsymbol{R}(n)\Delta\boldsymbol{w} = \boldsymbol{\beta_0}(n) \Rightarrow \Delta\widehat{\boldsymbol{w}}(n)$, $\boldsymbol{r}(i)$
4	$\widehat{\boldsymbol{w}}(n) = \widehat{\boldsymbol{w}}(n-1) + \Delta\widehat{\boldsymbol{w}}(n)$

Table 3.3 Solving Auxiliary Equations by RLS [95]

The existing residual vector $r(n-1)$ in Table 3.3 considered the previous calculation accuracy. By using iterative techniques, the previous solution is equivalent to being initialised when resolving the original problem. Under the same requirement of accuracy of $w(n)$ this method is a simpler way to reduce the complexity.

3.5.2 Fast Affine Projection (AP) Algorithm

The FAP algorithm is developed from the AP algorithm. Both use the most recent sampling data as an approximation of the regression matrix $\{R_{du}, R_u\}$ in regularised Newton recursion. As with most of the other adaptive algorithms, the FAP algorithm recursively uses system data to calculate the current parameter matrix in the current step. However, the difference is that FAP defines a positive integer *K* to determine how many step values are to be used in the approximation. This feature provides a superior convergence speed, low computational cost

and decent accuracy compared with other classic adaptive algorithms. The regressor matrix is obtained as follows [89]:

$$\hat{R}_u = \frac{1}{K}\left(\sum_{j=i-K+1}^{i} u_j^* u_j \right) \tag{3.8}$$

$$\hat{R}_{du} = \frac{1}{K}\left(\sum_{j=i-K+1}^{i} d(i) u_j^* \right) \tag{3.9}$$

To approximate the terms in regularised Newton recursion, the FAP regressive form can be defined as equation (3.10):

$$\omega_i = \omega_{i-1} + \mu U_i^* \left(\varepsilon I + U_i U_i^* \right)^{-1} \left[d_i - U_i \omega_{i-1} \right] \tag{3.10}$$

In the table 3.4 as shown below, *K* is the size of regressor. *M* is the size of weight vector. The complexity table is generated by the number of multiplications and summations. This reflects the number of calculations for each step and in total.

Term	×	+
$u_i \omega_{i-2}$	M	$M-1$
$\left[u_i u_{i-1}^* \quad u_i u_{i-2}^* \quad \mathrm{L} \quad u_i u_{i-K}^* \right]$	KM	$K(M-1)$
$U_i \omega_{i-2} + \mu U_i U_{i-1}^* \left(\varepsilon I + U_{i-1} U_{i-1}^* \right)^{-1} \left[d_{i-1} - U_{i-1} \omega_{i-2} \right]$	K^2	K^2
$d_i - U_i \omega_{i-1}$		K
$U_i U_i^*$	M	$M-1$
$\varepsilon I + U_i U_i^*$		K
$\left(\varepsilon I + U_i U_i^* \right)^{-1}$	K^3	K^3
$\mu U_i^* \left(\varepsilon I + U_i U_i^* \right)^{-1} \left[d_i - U_i \omega_{i-1} \right]$	KM	$(K-1)M$
ω_i		M
Total per iteration	$K^3 + K^2 + (2K+2)M$	$K^3 + K^2 + (2M+1)K + 2M + 2$

Table 3.4 Complexity of FAP Algorithm

The error matrix in the FAP algorithm is a vector-valued estimation error, and contains previous steps results which can flexibly reflect all previous data to update the current error value. The integer K can be varied to maintain the algorithm accuracy in different noise-environments. Compared with that, most other classic adaptive algorithms (i.e. RLS and Least Mean Squares (LMS)) use a scalar-valued estimation error, only reflecting the current step. The computational cost is summarised as the amount of summation and multiplication for each step, and is listed above in Table 3.4 [89].

3.6 System Identification Input Signal

As SI technique has the requirement of optimal and continuous excitation signals for the input signal, in the application of the research, the input signal of duty cycle needs to be combined with a rich-frequency excitation signal. There are two popular excitation signals among the research [96-99], which are white noise and PRBS. A continuous excitation signal means that the identified system should be excited in order to present all its transient dynamic responses. Therefore, the basic requirement is that the input excitation signal should have a bigger frequency bandwidth than the identified system. The inverse scalar function of the Fisher information matrix is always regarded as the indicator function *J* for most of the optimal input signal design as below:

$$J = \emptyset(\boldsymbol{M}^{-1}) \tag{3.11}$$

Where **M** is the Fisher Information Matrix:

$$\boldsymbol{M} = \boldsymbol{E}_{\boldsymbol{y|h}}\left\{\left[\frac{\partial logp(\boldsymbol{Y}|\boldsymbol{h})}{\partial \boldsymbol{h}}\right]\left[\frac{\partial logp(\boldsymbol{Y}|\boldsymbol{h})}{\partial \boldsymbol{h}}\right]^{T}\right\} \tag{3.12}$$

Formally, the partial derivative with respect to $\boldsymbol{h}$ of the natural logarithm of the likelihood function is called the "score". Under certain regularity conditions, if $\boldsymbol{h}$ is the true parameter (i.e. $\boldsymbol{Y}$ is distributed as $f(\boldsymbol{Y};\ \boldsymbol{h})$, it can be shown that the expected value (the first moment) of the score is 0. Therefore, an optimal input excitation signal is to make the scalar function *J* to a minimum value. The scalar function ∅ can be treated as a metric function for the accuracy of SI. Two general criteria based on this are:

A- rules: $$\boldsymbol{J} = Tr(\boldsymbol{M}^{-1}) \tag{3.13}$$

D- rules: $$\boldsymbol{J} = \det(\boldsymbol{M}^{-1}) \tag{3.14}$$

For an example of a discrete single input and single output (SISO) system which has considered a noise signal shown as below:

$$\boldsymbol{y}(k) = b_1 u(k-1) + b_2 u(k-2) + \cdots + b_n u(k-n) + v(k) \tag{3.15}$$

After applying the rules above, we can get the equation:

$$\frac{1}{N}\sum_{k=1}^{N} \boldsymbol{u}(k-i)\boldsymbol{u}(k-j) = \begin{cases} 1 & i = j \\ 0 & i \neq j \end{cases} \tag{3.16}$$

Which means if the output of the system is an independent and identically distributed normal sequence, it fulfils the optimal design D- rules, and the autocorrelation of input signal has the impulse format.

White noise signal is a stable and random signal or process when power spectral density *S(w)* is a non-zero constant within the whole frequency range.

$$S(\omega) = \sigma^2, \qquad -\infty < \omega < \infty \tag{3.17}$$

The autocorrelation of the white noise signal is shown below:

$$\boldsymbol{R_x}(n) = E[\boldsymbol{x}(k)\boldsymbol{x}(k+n)] = \sigma^2\delta(n) \qquad n = 0, \pm 1, \pm 2, \ldots \tag{3.18}$$

Where $\boldsymbol{\delta}(n)$ is Kronecker sign: $\boldsymbol{\delta}(n) = \begin{cases} 1 & n = 0 \\ 0 & n \neq 0 \end{cases}$.

From equation (3.18), the white noise sequence satisfies the requirement and can be used as an optimal input excitation signal for the purpose of SI.

The PRBS signal is generated by multilevel linear feedback shift register. Binary means that the signal is only comprised of two logical values‘1’ and ‘0’.The one with the longest cycle is also named the M-sequence (Maximal Length Sequence). The process is shown in Figure 3.5:

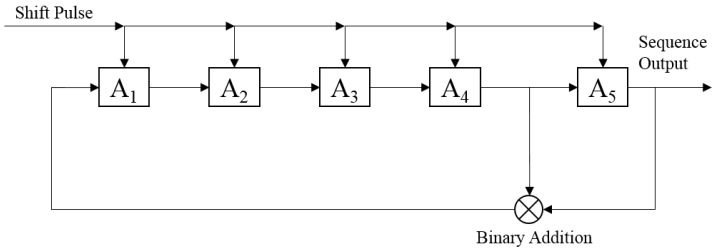

Figure 3.5 The structure of the PRBS process

A1, A2, A3, A4 and A5 are not all zeros. When a shift pulse is coming, the output of each register will become the input of the next level register. The output of the final level register is the PRBS signal. Its autocorrelation in discrete form is shown below:

$$\boldsymbol{R_{xx}}(\tau) = \frac{1}{N}\sum_{k=0}^{N-1} \boldsymbol{x}(k)\boldsymbol{x}(k+\tau) \tag{3.19}$$

Where N is the cycle of the M-sequence, and $N = 2^n - 1$. When $N \to \infty$, the autocorrelation of the M-sequence has the impulse format which satisfies the D- rule.

White noise and PRBS can both fulfil the purposes of the excitation signal for SI process. The M-sequence is similar to white noise, can be more easily applied in applications, and can also ensure a good identification accuracy. In this thesis, PRBS is adopted as the input excitation signal for SI.

3.7 Chapter Summary

In this chapter, different SI approaches have been introduced for simulation and experimental preparations. As the system model of SMPC is known in advance, and the task is to estimate the change of transfer function parameters, the SMPC SI in this research, therefore, belongs to a white-box parametric estimation approach.

Both RLS and FAP algorithms have been introduced along with their derivation steps. In order to make a convincing presentation of the results of the non-minimum phase parametric estimation, it was decided to apply the RLS algorithm in the experiment, since RLS is the most widely used adaptive algorithm in SMPC applications. Also, there is another key merit for choosing RLS, due to its more robustness compared to the FAP which will be shown in more detail by simulation in the next chapter. Additionally, two widely used identification-rich-frequency input signals have also been introduced in this section. Also, since PRBS is more suitable for digital system application, it will be used as the excitation input signal in the practical experiment.

In the next chapter, the performance of three SMPC parametric estimation and system parameters estimations will be presented in the simulation. The validity of the proposed solution to the parametric estimation of non-minimum phase converters will also be tested.

CHAPTER 4 PARAMETRIC ESTIMATION IN SIMULATION AND MODEL DISCUSSIONS

4.1 Introduction

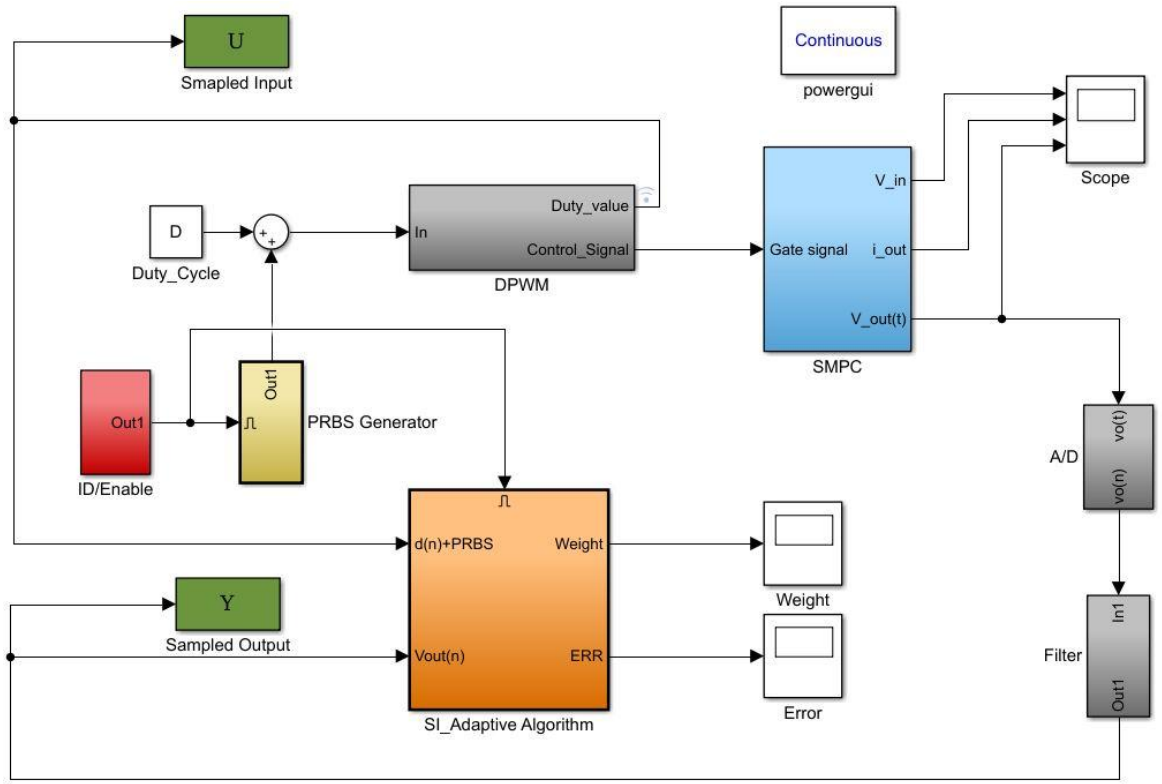

Figure 4.1 System Identification Block Diagram in Simulink

All simulation models are built and tested in Simulink. The block diagram of the parametric estimation of SMPCs in Simulink is shown in Figure 4.1. The blue block (SMPC) is the identified plant system. The grey block (DPWM) in the Simulink has the function of transferring the input signal duty cycle combined with PRBS to a PWM square-wave signal to drive the gate of the MOSFET in the SMPC blue block. The control signal of the DPWM block is a transformation signal from duty cycle to PWM signal. The name of DPWM also means transferring duty cycles to the PWM signal. The resolution of PWM should be at least on bit greater than ADC resolution to avoid the limit cycle oscillation phenomenon. This problem often arises in the digital control of SMPC during steady-state periods [100]. For the other two

grey blocks, A/D is an analogue to digital converter. There are two problems of practical design of ADC for DSP, namely resolution and sampling time. The resolution needs to be small enough to sense the output variation [101, 102]. The sampling frequency should be equal to or larger than the switching frequency, which is set to be the same as the switching frequency in the experiment. This is because each switching period will ensure the integrity of the data. The A/D and the filter are responsible for sampling the analogue output signal to a set of digital signals, for the pre-processing of the sampling output signal, and for removing unwanted noise. The ID/Enable block creates an enabled signal for the yellow block PRBS injection, and the orange block SI process, which behaves like a switch for the function of SI. When SI begins to work, the PRBS block will produce a rich-frequency signal simultaneously to excite the plant and the PRBS signal combined with duty cycle D is the input signal to the plant. The orange Adaptive SI adaptive algorithm block takes into the input and output signal of the SMPC and gives a best-fit estimated model parameters.

The percentage of estimation error can be used to evaluate the estimation results:

$$\mathrm{PE} = \frac{Real - Estimated}{Real} \times 100\% \tag{4.1}$$

The three sets of specifications of the three converters (buck, boost and buck-boost) have been determined as below. In the practical experiment, the buck SMPC and the boost SMPC use the same specifications as shown in the tables. The specifications of three SMPCs are listed in the following tables. Corresponding to equation (2.38), the four transfer function weights of each specification for both the averaged model and the TEOS model are presented following each converter specification in the table below.

Buck Converter:

Sampling Time (T_s)	5×10^{-5} s
Input Voltage (V_{in})	10 V
Output Voltage (V_{out})	3.3 V
Inductance (L)	220×10^{-6} μH
Inductor Impedance (R_L)	63 mΩ
Capacitance (C)	330 μf
Capacitor Impedance (R_c)	25 mΩ
Load Resistance (R_o)	3.3 Ω

Table 4.1 Buck SMPC Specifications

After the z-transformation of equation (2.12) by scripting in Matlab, the weights of averaged model can be achieved. The weights of TEOS model are calculated from equation (2.25).

Weights	Averaged	TEOS
a_1	-1.903	-1.914
a_2	0.9366	0.9485
b_1	0.05243	0.05682
b_2	0.2774	0.2901

Table 4.2 Buck SMPC Weights

Boost Converter:

Sampling Time (T_s)	5×10^{-5} s
Input Voltage (V_{in})	12 V
Output Voltage (V_{out})	20 V
Inductance (L)	680×10^{-6} μH
Inductor Impedance (R_L)	68 mΩ
Capacitance (C)	180 μf
Capacitor Impedance (R_c)	14 mΩ
Load Resistance (R_o)	6 Ω

Table 4.3 Boost SMPC Specifications

The weights of averaged model can be obtained from the z-transformation of equation (2.36). The TEOS model weights are calculated from the equation (2.48).

Weights	Averaged	TEOS
a_1	-1.948	-1.953
a_2	0.9548	0.9611
b_1	-0.8313	-1.255
b_2	0.975	1.512

Table 4.4 Boost SMPC Weights

Buck-boost Converter:

Sampling Time (T_s)	5×10^{-5} s
Input Voltage (V_{in})	10 V
Output Voltage (V_{out})	-14 V
Inductance (L)	840 μH
Inductor Impedance (R_L)	86 mΩ
Capacitance (C)	800 μf
Capacitor Impedance (R_c)	40 mΩ
Load Resistance (R_o)	4 Ω

Table 4.5 Buck-Boost SMPC Specifications

Weights	Averaged	TEOS
a_1	-1.9829	-1.9834
a_2	0.9835	0.9840
b_1	0.0010	0.4146
b_2	-0.0001	-0.4530

Table 4.6 Buck-Boost SMPC Weights

In this section, the three SMPCs (buck converter, boost converter, and buck-boost converter) is tested for parametric estimation in order to estimate their four model weights. All the converters are operating under CCM. In the first part, the performance of the RLS and FAP algorithms will be presented and compared. Then the performance of the three converters' on-line

parametric estimation is presented and compared for both the averaged modelling method and the proposed TEOS modelling method. Finally, the system parameters estimation results of load resistance and capacitance are presented. In the last part, the superiority of the proposed model for non-minimum phase system parametric estimation will be discussed and concluded from the results. All the results are based on the specifications above, and all the results in this section are simulation results. The experimental results will be presented in Chapter 6.

4.2 Open-Loop and Closed-Loop Performance

The performance of the system parametric estimation is compared for both open-loop and closed-loop situations in the simulation. This comparison is aimed to observe the effects of controller implementation on system parametric estimation. A boost converter with specifications from table 4.3 is adopted. The boost converter is controlled by a PI controller as shown in Figure 4.2.

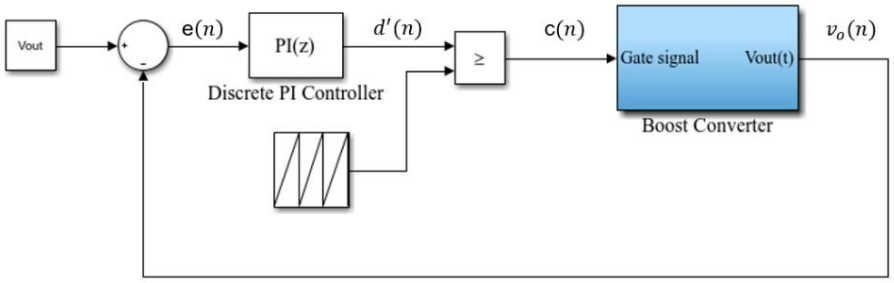

Figure 4.2 Boost Converter Closed Loop Block Diagram

The widely used Ziegler-Nichols method is used in the first step to obtain an initial set of controller gains [53, 103]. Following the rules of Ziegler-Nichols method, set gains of K_i and K_d to zero firstly and gradually increase K_p until the output response reaches a stable and consistent oscillations. Then, this K_p is named ultimate gain or critical gain K_u, at which, the period of oscillations is T_u. After tuning, K_u is found to be 0.0514 and T_u is 0.02 s as shown in Figure 4.3. The final gains of K_p and K_i can be obtained following the rules in the table 4.7.

Control Type	K_p	T_i	T_d
P	0.5Ku		
PI	0.45Ku	Tu/1.2	
PID	0.6Ku	Tu/2	Tu/8

Table 4.7 Ziegler-Nichols Table [103]

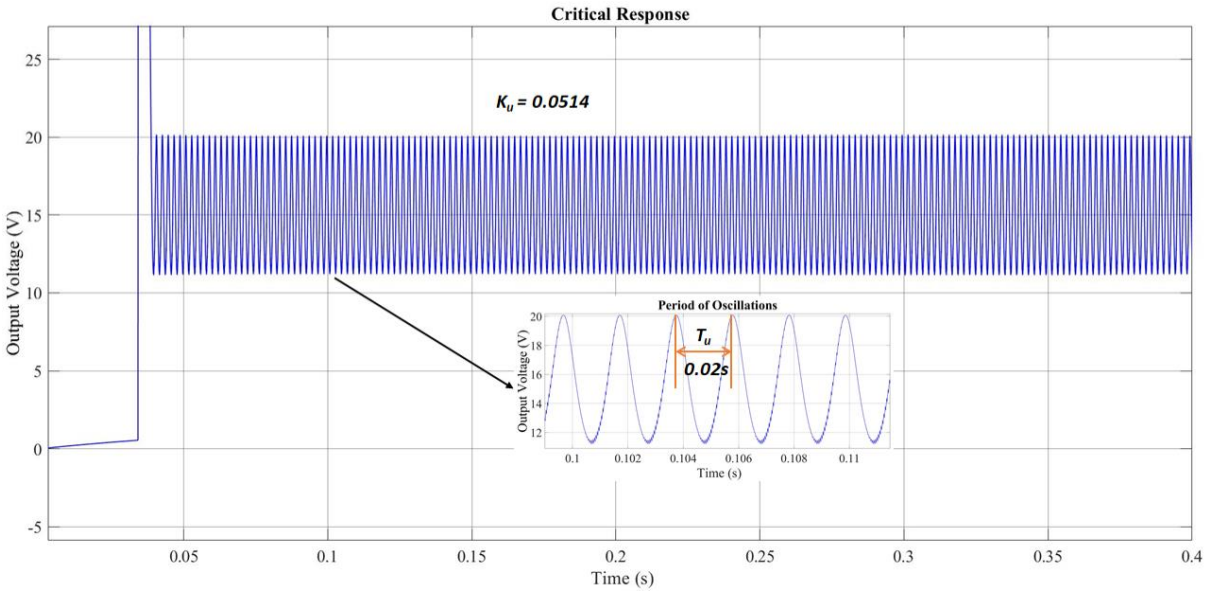

Figure 4.3 Output Voltage Critical Response

Therefore, the controller gains are determined as:

$$K_p = 0.45 \times K_u = 0.45 \times 0.0514 = 0.02313$$

$$K_i = \frac{K_p}{T_i} = 1.2 \times 0.45 \times \frac{K_u}{T_u} = 1.2 \times 0.45 \times \frac{0.0514}{0.02} = 1.3878 \qquad (4.2)$$

With the calculated gains in equation (4.2), the output voltage response is given in Figure 4.4.

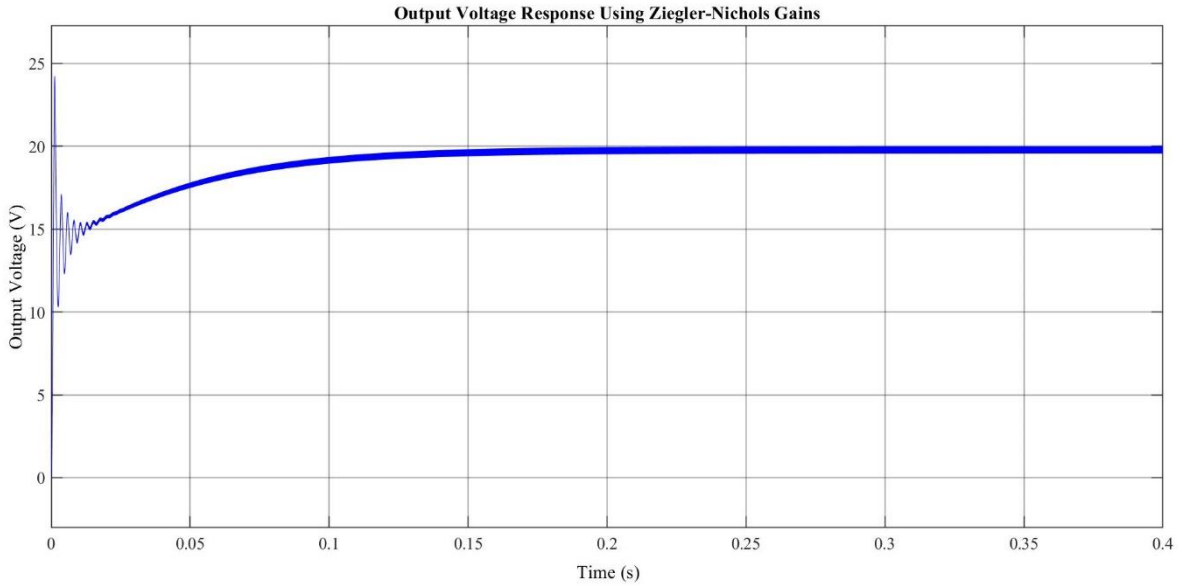

Figure 4.4 Output Voltage Response using Ziegler-Nichols Gains

From the results as shown in Figure 4.4, the output voltage achieved a reasonably good response. However, the overshoot in the first step response was big shooting up to 24V which is much

higher than the steady-state 20V. Ziegler-Nichols method can give a good start where it needs a bit more manual adjustment to reach an optimal control performance. Based on the principle to achieve a small overshoot, fast response and no steady-state error, the final controller gains after adjustment are K_p = 0.0001 and K_i = 1.

Figure 4.5 combines the open-loop with final tuned close-loop output voltage response. The overshoot voltage is controlled from 28 V for open-loop to 19 V for closed-loop. The system was operated for 0.4 s, and it takes 0.15 s to reach its steady state. Therefore, PRBS signal is injected from 0.25 s when the system response is stable. The injected signal can be observed as the effect of small oscillations in the Figure 4.5 during a period (from 0.25 s to 0.4 s).

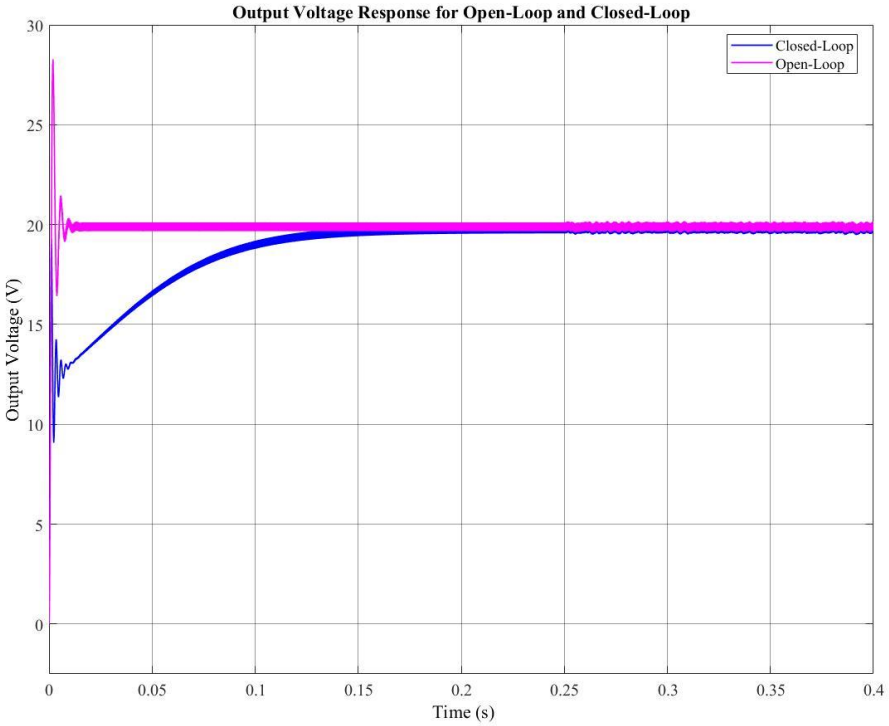

Figure 4.5 Output Voltage Response for Open-Loop and Closed-Loop

Figure 4.6 and 4.7 present the performance of parametric estimation in both open-loop and closed-loop respectively. RLS algorithm is applied as the adaptive algorithm for the SI purpose from 0.25 s. Four transfer function parameters are estimated.

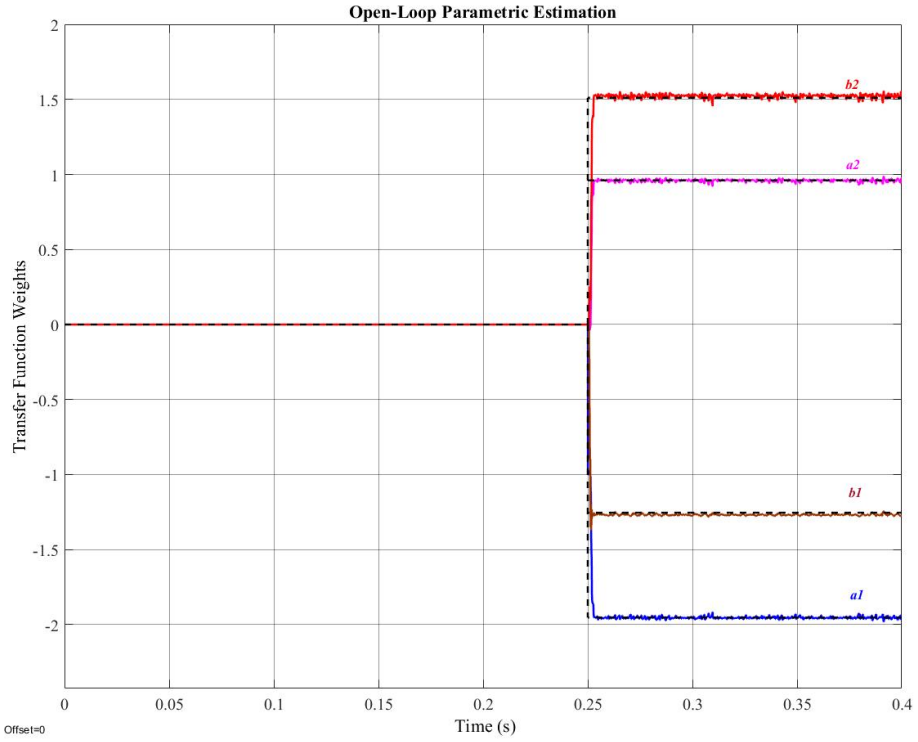

Figure 4.6 Open-Loop Parametric Estimation

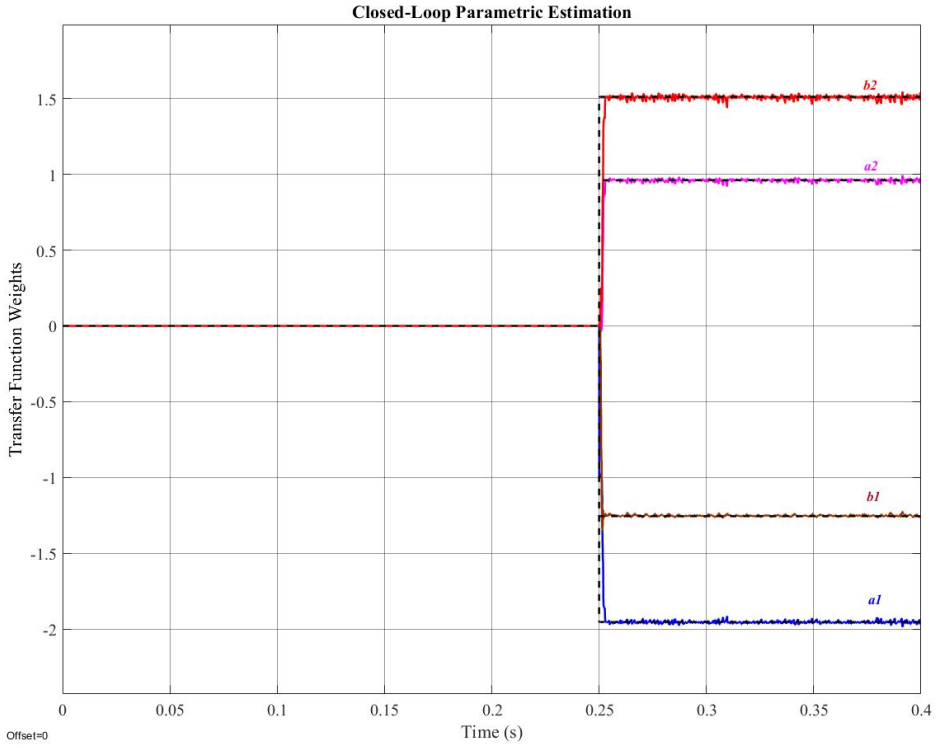

Figure 4.7 Closed-Loop Parametric Estimation

From the results in Figure 4.6 and 4.7, it can be observed that the parametric estimation for both open-loop and closed-loop is accurate. b_1 has a 0.01 weight estimation difference (-1.26 for open-loop and -1.27 for closed-loop). It is hard to recognize more differences from the results. Therefore, in the following tests and experiments, to make it clearer for verifying the proposed

parametric estimation solution to non-minimum phase converters, all the systems will be based on the open-loop performance.

4.3 RLS & FAP Performance Comparison

The FAP algorithm is tested for the identification process in this research due to its fast convergence speed. Therefore, in this part, a comparison of performance between the two adaptive algorithms of RLS and FAP will be provided via their estimation performances. Based on the comparison result, the reasons why to choose RLS is presented. As different converters and different modelling methods do not influence the performance of parametric estimation techniques (such as estimation speed, accuracy and robustness), however, to make the results comparable, the buck converter and the commonly used averaged model are chosen here for the comparison test. When we apply the two adaptive algorithms on the same buck converter, whose specifications are highlighted in Table 4.1, the two weighted estimation performances are depicted in one figure, as shown below. The identification process is enabled at 0.01 s.

The same PRBS signal with the magnitude of 0.0035 is applied as the excitation signal to the input of the converter. The four black dashed lines in Figure 4.8 are the real model weights values which are also presented in values in Table 4.2, and the solid lines are the estimated weights as calculated by the two algorithms. The blue line is the estimation result by the RLS algorithm, and the pink line is by the FAP algorithm. From the result in Figure 4.8, it can be observed is the steady-state estimation results are sitting on the dashed lines, which means that the estimation results of both adaptive algorithms are very accurate. It is also clear that the pink line of all four weight estimations is about 0.001 s faster in converging to the final value than the blue line, which means that, given the same conditions, the FAP algorithm has a faster convergence speed than the RLS algorithm. Figure 4.9 shows that both algorithms have a very small estimation error that is less than 0.1% reading from the graph; which indicates that they can both correctly describe the characteristics of the system. The estimation error is the calculated difference between the actual output and the estimated output signals. The difference between those two errors can barely be observed.

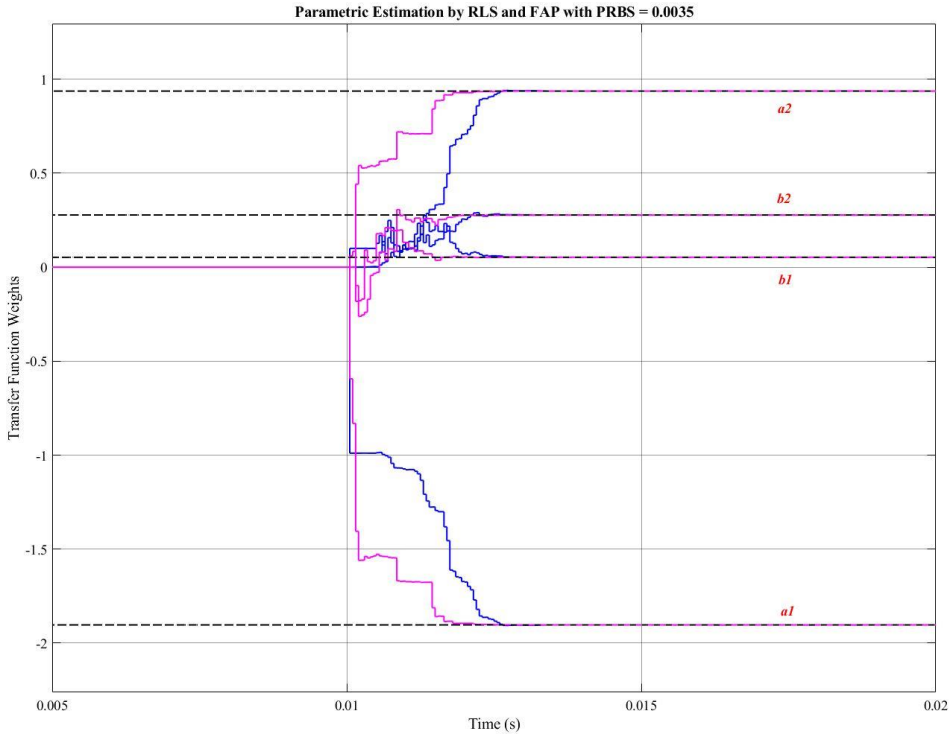

Figure 4.8 Parametric Estimation Results of both RLS and FAP Algorithms

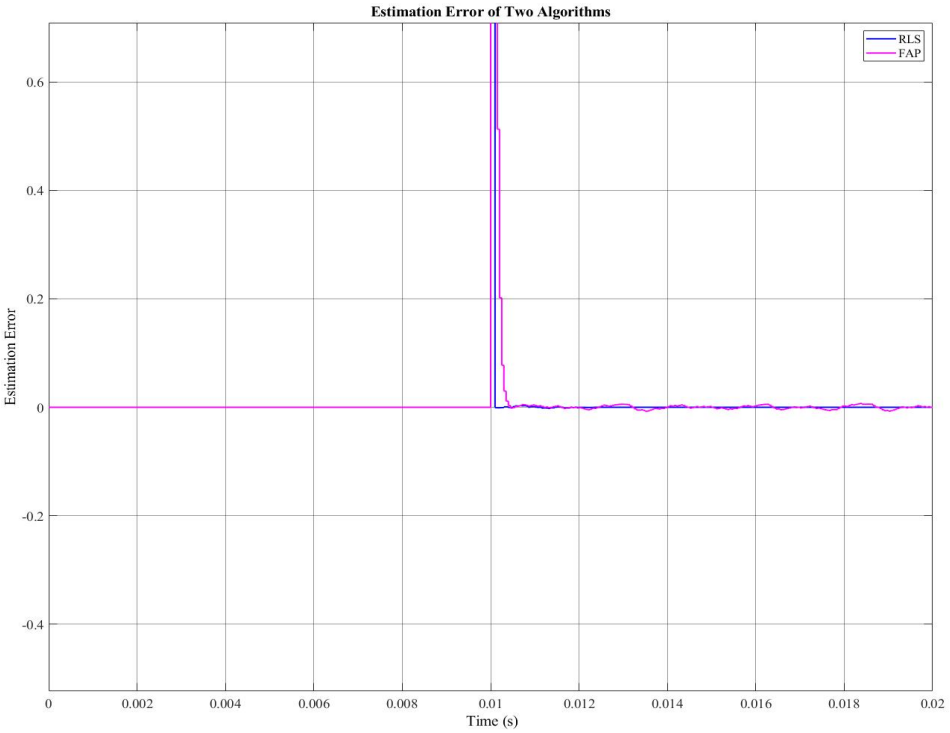

Figure 4.9 Estimation Error of Two Algorithms when PRBS = 0.0035

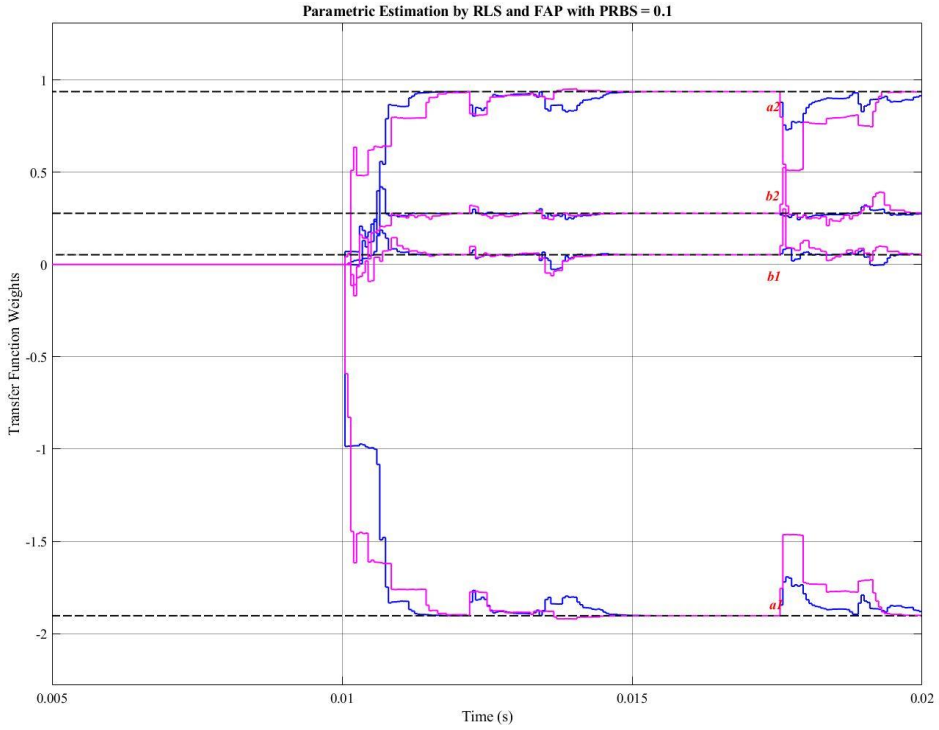

Figure 4.10 Parametric Estimation Results with PRBS = 0.1

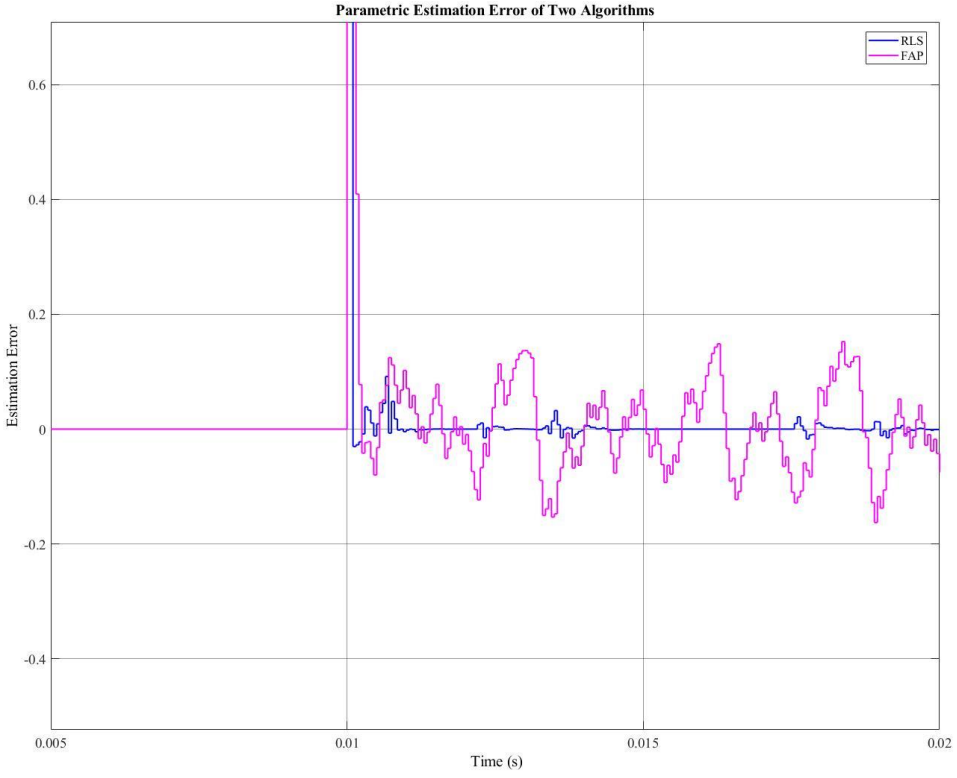

Figure 4.11 Parametric Estimation Error of Two Algorithms when PRBS = 0.1

Next, the PRBS signal is set to have a magnitude of 0.1 and the result is presented in Figure 4.10. The identification process is enabled at 0.01 s for both estimations. From the result, the estimation keeps oscillating through the whole period. It can be concluded that PRBS 0.1 signal cannot present all its transient dynamic responses of the identified system for SI to catch. Another observation from the result is that FAP responds faster but the RLS converges faster to the final steady-state value. The RLS estimation also has fewer oscillations than the FAP estimation as RLS has considered all previous data in calculation rather than FAP only considering the recent data instead of all previous data. Consequently, it shows that the performance of the RLS algorithm is more robust compared to the performance of the FAP algorithm. As PRBS is a random rich-frequency signal, which can represent a noise signal in a practical situation, another point can be found from the results is that the RLS has more immunity to the noise.

From Figure 4.11, two estimation errors are oscillating around zero with a value less than 0.2 which means 0.2 V difference between the estimated output and the actual output, but it is obvious that the estimation error of FAP is much bigger than that of RLS. From the two figures above, it can also be found that if it is close to an ideal condition with little noise, then the FAP algorithm will give a better performance than RLS, with a faster convergence speed. However, if it is not in an ideal condition, in which situation with a big noise, then RLS will be a better choice as it has a more robust performance. In the following content, the RLS algorithm will be mainly adopted for the identification process for two reasons. The first is that RLS can have more robustness in the practical experiment environment while the second reason is due to the greater popularity of the RLS algorithm, which can make the superiority of the proposed model more convincing in the application of non-minimum phase converter SI.

4.4 Parametric Estimation Simulation Results of Both Models Comparison

4.4.1 Buck Converter Parametric Estimation

In this sub-section, the parametric estimation of both the averaged model and the TEOS model are tested on the buck converter. As a buck converter is a minimum-phase converter, it does not have an RHP-zero in its transfer function. However, the TEOS model is still worthy to be tested on the buck converter in order to test the validity of the model on the application of minimum-phase SI. Therefore, the RLS algorithm is applied to the buck converter to estimate its model parameters on-line. Theoretically, if the modelling method can accurately describe the dynamic

characteristics of the buck converter system, the estimated parameters should be the same as the weights calculated from the modelling method. In addition, different modelling methods do not affect the identification speed as this is mainly controlled by different chosen identification algorithms. Thus, for the comparison of the two models, the estimation accuracy is the key point that needs to be analysed. The buck converter simulation results of both models are shown below. The magnitude of the PRBS signal is set to be 0.0035.

It can be observed from the results in Figure 4.12 that the weights identification speed is about 0.003 s, the same as presented in the previous part. Again, there are two kinds of dashed lines. The four red ones are the weights calculated from the TEOS model, while the four black dashed lines are calculated by the averaged model. The four estimated weights are labelled. It is obvious that the four estimated parameters are almost coinciding with the averaged model weights. However, for the TEOS model the estimation of parameters a_1 and a_2 has a small estimation error, which is within 0.5%. Once we get the four estimated weights, they can then be put into the transfer function, as shown in equation (2.38) to further estimate the output voltage, as the equation is output to the duty-cycle transfer function. The output voltage estimation error is depicted in Figure 4.13. The estimation error is the difference between the real sampled output voltage and the estimated output voltage calculated from the estimated weights, which is an index to check whether the estimated weights can correctly describe the dynamic response of the system.

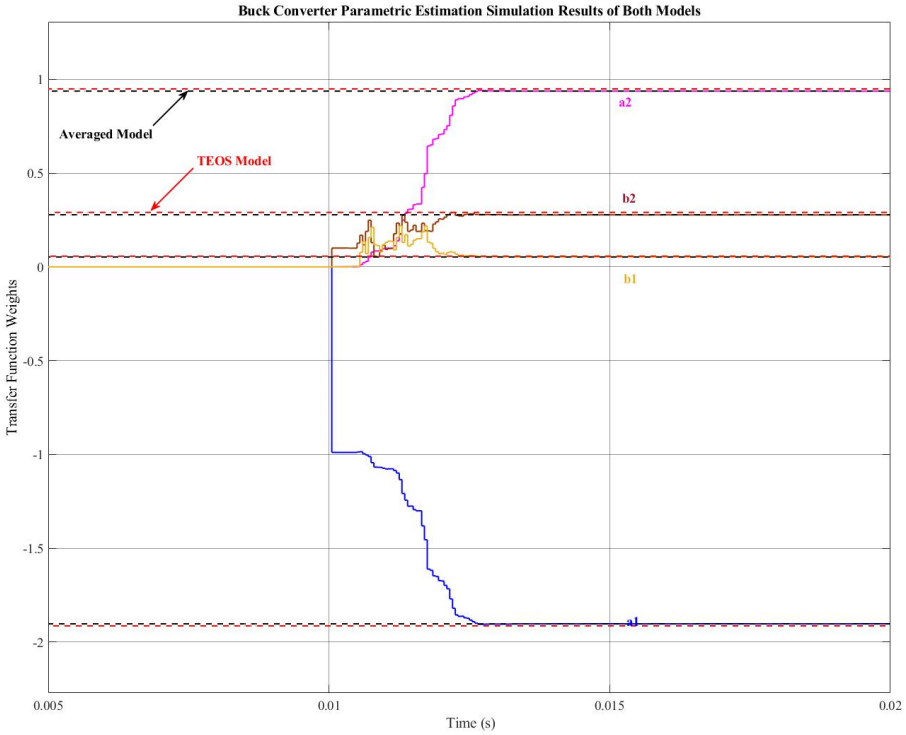

Figure 4.12 Buck Converter Parametric Estimation Simulation Results of Both Models

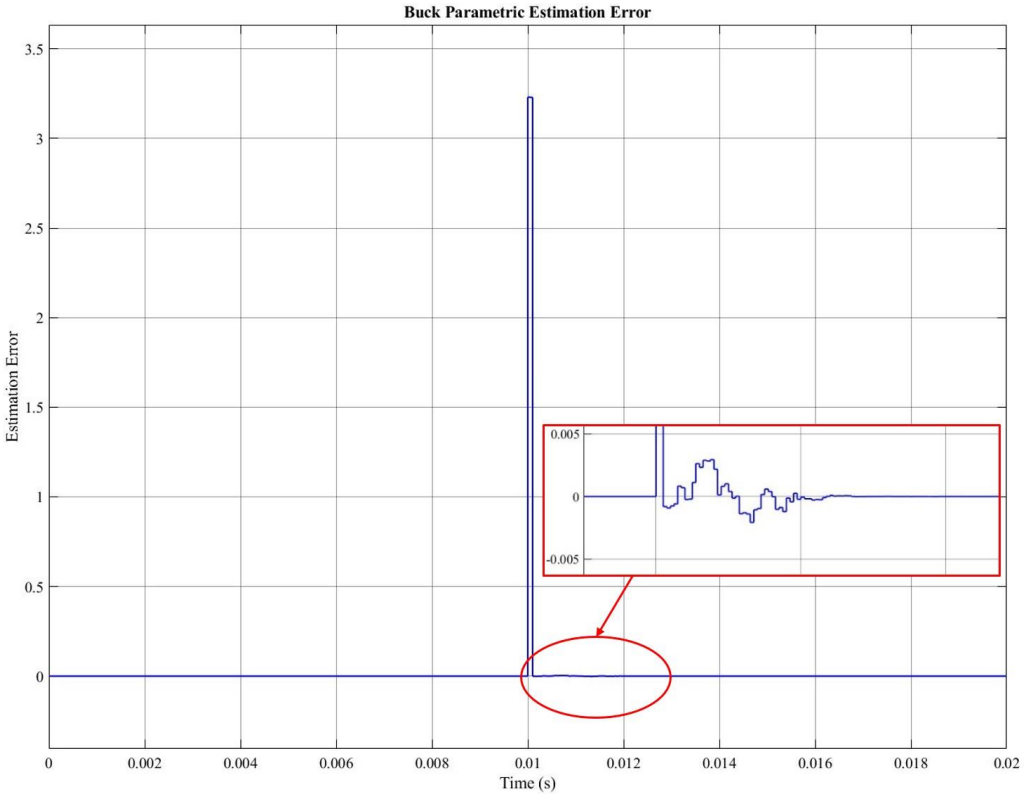

Figure 4.13 Buck Converter Parametric Estimation Error

From figure 4.13, it can be observed that the final estimation error is 0.003 which means a difference of 0.003 V between the estimated output voltage and the actual output voltage. It can also be evidenced that the adaptive algorithm RLS works well for the parametric estimation process, as the estimated weights can correctly describe the dynamic response of the system. Therefore, the weights a_1 and a_2 estimation error problem in Figure 4.12 is not caused by the algorithm. Apart from that, it can be found that there is a reason behind the cause of the weight estimation error problem. It is because that the derivation of the TEOS model has approximation steps when calculating X_i from equation (2.21), and the exponential to discrete-time approximation equation. The TEOS model used here is equation (2.24) including the term R_c. However, this estimation error can be accepted, to some extent, as it is within the range of 1.5%.

The simulation results in this part verify that both the proposed TEOS model and the averaged model can work well for the parametric estimation of minimum-phase buck converter systems. Additionally, if the error within 1.5% can be accepted, the two models can both correctly describe the dynamic response of the minimum-phase buck converter. However, the averaged model has a slightly higher accuracy than the TEOS model on the buck converter.

4.4.2 Boost Converter Parametric Estimation

In this sub-section, the parametric estimation of the two models is tested on the boost converter. The boost converter is a classic non-minimum phase converter system, which has the RHP-zero effect on its output voltage as explained earlier in Figure 2.7. Therefore, as discussed in the previous sections, there is an expectation for the simulation results that the estimation results can fit the TEOS model weights correctly but cannot correctly fit the averaged model weights. The magnitude of the PRBS signal is set to be 0.0025, which is tuned manually for an optimal estimation performance. The on-line estimation results in the simulation are shown below.

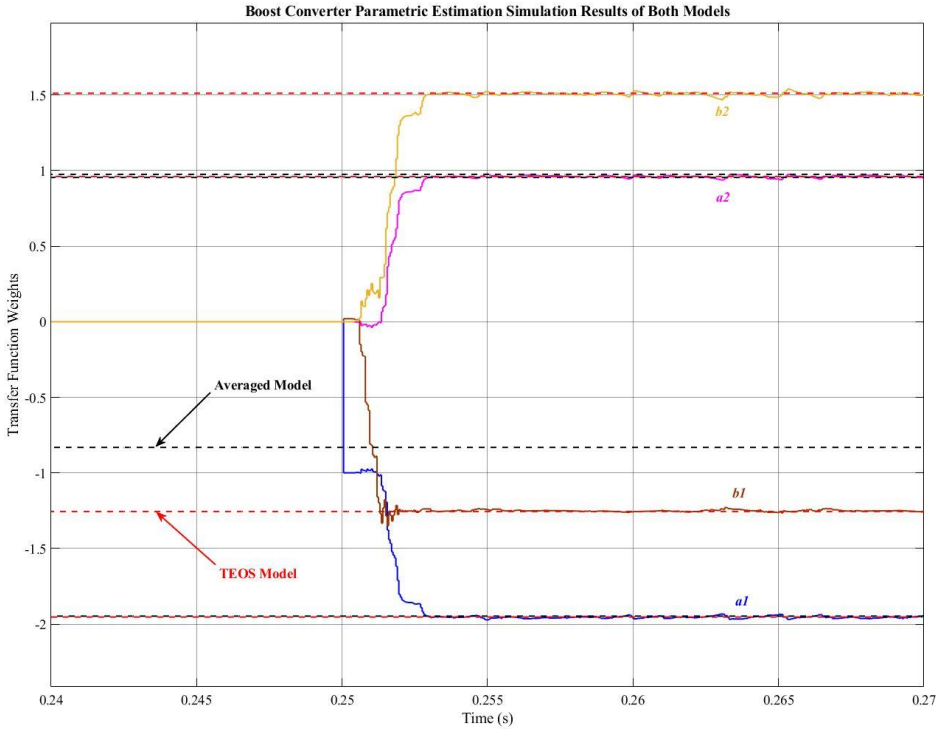

Figure 4.14 Boost Converter Parametric Estimation Simulation Results of Both Models

The results shown in Figure 4.14 show that it has verified the expectation. The denominator weights a_1 and a_2 calculated from both models are almost the same, as it can barely present any difference on the graph. However, the numerator weights, b_1 and b_2, have a big difference. After the identification process is enabled at 0.25s, the four estimated weights have taken 0.003s to revert to the final steady-state value, which is the same estimation speed as that with the buck converter, which is also evidence that the estimation speed will not be influenced by changing to another plant system. However, from the results it is obvious that the two numerator estimated weights are sitting at the TEOS model weights and are far away from the averaged model weights. From the boost simulation result, it has proven that the TEOS model weights are more of a fit to the estimation results than the averaged model. However, this does not mean that the TEOS model can better describe the system dynamics response because in the previous sections, there were discussions that the SI is misled by the RHP-zero effect, and using the TEOS model can help to ignore the effect of RHP-zero to a maximum degree. Therefore, the estimated weights can fit to the model weights perfectly, which has also verified the validity of the proposed theory behind the non-minimum phase converter parametric estimation problem.

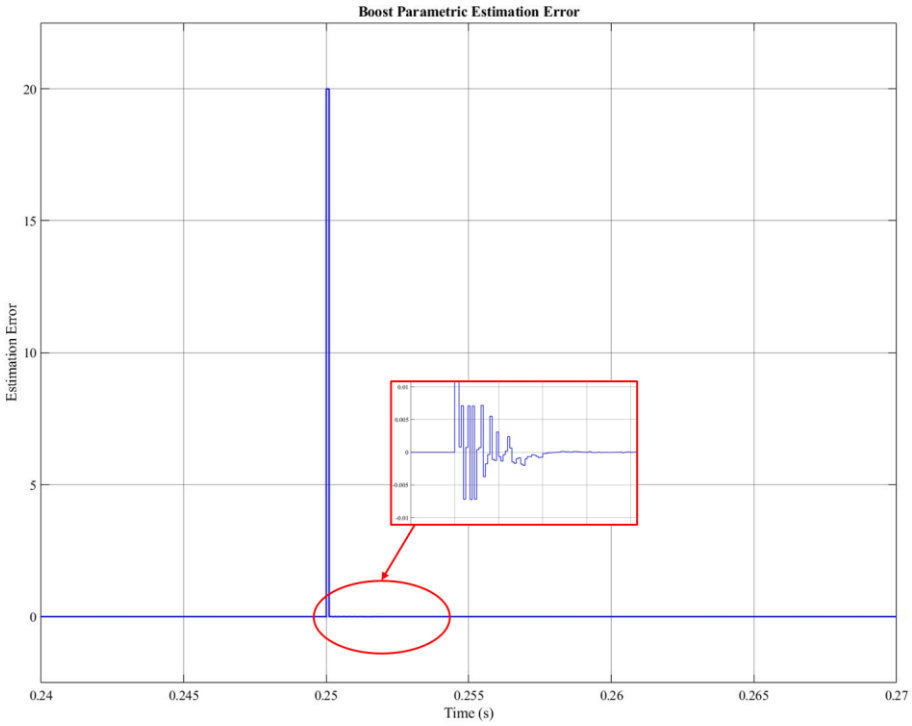

Figure 4.15 Boost Converter Parametric Estimation Error

From Figure 4.15, it also presenting a small voltage estimation error less than 0.007 V. Many control methods of the boost converter are able to combine SI techniques to improve control performance, as the author in [104] suggests that his method is better combined with SI technique and an Improved Time Optimal Control (ITOC) scheme.

4.4.3 Buck-Boost Converter Parametric Estimation

In order to further verify the validity of the TEOS modelling method on other non-minimum phase DC-DC converters, another classic non-minimum phase converter, the buck-boost converter, is chosen to be tested using the same steps as shown in the previous sub-section. The specifications are presented in Table 4.5., the magnitude of PRBS is set to be 0.0035., and the simulation results are presented below.

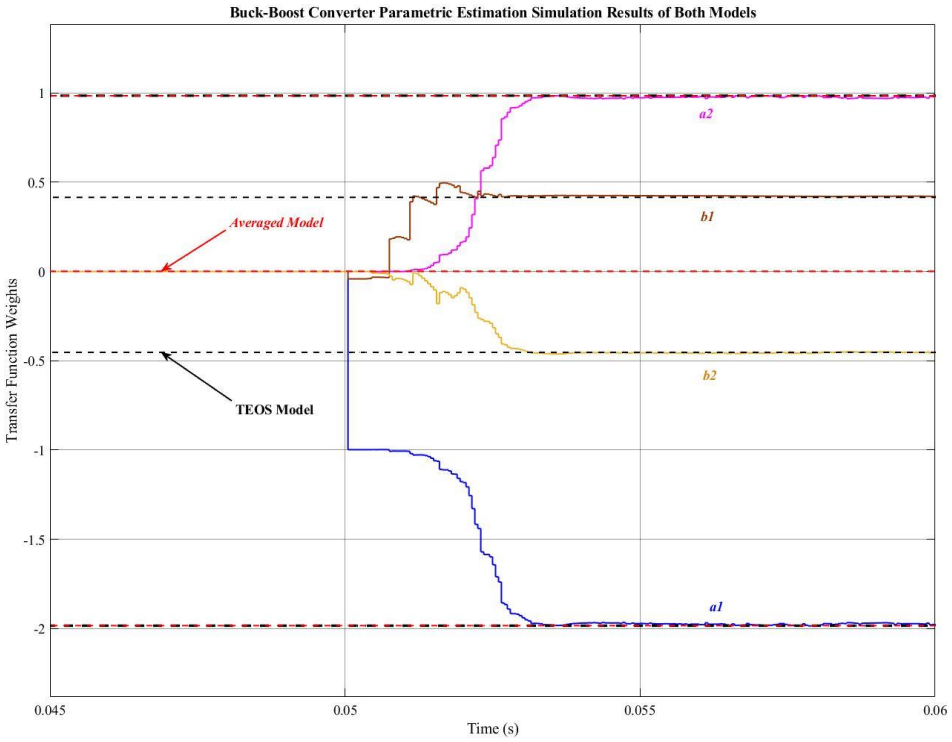

Figure 4.16 Buck-Boost Converter Parametric Estimation Simulation Results of Both Models

From Figure 4.16, after the estimation process is enabled at 0.05 s, it takes 0.03 s to reach a steady-state value. The four estimated parameters of the buck-boost converter are almost collapsing with the TEOS model weights but are not a fit to the averaged model weights of b_1 and b_2. As the capacitor and inductor impedance has been considered, the TEOS model can considered to be more accurate.

The buck-boost converter estimation error in Figure 4.17 also shows a small error to ensure that the algorithm works fine to estimate the dynamic characteristics of the system. Above all, it can be concluded that the TEOS model is suitable for the parametric estimation of boost converters and buck-boost converters, and it also has the potential to be adapted to any other non-minimum phase converters. There are many control methods which are better to combine with parametric estimation technique to improve control performance, as the author in [104] suggests that the control method he adopted (ITOC) is better combined with the parametric estimation technique.

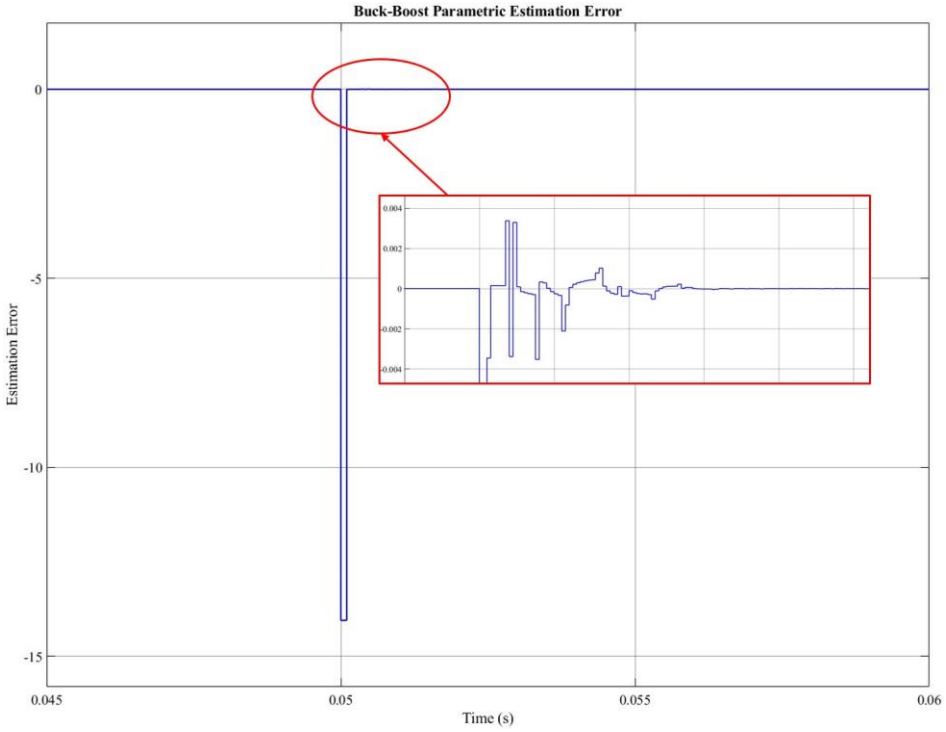

Figure 4.17 Buck-Boost Converter Parametric Estimation Error

4.5 On-line System Parameters Estimation

The TEOS model is a discrete form transfer function, which show a clear relationship of each system parameter inside a converter circuit. The averaged model is either in a state-space form or a continuous form transfer function. After z-transformation by scripting in Matlab® or other software, it cannot present a clear relationship between each system parameter. Therefore, when using the TEOS model, and once the correct set of estimated weights are determined, the system parameters of capacitance, load resistance or the inductance inside the converter circuit can then be estimated. There are two parameters which are widely monitored. One is the load resistance, as load change is a common seeing situation; while the other one is capacitance in a circuit, which can easily have faulty conditions. In this research, load resistance and capacitance are the two key system parameters that will be estimated; and the inductance is assumed to be known in advance and will not change. In order to test the TEOS model relationships and to further check the validity of the model simplification steps, buck converters and boost converters are chosen to conduct the experiment for on-line system parameter estimation. The specifications of both converters remain the same, as shown in the tables in Section 4.1, and have not changed.

4.5.1 Buck Converter

As discussed in Section 2.5, for a buck converter, the system parameters are better estimated from the transfer function denominator weights a_1 and a_2, since the two equations in equation (2.45) have R_o and C in each equation, and thus each of them can be cancelled out respectively in order to give a better accuracy. The estimation process is enabled at 0.01 s and the results are shown below.

Both results in Figure 4.18 and 4.19 took 0.003 s to settle at a steady-state value; and both of the results' estimation error shown above are within a range of 3%. The error might be accepted depending on different requirements. However, for general applications, this error is small enough, in that it is smaller than 5%. It can be concluded from the two simulation results above that system parameters can be estimated from the denominator weights a_1 and a_2 in the simulation. Apart from the estimation from the denominator weights, the numerator weights b_1 and b_2 are also estimated. The results are shown in Figure 4.20 and 4.21.

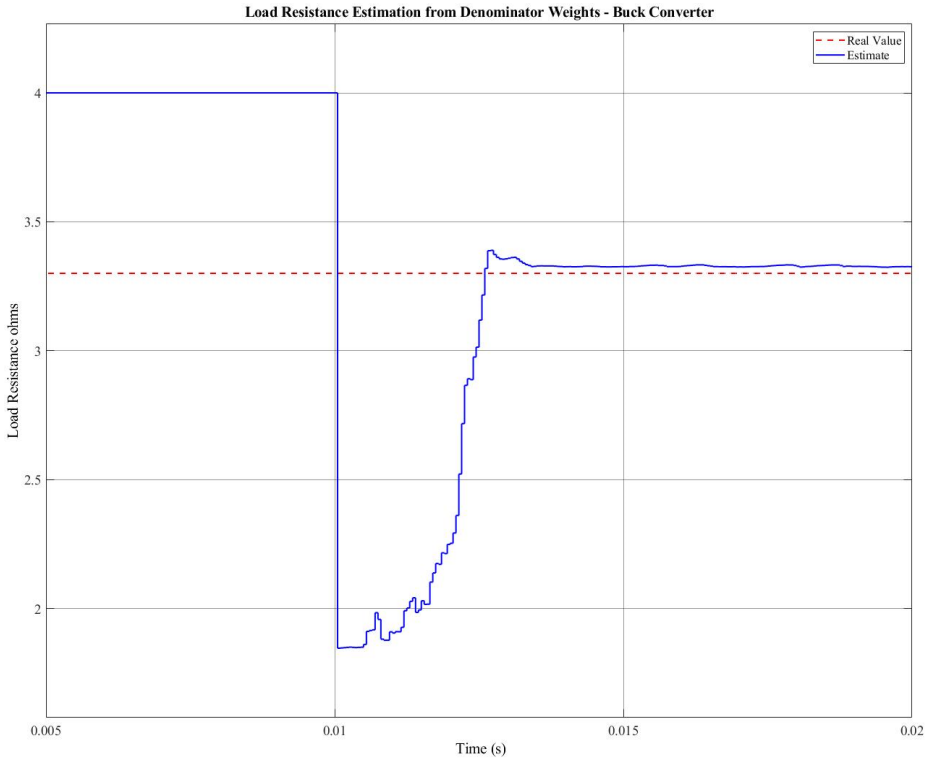

Figure 4.18 Load Resistance Estimation from Denominator Weights - Buck Converter

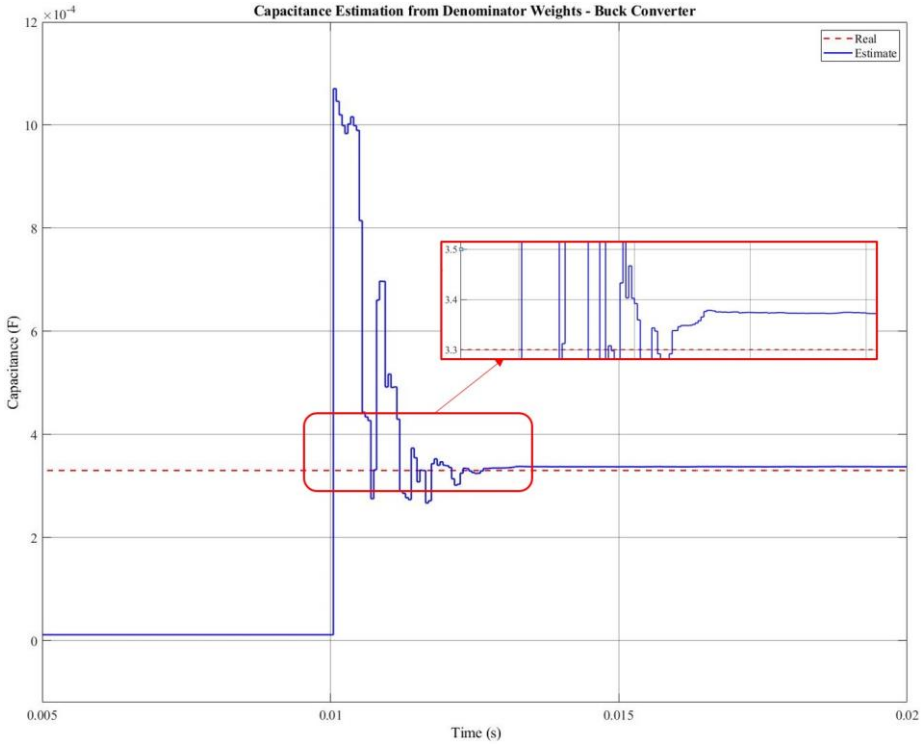

Figure 4.19 Capacitance Estimation from Denominator Weights - Buck Converter

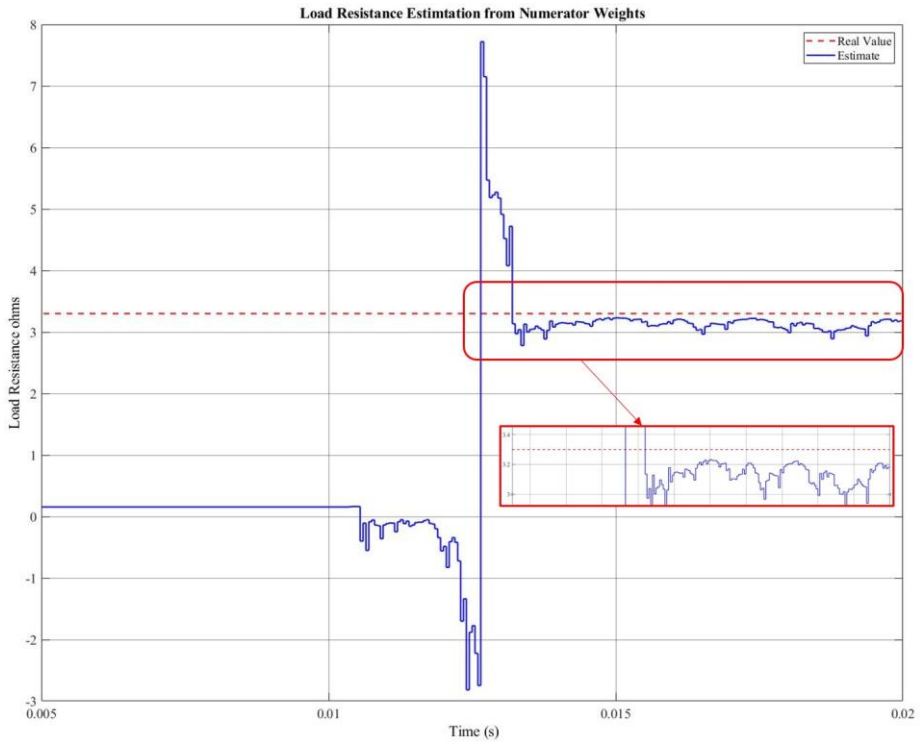

Figure 4.20 Load Resistance Estimation from Numerator Weights - Buck Converter

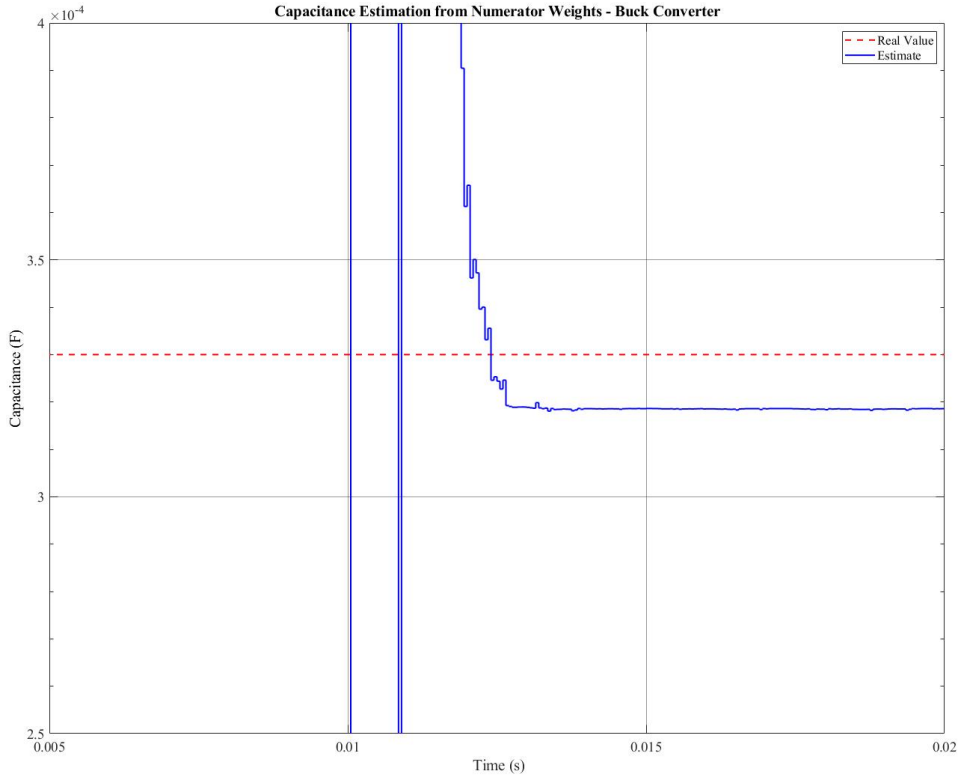

Figure 4.21 Capacitance Estimation from Numerator Weights - Buck Converter

As the result shows in Figure 4.20, the load estimation shows more oscillations than were estimated from the denominator weights, which is due to a more complex computation from equation (2.52). However, the estimation error can still be within 5%. But for the capacitance estimation in Figure 4.21, the estimation error is within 3%. Therefore, it can be concluded that system parameter estimation from both pairs of weights can work well in the simulation.

4.5.2 Boost Converter

For the boost converter estimation, both the R_o and C estimations are tested from both sides of its equation. Firstly, the two estimation results from numerator side are shown in Figure 4.22 and 4.23.

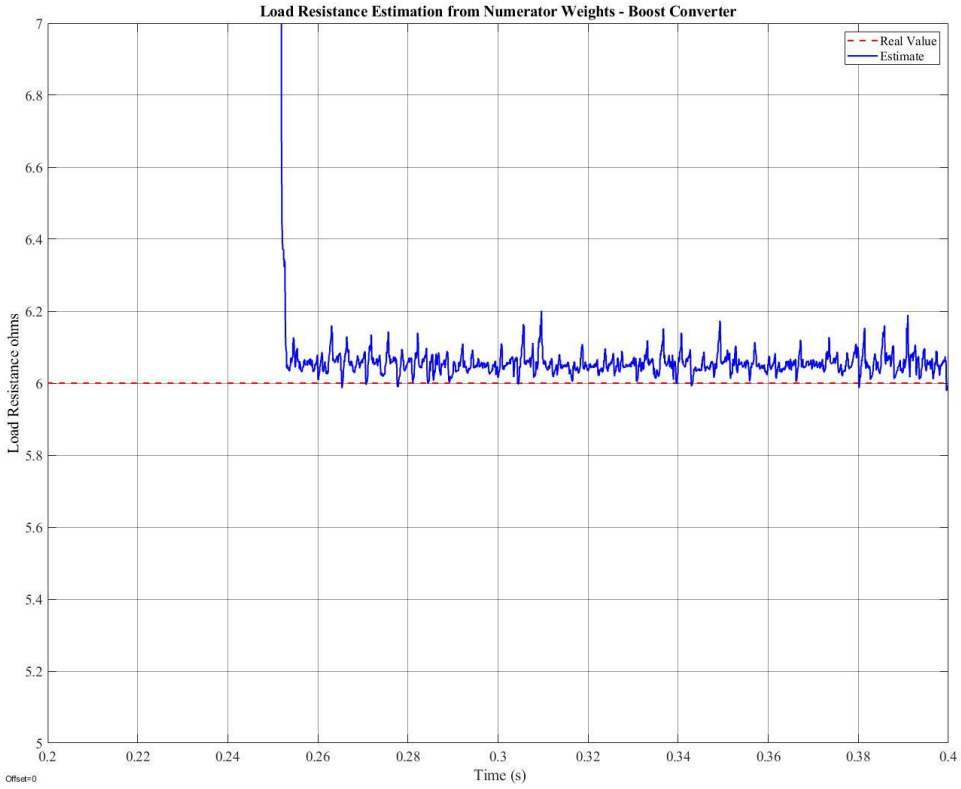

Figure 4.22 Load Resistance Estimation from Numerator Weights - Boost Converter

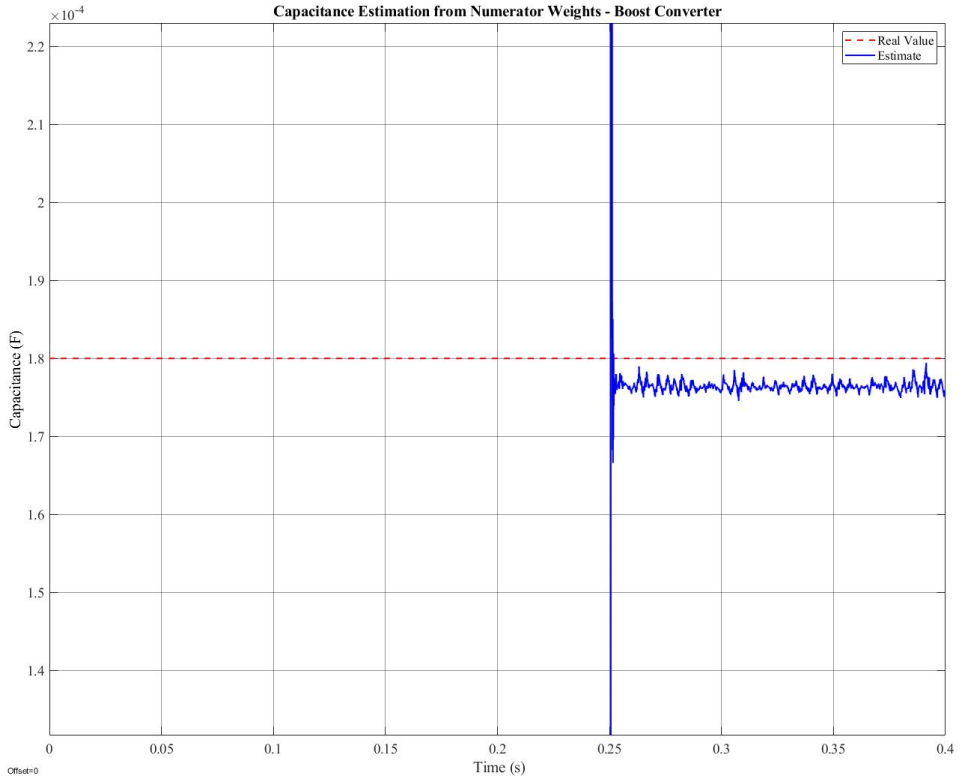

Figure 4.23 Capacitance Estimation from Numerator Weights - Boost Converter

The load resistance estimation result in Figure 4.22 presents an estimation accuracy within a 2% range of error, which is still a small estimation error as it is less than 5%. However, the capacitance estimation in Figure 4.23 has shown an estimation error within the range of 3%. This raises the possibility that the small magnitude of capacitance is more sensitive to being estimated. Another reason could also be due to its complex form of calculation from equation (2.53). Then the estimation is tested from the denominator pair of weights (a_1 and a_2).

The load estimation in Figure 4.24 has shown very big oscillations, which will barely be able to give an accurate value. Therefore, it was decided to filter the high-frequency noise in order to stabilise the estimation result. A low-pass filter $\frac{100}{s+100}$ with a cut-off frequency of 16 Hz was added to filter the response. The result, after adding the filter, is shown in Figure 4.25 whose estimation error is now within 3%.

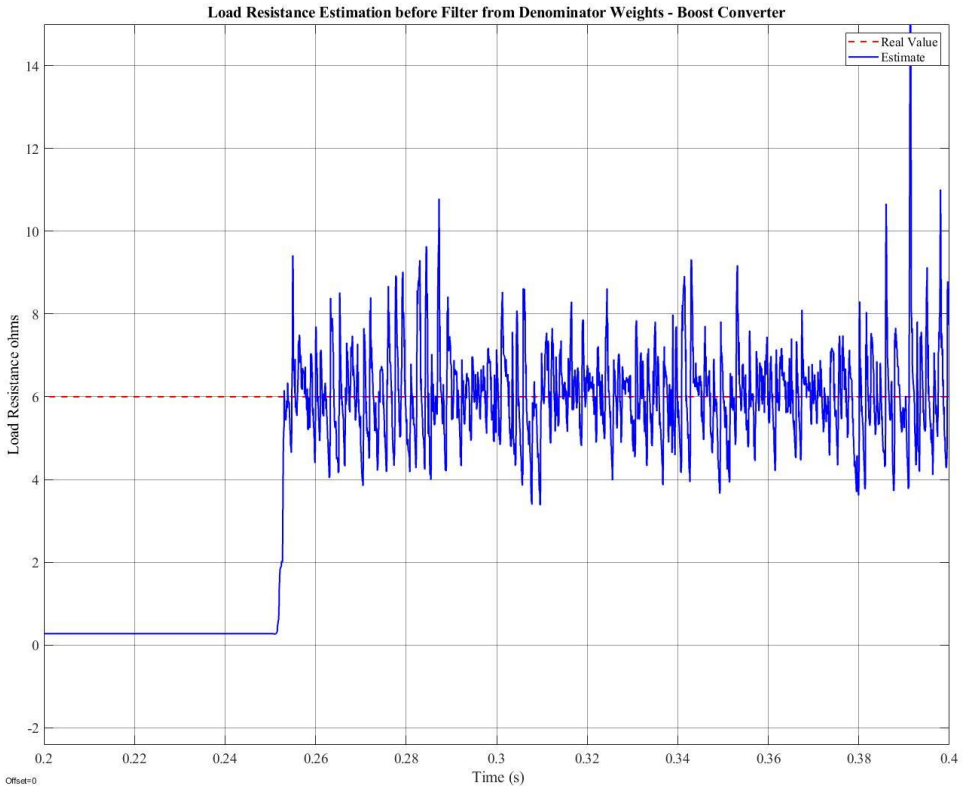

Figure 4.24 Load Resistance Estimation from Denominator Weights - Boost Converter

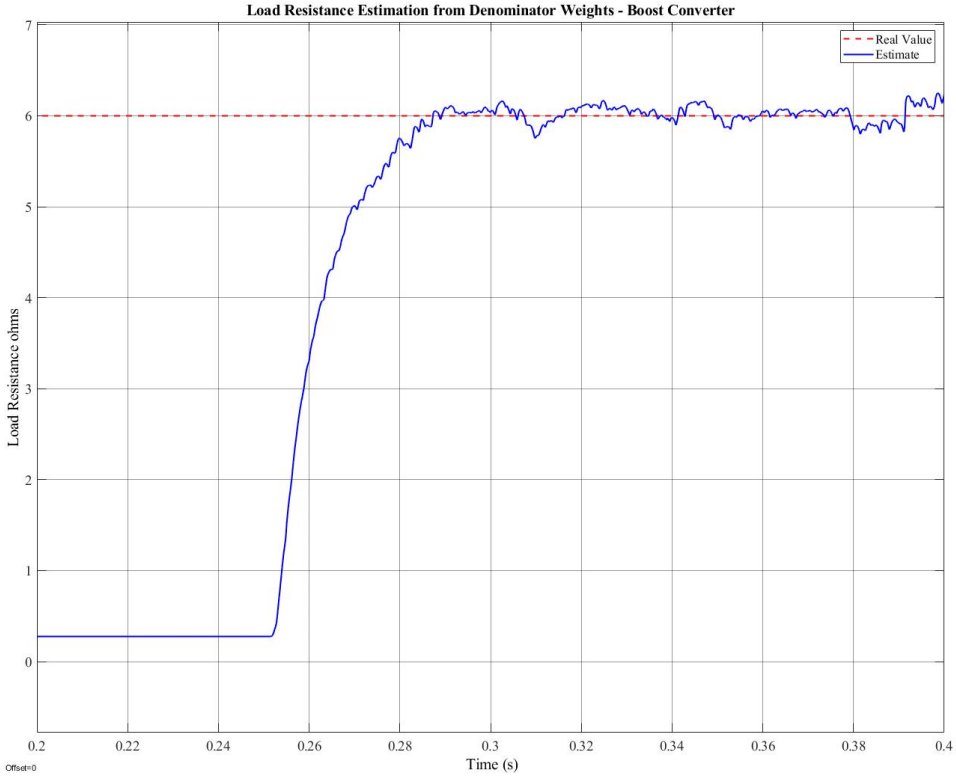

Figure 4.25 Load Resistance Estimation from Denominator Weights – Boost Converter – after Filter

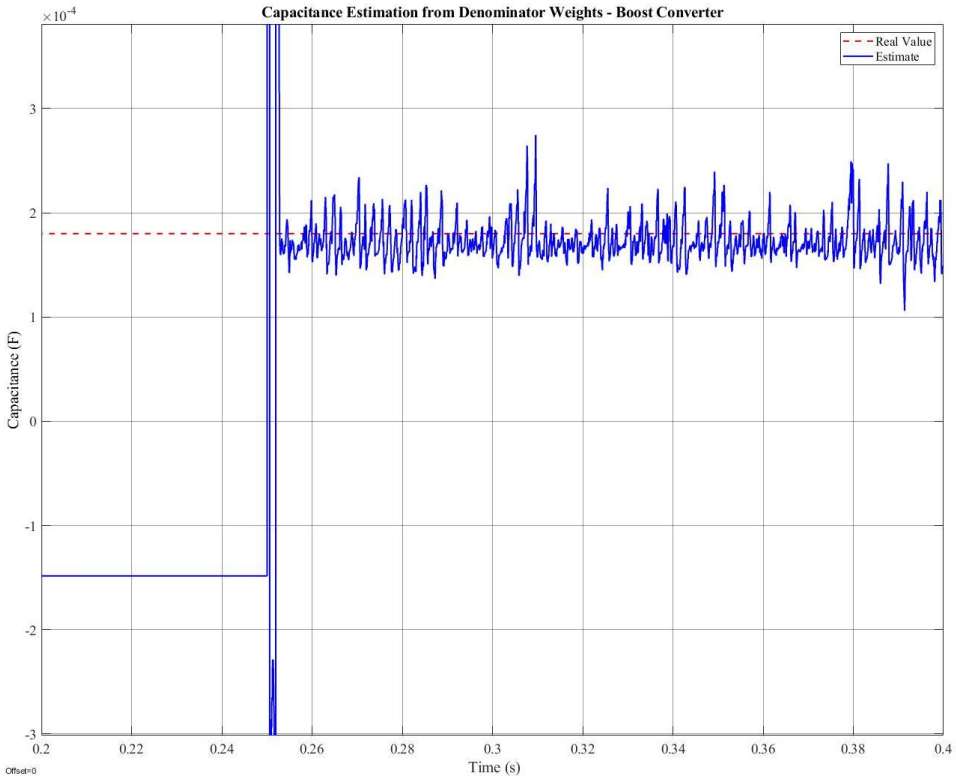

Figure 4.26 Capacitance Estimation from Denominator Weights - Boost Converter

From Figure 4.26, the capacitance estimation has shown that the average estimation value is maintained at the real value. However, it has the same big oscillation problem. It can be concluded from the boost simulation results that the system parameters estimation is more accurate and has less oscillations if estimating from the numerator pair of weights than from the denominator weights.

4.6 Chapter Summary

This chapter has presented all the simulation results in this research. The first aim was to compare the performance of the performance of parametric estimation in both open-loop and closed-loop situations. From this test, it was decided to conduct all the tests and experiments in this research in open-loop situation. The second was to compare two adaptive algorithms estimation performance: RLS and FAP, in the application of parametric estimation. Finally, due to the robustness and popularity of the RLS algorithm, it was decided to adopt RLS in the following tests. The third aim was to verify the validity of the TEOS modelling method on the parametric estimation of buck, boost and buck-boost converters. The fourth aim, which is the key point, was to verify the validity of the proposed solution of non-minimum phase converter parametric estimation with the TEOS model. The final aim, which is also an essential contribution, is to illustrate the possibility of system parameters (R_o and C) estimation with the TEOS model.

From the simulation results in Figure 4.8, three conclusions can be drawn. The first is that the convergence speed of FAP is faster compared to RLS under the same conditions. However, RLS is more robust than FAP under a big noise situation. The second conclusion is that all three adaptive algorithms are accurate in their parametric estimation, in that all of them tried and succeeded in solving the normal equation (3.5). The conclusion is that all three algorithms can work well for parametric estimations if given a proper excitation input signal. And finally, in order to make the estimation results in Section 4.4 and 4.5 more convincing, the most commonly used RLS algorithm was adopted for those tests.

There are also several conclusions that can be drawn from the simulation results in Figure 4.9. The first conclusion is that averaged model shows a slightly better fit than the TEOS model in the parametric estimation test, particularly for the denominator weights a_1 and a_2 estimation. This is because the TEOS model is based only on OFF-time sampling, which has lost some dynamics of the system in the estimation. The second conclusion is about the advantage of the

TEOS model. Chapter 2 has pointed out the superior performance of the TEOS model compared to the averaged model. From the simulation test in this chapter, it has been verified, in simulation, that the proposed theory of OFF-time sampling can ignore the RHP-zero effect in order to be a best-fit to the non-minimum phase converter parametric estimation results. This point still needs to be further verified in the practical experiment, which will be tested in Chapter 6.

The results in Section 4.5 show the possibility of on-line system parameter estimation in simulation. However, there appears a big oscillation for the system parameters estimation from the denominator weights of the boost converter as shown in the figure 4.24 and figure 4.26. As the approximation steps when deriving the final equation may have led a slight error to the model accuracy which consequently influences the estimation results. Thus, in the practical experiment in chapter 6, system parameters estimation from the denominator weights might also have a bigger oscillation than the simulation results. A proper filter is necessary for reducing the oscillations.

CHAPTER 5 DSP IMPLEMENTATIONS AND PLATFORM DESIGN

5.1 Introduction

This chapter is a brief illustration of the experiment platform setup, including converter parameters calculation, components selection, PCB design, wired-connection and auto-coding between Simulink and CCS®.

5.2 Boost DC-DC SMPC Parameters Design

The experiment on boost converter is the key experiment for this research work. To design all the of parameter setups, there are some requirements: input voltage, output voltage, switching frequency and output current. The initial conditions of the boost converter are assumed, as shown in Table 5.1, and this converter is designed to work under CCM operation.

Input Voltage V_i	12 V
Output Voltage V_o	20 V
Switching Frequency (f)	20 kHz
Output current (I_o)	1.7 A (12 Ω) ~ 3.4 A (6 Ω)

Table 5.1 Initial conditions for boost converter design

As shown in Figure 2.5, the boost converter has two operating states. When the switch is on and the diode is off, the current going through the inductor L and the switch S will increase gradually. The voltage across the inductor is V_L. Considering the voltage drop on the switch (V_s), the increment of the inductor current ΔI_{Lon} when switch is on would satisfy the equation:

$$\Delta I_{Lon} = \frac{(V_L - V_s)t_{on}}{L} \tag{5.1}$$

V_s: the voltage drop of the switch plus the voltage of the switch resistance R_s. In the PCB design, the switch that has been chosen is a power MOSFET BSC014N04LS. The forward voltage is 0.82 V and the R_s is 1.1 mΩ. As the voltage across R_s is very small, V_s could be 0.82 V.

When the switch is OFF and the diode will be ON, the energy stored in the inductor will charge the output. The current going through the inductor *L* and the switch *S* will be decreased. During the switch-off state period, the inductor voltage is ($V_o + V_f - V_i$). The diminution of the inductor current ΔI_{Loff} would satisfy the equation:

$$\Delta I_{Loff} = \frac{(V_o + V_d - V_i)t_{off}}{L} \tag{5.2}$$

V_d: The forward voltage of the diode. In the practical PCB design, the diode position is used as the same power MOSFET BSC014N04LS which will have the same function of a diode. Thus, V_d is 0.82 V and the R_f is 1.1 mΩ.

When the system is stable, $\Delta I_{Lon} = \Delta I_{Loff}$. From equations (5.1) and (5.2), it can be re-arranged as below:

$$\frac{t_{on}}{t_{off}} = \frac{V_o + V_d - V_i}{V_i - V_s} \tag{5.3}$$

Since $D = \frac{t_{on}}{T_s}$, thus the duty-cycle is:

$$D = \frac{V_o + V_d - V_i}{V_o + V_d - V_s} \approx \frac{V_o - V_i}{V_o} = \frac{20 - 12}{20} = 0.4 \tag{5.4}$$

As the power consumed on the inductor is very small compared to the input or output power, the dissipation of the inductor can safely be ignored. Thus, the output power should be equal to the input power:

$$V_i \times I_{Lave} = V_o \times I_o \tag{5.5}$$

Where I_{Lave} is averaged inductor current and I_o is output current.

It is assumed that the load is the maximum load, which means $I_o = 1.7\ A$. If we consider a 10% tolerance of the load resistance, for the calculation, the output current is assumed to be 1.5 A. From equations (5.4) and (5.5), the I_{Lave} can be calculated as:

$$I_{Lave} = \frac{I_o}{1 - D} = \frac{1.5}{0.6} = 2.5\ A \tag{5.6}$$

From equation (5.1), the inductor ripple current should be:

$$\Delta I_L = \frac{(V_i - V_s)D}{Lf} \tag{5.7}$$

As the boost converter is working in CCM, the inductor current should therefore satisfy the equation:

$$I_{Lave} \geq \frac{\Delta I_L}{2} \tag{5.8}$$

To further ensure the boost converter is working in CCM, the proper inductance can be calculated as equation (5.9) from equations (5.6), (5.7) and (5.8).

$$L \geq \frac{(V_i - V_s)D(1-D)}{2I_o f} = \frac{(12 - 0.82) \times 0.4 \times 0.6}{2 \times 1.5 \times 20 \times 10^3} = 44.72\ uH \tag{5.9}$$

For most practical design applications, the inductor ripple current should be 20%–30% of the average current. Therefore, the inductor ripple current is:

$$\Delta I_L = 20\% \times I_{Lave} = 20\% \times 2.5 = 0.5\ A \tag{5.10}$$

From equations (5.7) and (5.10), the minimum value of inductance can be calculated below:

$$L = \frac{(V_i - V_s)D}{\Delta I_L f} = \frac{(12 - 0.82) \times 0.4}{0.5 \times 20000} = 450\ uH \tag{5.11}$$

In order to make the response much smoother in order to present a much clearer response performance, the inductance has been determined as 680 uH, which is 50% more than the minimum value 450 uH.

From the boost converter structure, it can be found that the inductor peak current I_{LP} should be equal to the switch peak current I_s and equal to the diode peak current I_d. To ensure it is safe when the load changes to 6 Ω and the output current is 3.4 A, the peak current should be calculated from the 3.4 A output current. Therefore, the peak current can be obtained from equation (5.12).

$$I_{sP} = I_{dP} = I_{LP} = I_{Lavd} + \left(\frac{\Delta I_L}{2}\right) = 1.1 \times \frac{I_o}{1-D} = 6.233\ A \tag{5.12}$$

Thus, the selected inductor should satisfy the conditions of inductance larger than 450 uH and current bigger than 6.3 A.

The voltage drop of the switch should be:

$$V_{s(off)} = V_o + V_d = 20 + 0.82\,V = 20.82\,V \tag{5.13}$$

Considering 20% tolerance, the selection should be larger than 8 A/25 V. The rating voltage of the diode should be able to work under the reverse output voltage; and the rating current should be able to transport the maximum output current. The parameters of the diode should be larger than 8 A/25 V.

As discussed above, the switch is the power MOSFET BSC014N04LS. Its parameters are 100 A/40 V/1.1 mΩ which can completely fulfil the requirement.

The selection of the capacitor is determined by the requirement of the ripple voltage, which is related to the equivalent series resistance (ESR). The rating capacitor ripple current should be larger than the ripple current of the circuit. The requirement of the ripple voltage is commonly assumed to be 3% of the output. As shown in equations (5.6) and (5.10), when the output current is 3.4 A, the inductor ripple current is 1.133 A. The ESR should satisfy:

$$ESR < \frac{\Delta V_o}{\Delta I_L} = \frac{20 \times 1\%}{1.133} = 0.1765\ \Omega \tag{5.14}$$

According the capacitor equation, $C\frac{dU}{dt} = i$. Therefore:

$$C\frac{\Delta U}{DT_s} = I_o \tag{5.15}$$

The ripple voltage is:

$$\Delta U = 20 \times 3\% = 0.6\,V \tag{5.16}$$

From the equations (5.15) and (5.16), the output capacitance should be:

$$C \geq \frac{DI_o}{\Delta U f} = \frac{0.4 \times 3.4}{0.6 \times 20000} = 113.33\,uF \tag{5.17}$$

From the practical design case experiences, the capacitance should be 20%–100% larger than the minimum value. In this experiment, the capacitance is chosen as 180 μF. The ESR is 28 mΩ. There are two same output capacitors connected in parallel which could consequently make the ESR as 14 mΩ.

In summary, the inductor is selected as 680 μH, and the rated current should be greater than 6.3 A. The capacitor is selected as 180 μF. The power of the circuit is 67 W if the load resistance is 6 Ω in the practical experiment. Some of the important readings of the components are presented in the Appendix.

5.3 Components Selection and PCB Design

With the results obtained from calculated requirements of the components in the previous section, suitable components can be selected. In addition, some X7R and C0G/NP0 capacitors are selected for the function of the bypass and decoupling filters. The final selected components are presented in the Appendix. With the package size of the selected components, the PCB layout can be sketched. The schematic is drawn in Multisim® software, which is shown in Figure 5.1. There are three voltage levels in the circuit: ±12 V, 5 V and 3.3 V. In addition, two linear voltage regulators are used to transform the voltages – 12 V to 5 V and 3.3 V respectively. The 12 V power supply provides an input voltage for the analogue circuit and also to the instrumentation amplifier. ±12 V supplies the instrumentation amplifier and 5 V supplies the current sensor. Output voltage is sampled with the help of a voltage divider with a gain of 0.2. The PCB layout is drawn using Ultiboard® software, which is shown in Figure 5.2.

As the schematics show in Figure 5.1, there are five main sections. The converter part is the analogue circuit, while the rest of it is made up of other parts belonging to the digital circuits. Each part uses its own ground connection and there is a zero-resistor connecting between the two-part ground connections. A zero resistor can represent a narrow current path. The purpose is to suppress the loop current in order to finally reduce the noise. The digital part includes a MOSFET driver, the voltage and current measurements, and the voltage regulator.

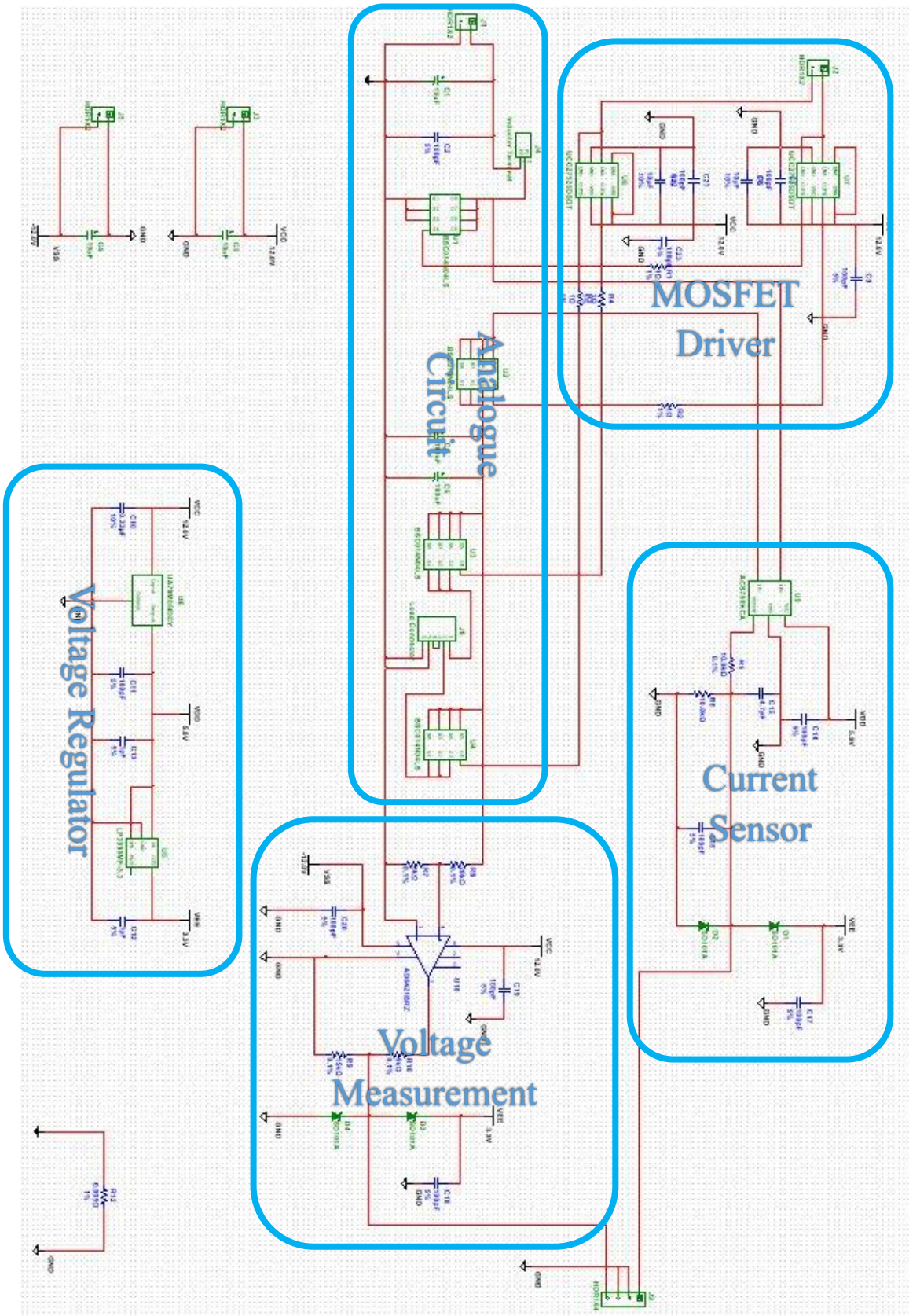

Figure 5.1 Schematic of the boost converter in Multisim

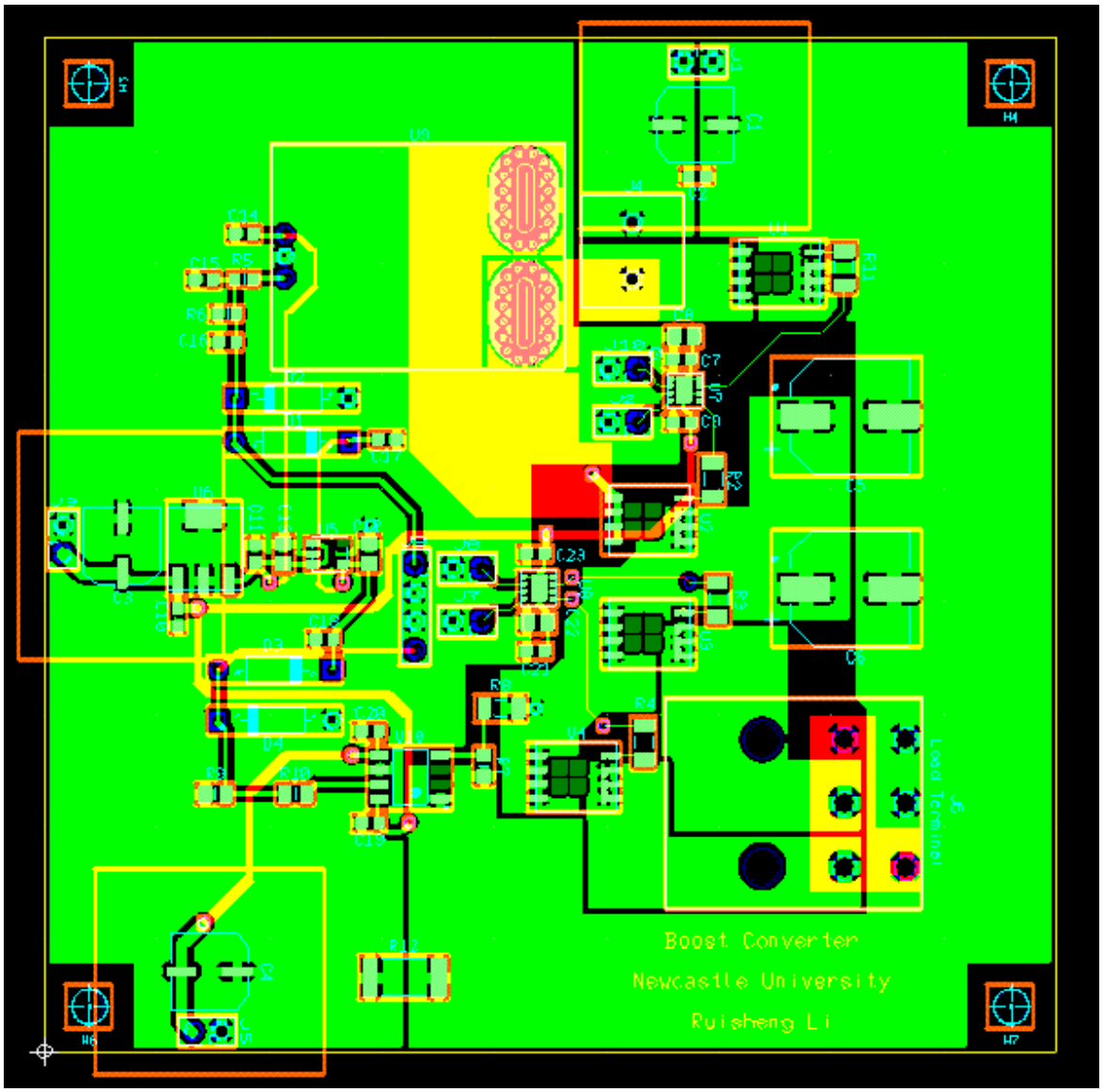

Figure 5.2 Boost Converter PCB

The final layout as shown in Figure 5.2 is designed based on several considerations. The first consideration is to separate the analogue and digital circuits, which are shown in Figure 5.2. The left part is the digital circuit and the right part is the analogue circuit. The second consideration is to make the current paths as short as possible, with the consideration of the temperature control. The third one is to put the filter close to their filtered components (i.e., MOSFET driver, instrumentation amplifier, current sensor, and voltage regulator). There are also three other test boards designed to test the regulator, the MOSFET driver and the sensors, which are shown in Appendix D. The final boost PCB is presented in the figure 5.3.

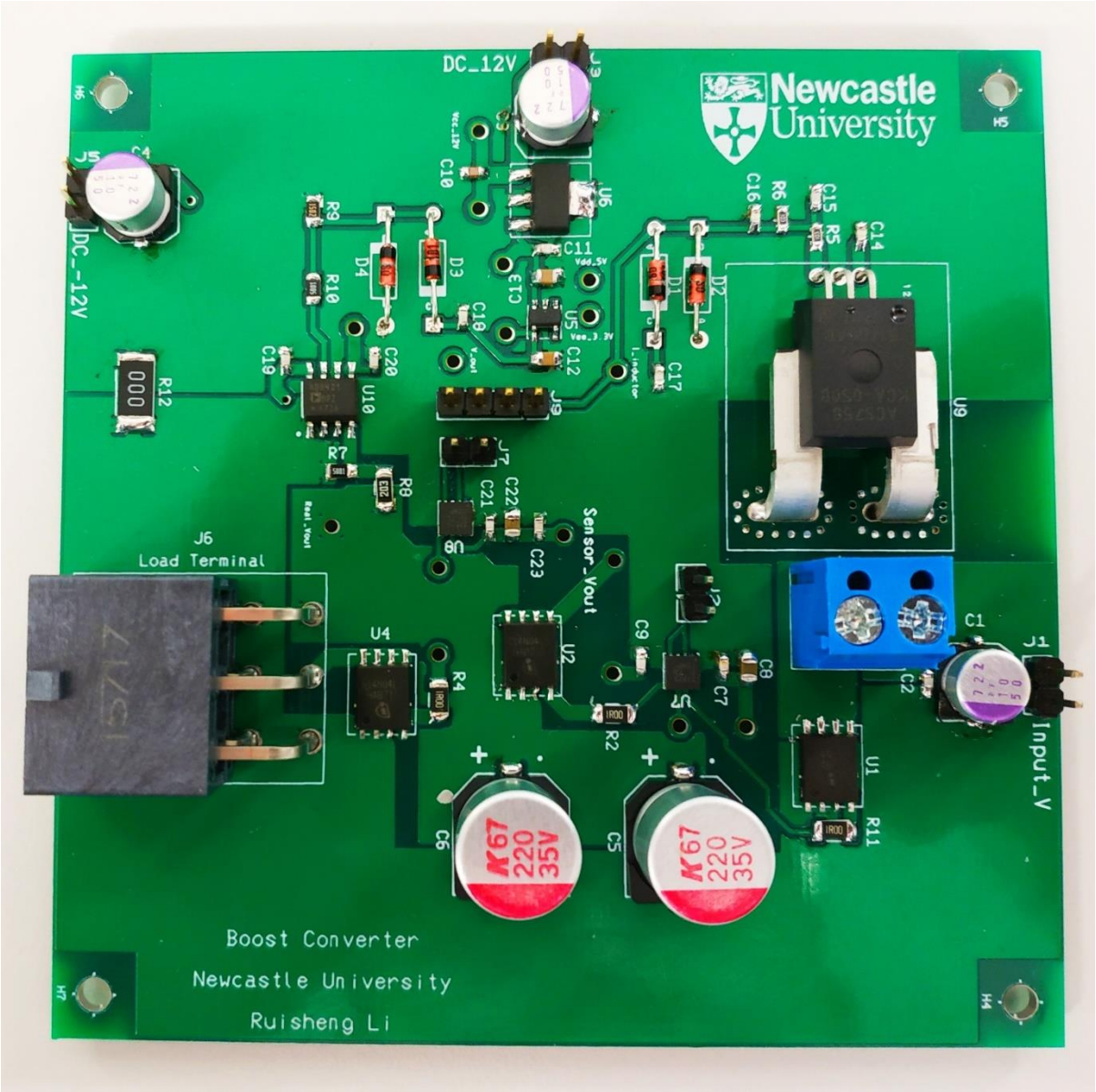

Figure 5.3 Final Boost PCB

5.4 Experimental Platform Interface Setup and DSP Implementation

The DSP used in this experiment is the Texas Instruments^{TM} TMS320F28335 eZdsp board. This microprocessor board can be used by simple programming for an optimal system operation. The DSP is developed for fast and effective operation of digital signal processing algorithms. It will help realise the function of identification algorithms and the DC-DC SMPC controller implementation. This platform TMS320F28335 includes 512 KB flash memory, 68 KB RAM, and six channels of direct access memory (DMA), which is similar to other general-purpose microprocessors based on Harvard architecture design, as shown in Figure 5.4.

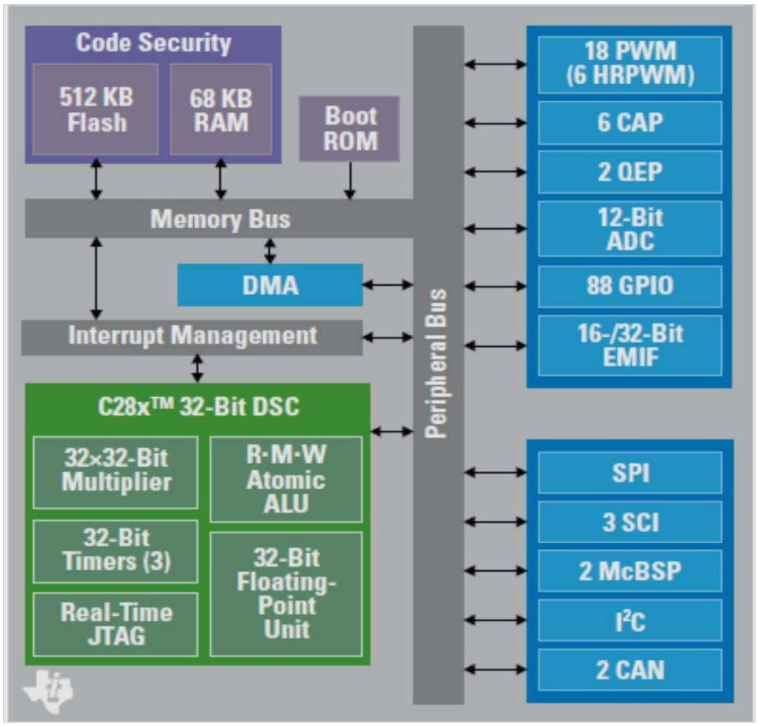

Figure 5.4 TMS320F28335 eZdsp Architecture [105]

The programming codes are developed and written in Texas Instruments CCS® based Integrated Development Environment (IDE), and are then compiled and downloaded onto the DSP through this software. In this experiment, before downloading the codes via CCS®, Simulink on the Matlab platform is employed to build the model, and this automatically generates a C-code from the model (with the help of its embedded 28335 Target Support Package (TSP) and Real-time Workshop (RTW)). The detailed interface setup can be retrieved from the website. The function is similar to the function of dSPACE. After generating the report by building the model in the Simulink via C language auto-coding, the generated file is downloaded onto the DSP via CCS® to realise the DSP settings. The experiment also includes buck converter test, the figure 5.5 is presenting the connection of the DSP with the buck converter board. The entire experiment platform is shown in Figure 5.6.

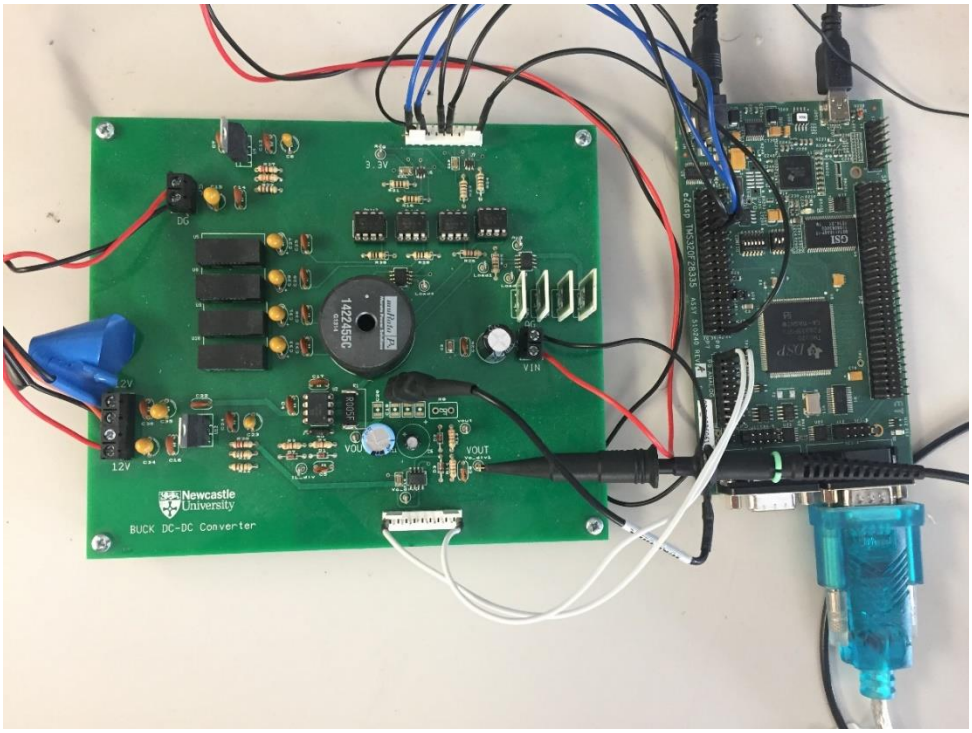

Figure 5.5 DSP Connection with the Converter Board

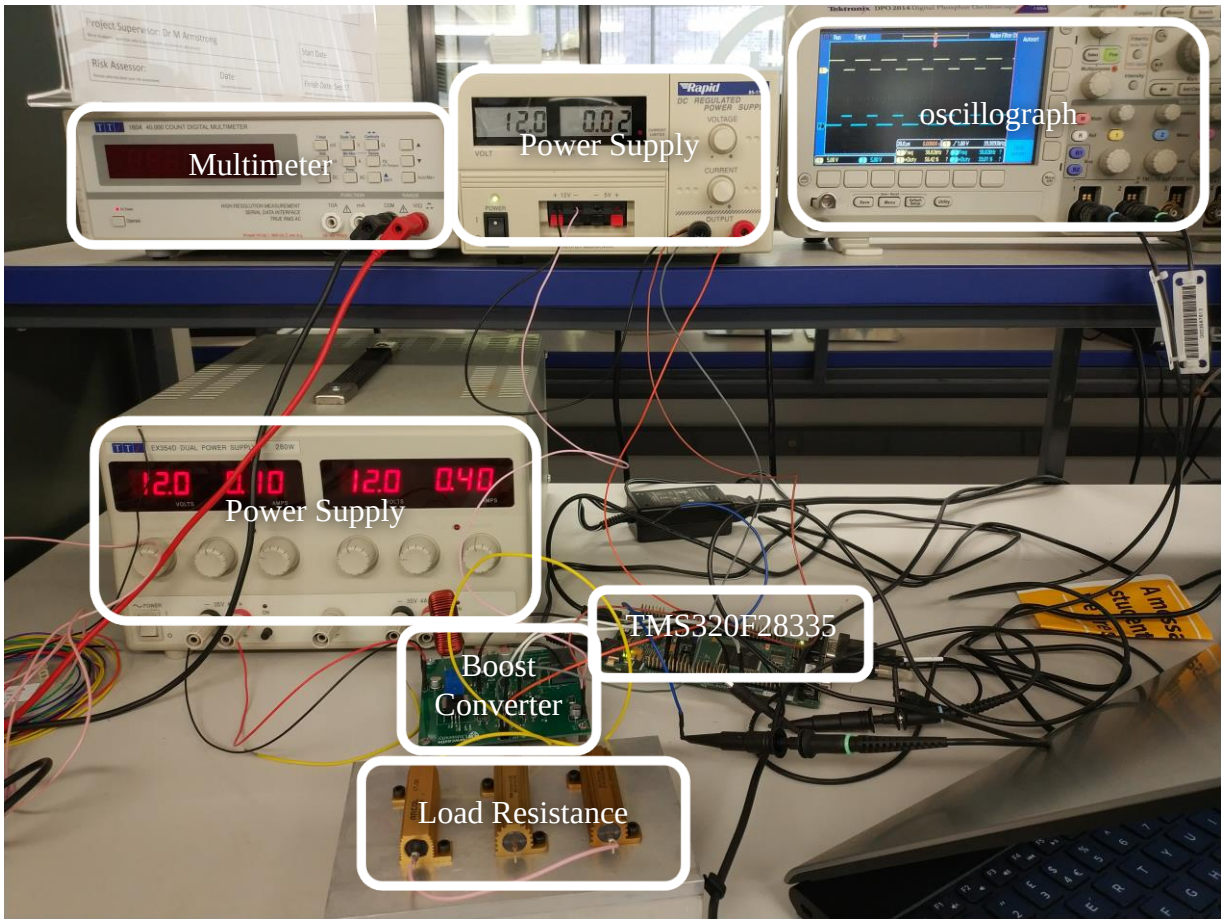

Figure 5.6 Experiment Platform

5.5 Chapter Summary

In this chapter, we have presented the software and hardware preparations for the experiment. Based on the voltage, frequency and ripple requirements, the system parameters of capacitance and inductance of the converter have been calculated. In addition, a boost converter board was designed for the experiment with component selection and PCB design. The buck converter used in the experiment test is ready for use in the lab, whose specifications are shown in Table 4.1. The microprocessor used in this experiment is TMS320F28335. The following experimental results are the outcome from the experiment platform shown in Figure 5.6.

CHAPTER 6 ESTIMATION OF SMPCs – EXPERIMENTAL RESULTS

6.1 Introduction

The simulation results have been presented in Chapter 4, which verified the validity of the proposed solution, for the non-minimum phase converters parametric estimation problem in an ideal environment. In this chapter, the solution will be further tested on the buck converter and boost converter in the practical experiment. The detailed specifications of each practical converter are the same as those tested in the simulation, as shown in Table 4.1 and Table 4.4. This chapter will also introduce, in the following three sections: different sampling points effects, buck converter identification results and boost converter identification results. In the practical experiment, each of the input (duty cycle) and output (voltage) signals are sampled at 600 points, which is about 0.03 s operation for the off-line estimation experiment. In the first section, the results will be shown for both models different sampling approaches to analyse the difference between two modelling methods in the practical experiment. The second and the third sections will present the parametric estimation results and system parameters estimation results for the buck converter and boost converters, respectively followed by discussions. At the end of the three sections, the chapter will be summarised.

6.2 Parametric Estimation and Sampling Points Effects

The two modelling methods have two differences in the practical experiment: one is adopting different types of PWM signal, and the other is sampling different points of the output signal. The averaged modelling method is commonly done using the centred pulses PWM signal with sampling at the switch-OFF-to-ON state edge. In addition, the proposed TEOS model can be done using the trailing-edge PWM signal, with sampling during the switch-off time. Both of the settings in ePWM block in the practical experiment are shown below. In addition, some other settings within the Simulink block are shown in Appendix C.

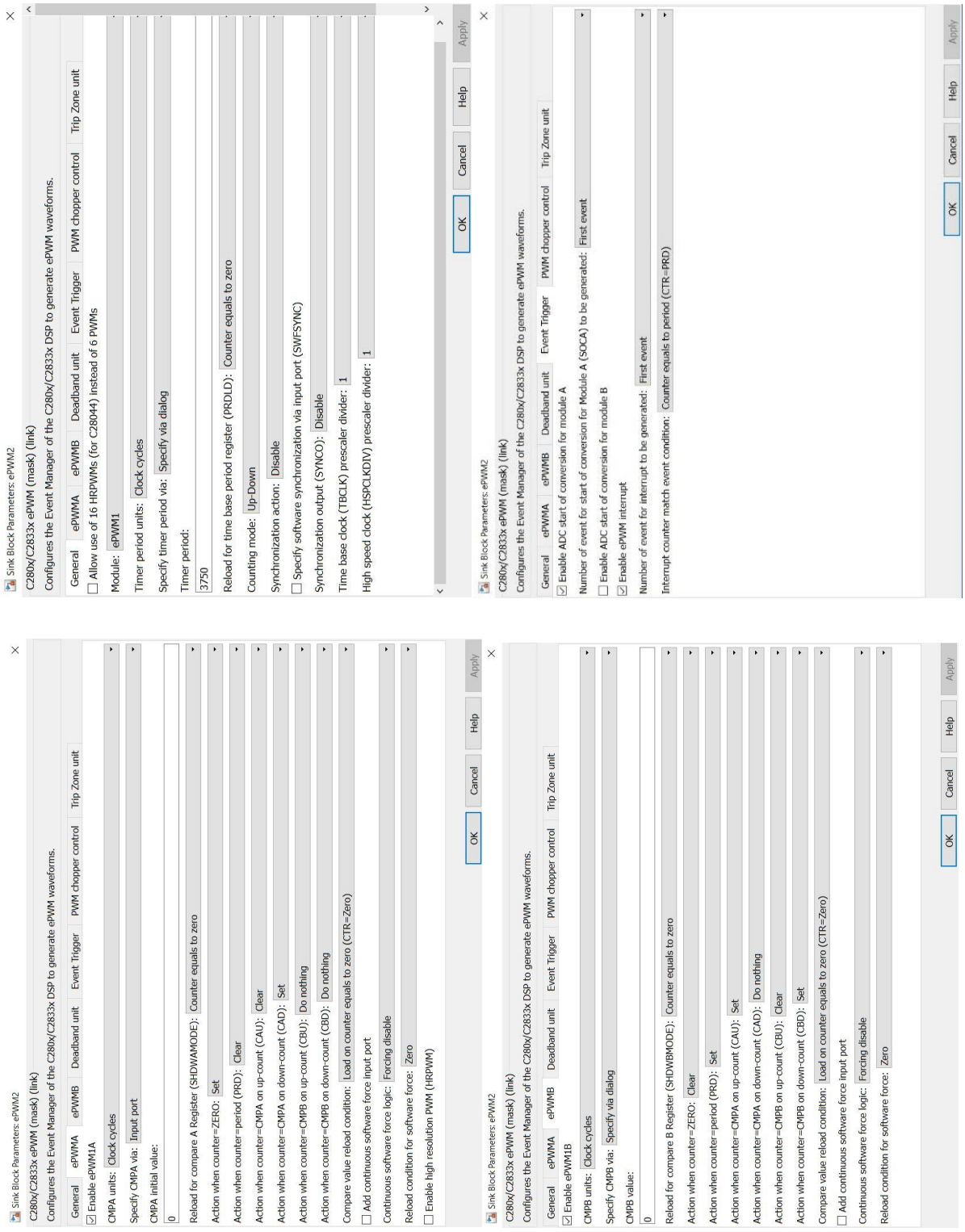

Figure 6.1 Averaged Model ePWM Block Settings

Figure 6.2 TEOS Model ePWM Block Settings

In the averaged model test, ePWMA is the input signal, which is also used to trigger the ADC event. In the TEOS model test, ePWMB is the input signal to the converter, and the ePWMA signal is used for triggering the ADC event during the switch-off time. The experimental results are shown below.

The results in Figure 6.4 and Figure 6.6 are the parametric estimation error results, which are both stable around zero after a start period of 0.005 s. It indicates that the estimation process is able to estimate the output voltage accurately, which also indicates that the estimation can correctly predict the dynamic response of the system. This also provides confidence for further analysing the difference of parametric estimation with two different models.

The results shown in Figure 6.3 and Figure 6.5 are the parametric estimation experimental results of the buck converter. There are four parameters to be estimated: a_1, a_2, b_1 and b_2. The black dashed lines are the real averaged model weights, and the red dashed lines are the real TEOS model weights. The denominator weights, a_1 and a_2, are likely to be stable, but the two numerator weights, b_1 and b_2, are oscillating around their real values. However, the trends of the numerator weights oscillations seem to be the same but in an opposite direction. In other words, the ratio relationship between b_1 and b_2 seem to be stable and have not changed. This ratio relationship is the relationship between each system parameter, which will be tested in the next two sections by estimating the system parameters from the two pairs of estimated weights (a_1 and a_2, b_1 and b_2).

From the estimation results, it is obvious that when using the averaged sampling settings, the estimation results of a_1 and a_2 are mostly coinciding with the averaged model weights. And when changed to the TEOS settings, the estimation results are collapsing exactly with the red dashed lines, which are the TEOS model weights. Although the two model weights for b_1 and b_2 are close to each other, it is difficult to find a clear difference. Although, for the denominator weights, a slight difference can still be observed, in that the estimated a_1 and a_2 are much closer to their real model weights depending on its specific sampling mechanism. However, from the results shown above, using different sampling points will only have a slight effect in the estimation result, which can barely be observed.

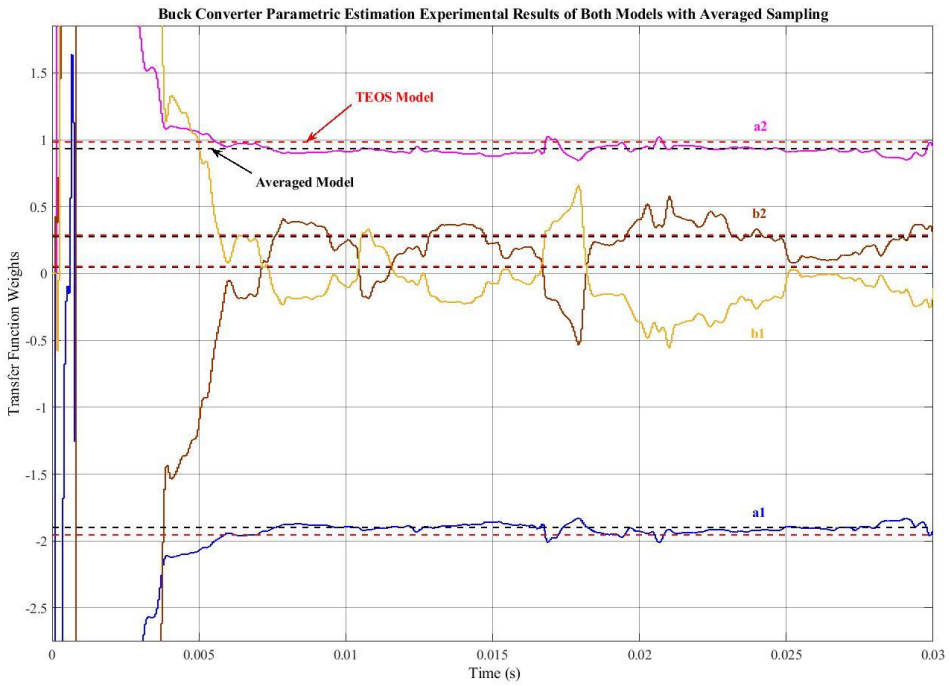

Figure 6.3 Buck Converter Parametric Estimation Experimental Results of Both Models with Averaged Sampling

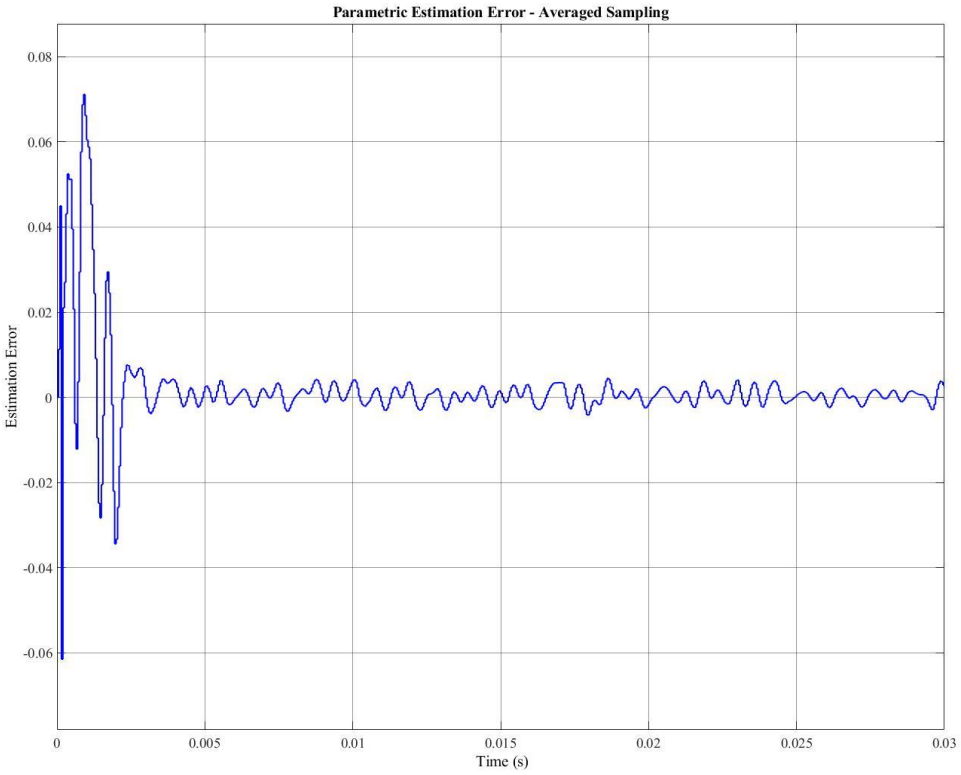

Figure 6.4 Buck Parametric Estimation Error - Averaged Model Sampling

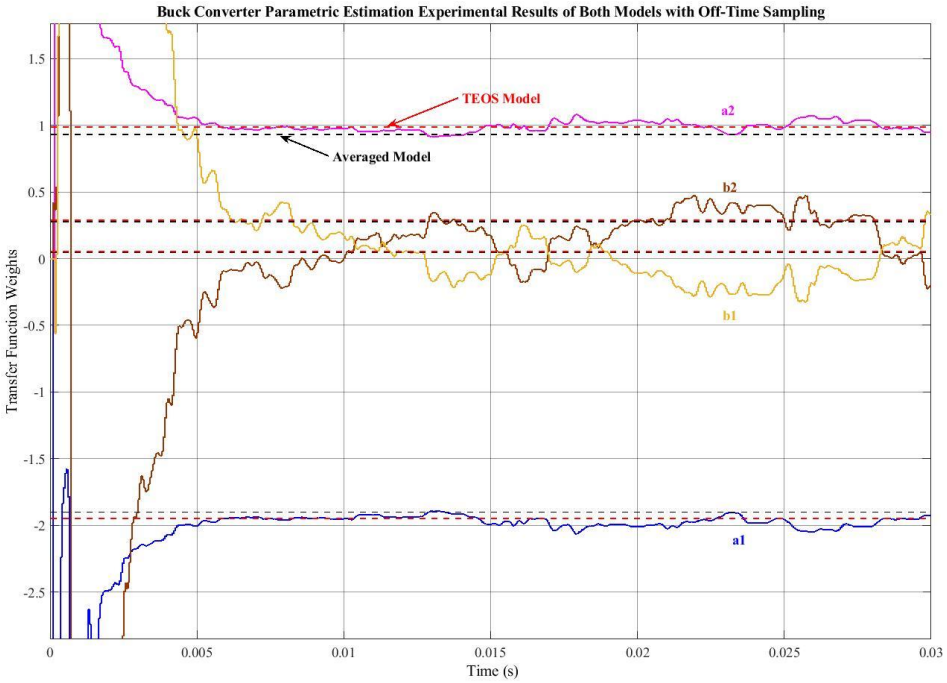

Figure 6.5 Buck Converter Parametric Estimation Experimental Results of Both Models with Off-Time Sampling

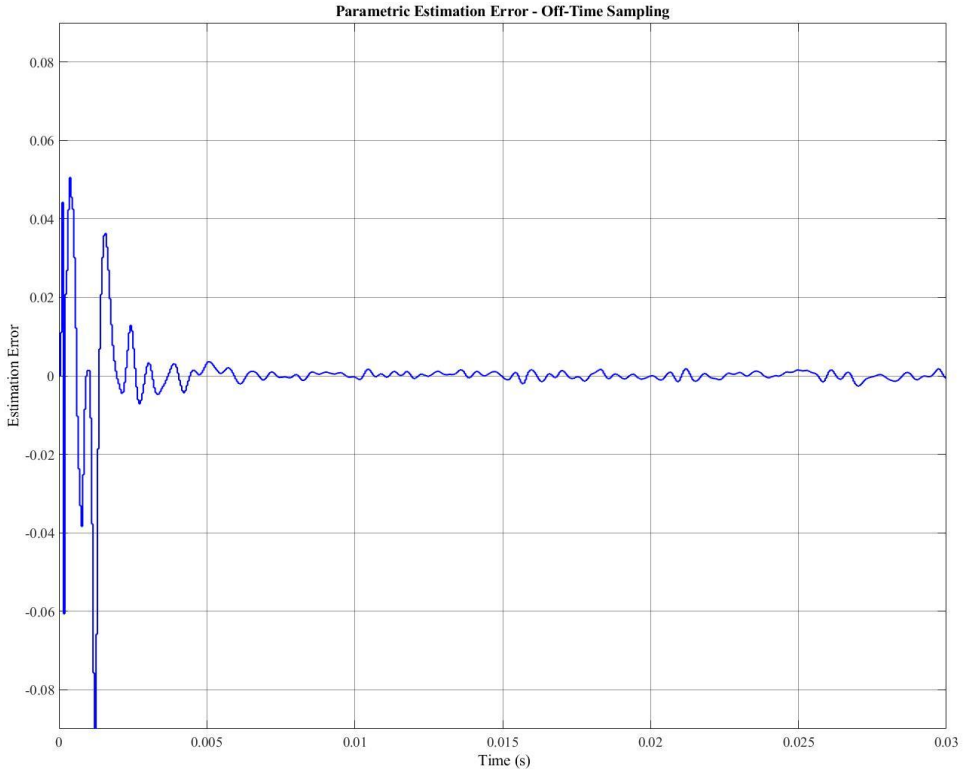

Figure 6.6 Buck Parametric Estimation Error - Off-Time Sampling

The boost converter is also tested with two sampling mechanisms. From Figure 6.7 to Figure 6.10, they are the parametric estimation experimental results of the boost converter test. For the boost test, it is expected that there will be a big difference observed between each model's estimated numerator weights, as the weights calculated by the two models are quite different. However, the difference between the estimated denominator weights are barely observable.

As shown in Figure 6.7 and Figure 6.9, when using different sampling mechanisms the two estimated numerator weights are both far away from the real averaged model weights but are quite close to the real TEOS model weights. The average value of the estimated numerator weights in Figure 6.7 are ($b_1 \approx$ -1.1) and ($b_2 \approx 1.3$), which have an approximated estimation error with averaged model weights as shown below.

$$b_{1error} = \frac{-1.1 - (-0.8313)}{-0.8313} \approx 32\%$$

$$b_{2error} = \frac{1.3 - 0.975}{0.975} \approx 33\% \tag{6.1}$$

In addition, due to the result shown in Figure 6.9, the estimation error with the averaged model is:

$$b_{1error} = \frac{-1.15 - (-0.8313)}{-0.8313} \approx 38\%$$

$$b_{2error} = \frac{1.4 - 0.975}{0.975} \approx 44\% \tag{6.2}$$

However, if using the weights of the TEOS model with averaged sampling, the estimation error in Figure 6.7 is:

$$b_{1error} = \frac{-1.1 - (-1.255)}{-0.8313} \approx 12\%$$

$$b_{2error} = \frac{1.3 - 1.512}{0.975} \approx 14\% \tag{6.3}$$

And if using OFF-time sampling mechanism in Figure 6.9, the estimation error is:

$$b_{1error} = \frac{-1.15 - (-1.255)}{-0.8313} \approx 8\%$$

$$b_{2error} = \frac{1.4 - 1.512}{0.975} \approx 7\% \tag{6.4}$$

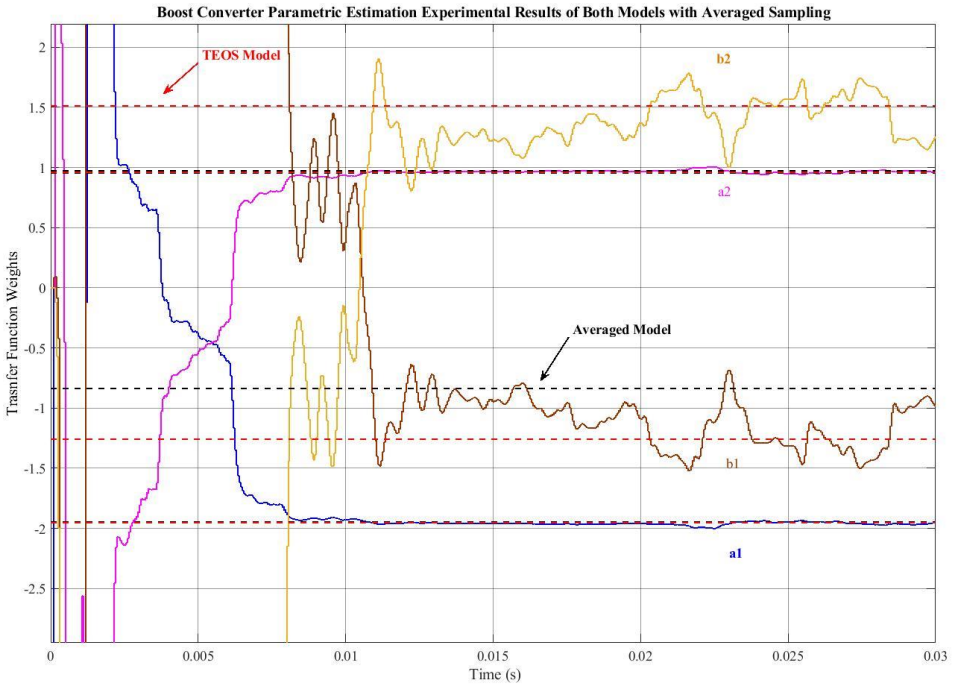

Figure 6.7 Boost Converter Parametric Estimation Results of Both Models with Averaged Sampling

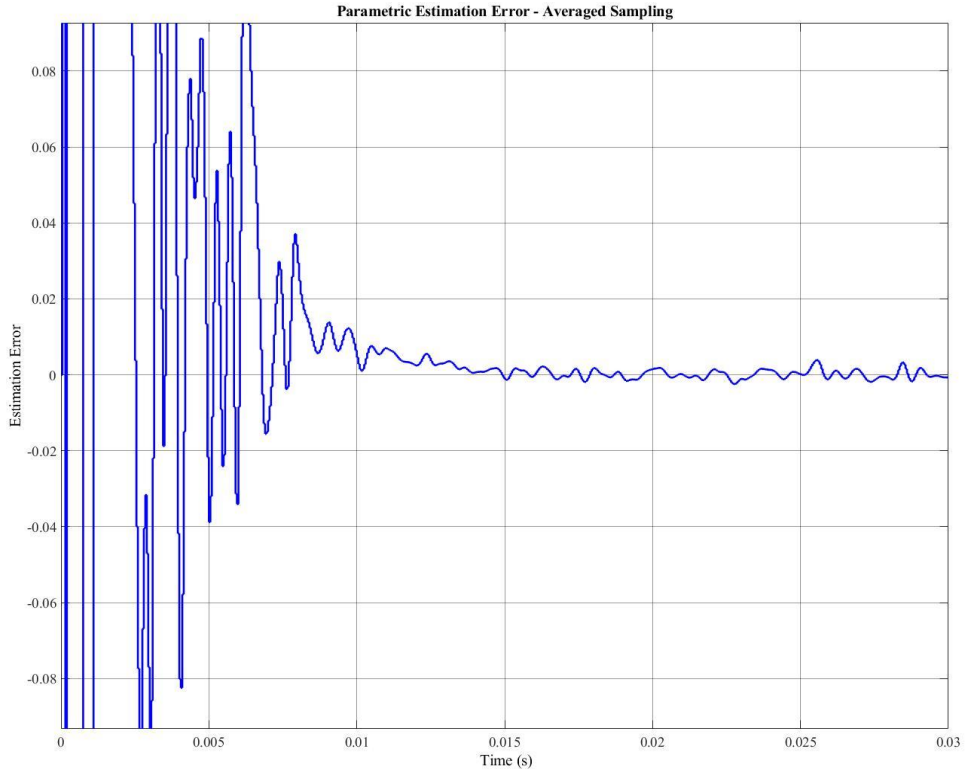

Figure 6.8 Boost Converter Parametric Estimation Error - Averaged Sampling

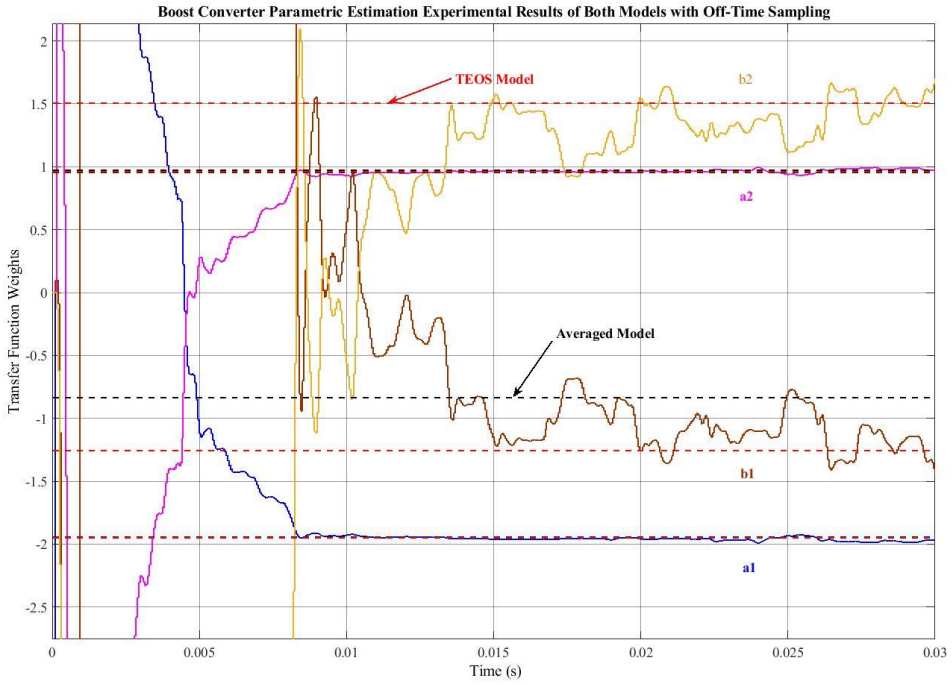

Figure 6.9 Boost Converter Parametric Estimation Experimental Results of Both Models with Off-Time Sampling

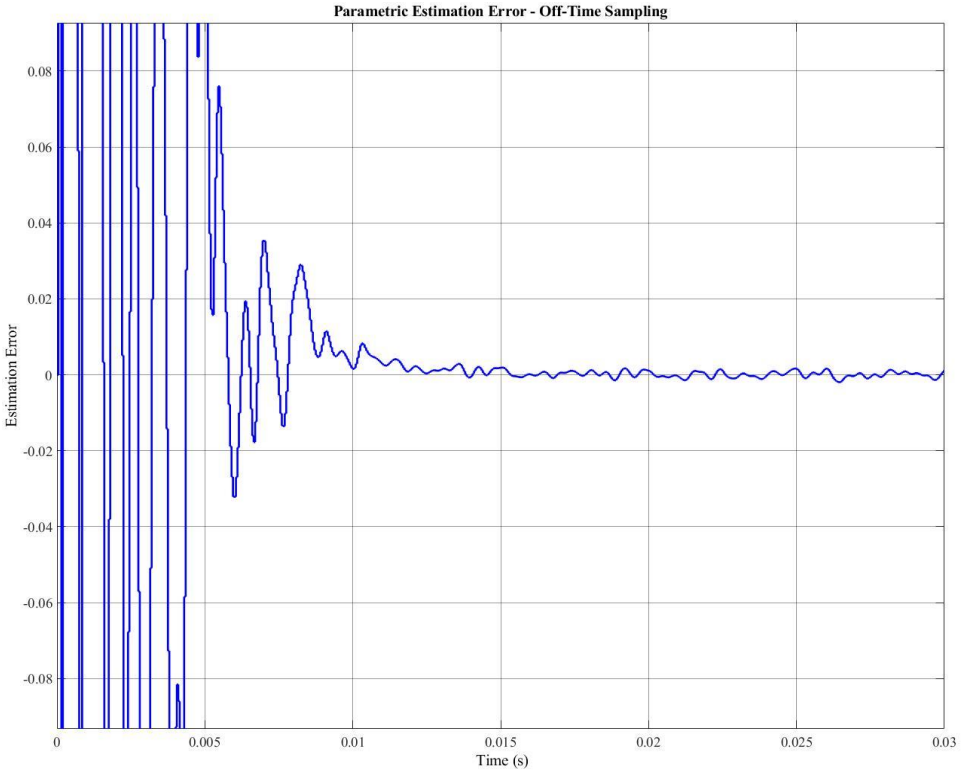

Figure 6.10 Boost Parametric Estimation Error - Off-Time Sampling

The averaged values chosen above are based on the approximate readings from the graph, which may not be particularly accurate. However, it is apparent that the TEOS model weights fit much better to the parametric estimation results. It can improve the estimation accuracy by more than 20%.

The results in this section have shown that the parametric estimation of the buck converter can work well for both models. However, the boost converter estimation results have also shown that the TEOS model is 20% more accurate than the averaged model for the parametric estimation, particularly for the numerator weights estimation. In addition, the results have shown that changing different sampling points only has a limited effect on the parametric estimation process. However, for the boost converter test, the OFF-time sampling with trailing-edge PWM signal is more accurate than the averaged sampling which is using centred pulses PWM signal. In the next section, the TEOS model will be further tested for the system parameters estimation, which is another advantage of this modelling method. In addition, if the system parameters estimation from the estimated weights, especially from the pair of (b_1 and b_2) is accurate and stable for both buck converter and boost converter, it can prove that the estimated weights can successfully describe the characteristics of the system.

6.3 System Parameters Estimation Experimental Results

Based on the parametric estimation results with the TEOS model in the previous section, system parameter estimation can be done for both the buck converter and boost converter. The way to estimate the system parameters from the TEOS model has already been illustrated in Chapter 2. In the experiment, the system parameters are estimated from both sides of the transfer function weights, which are a_1 and a_2, b_1 and b_2, the same as in the simulation test.

6.3.1 Buck SMPC Experimental Test

Figures 6.11 and 6.12 are the system parameters estimation results from numerator weights for the buck converter. Both figures have shown that it will take 0.005 s to reach a steady-state point. Figure 6.11 has shown that the estimation error of load resistance is within $\pm$10%., while Figure 6.12 has shown that the estimation error of capacitance is within $\pm$8%. These two

figures have shown the possibility of estimating the system parameters from the numerator weights.

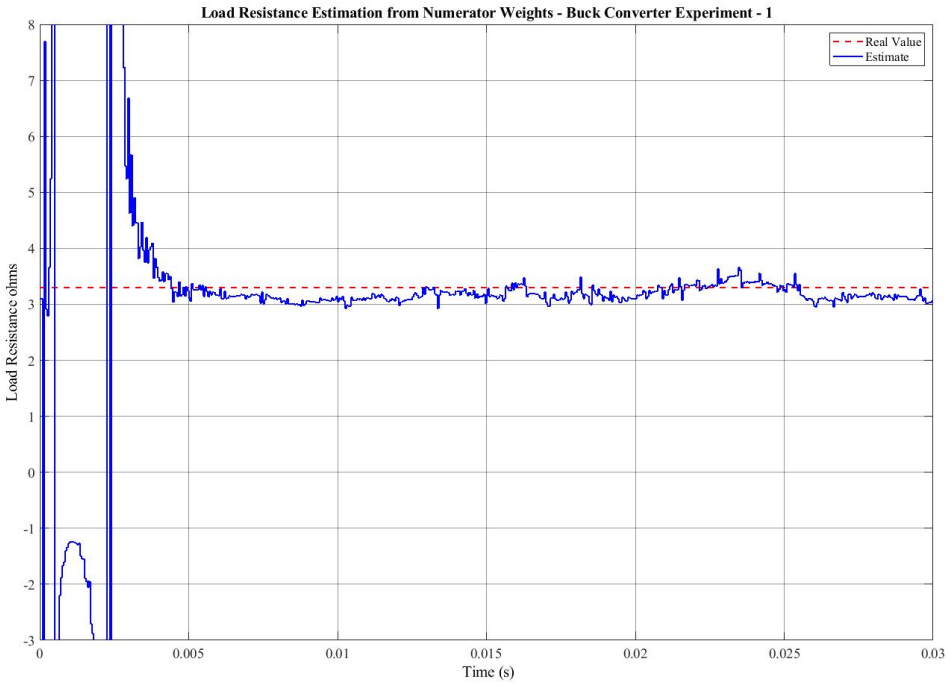

Figure 6.11 Load Resistance Estimation from Numerator Weights - Buck Converter Experiment – 1

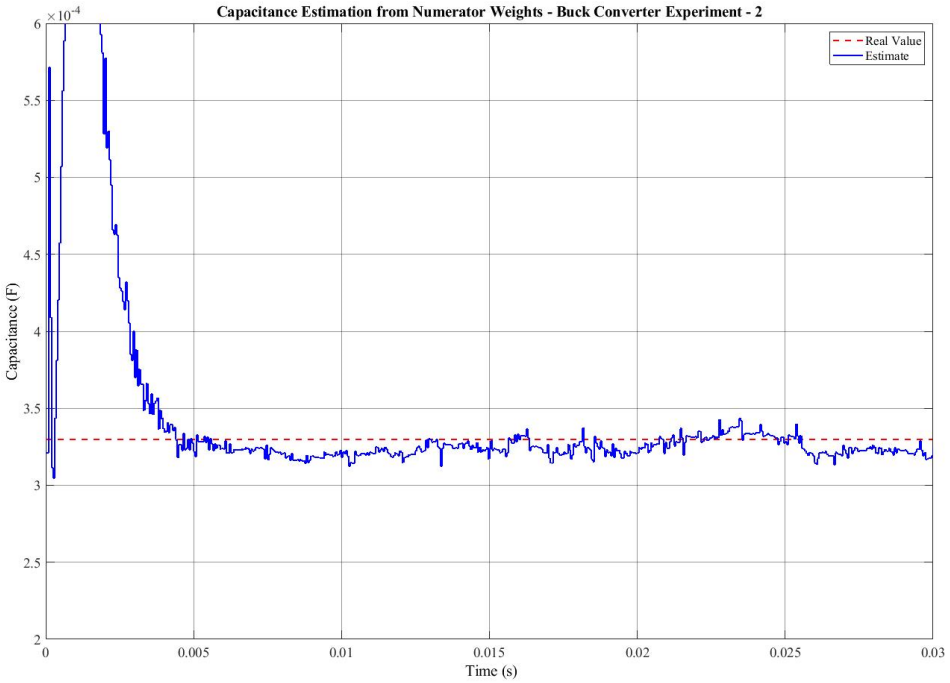

Figure 6.12 Capacitance Estimation from Numerator Weights - Buck Converter Experiment – 1

The two figures below are the system parameters estimation from the denominator weights.

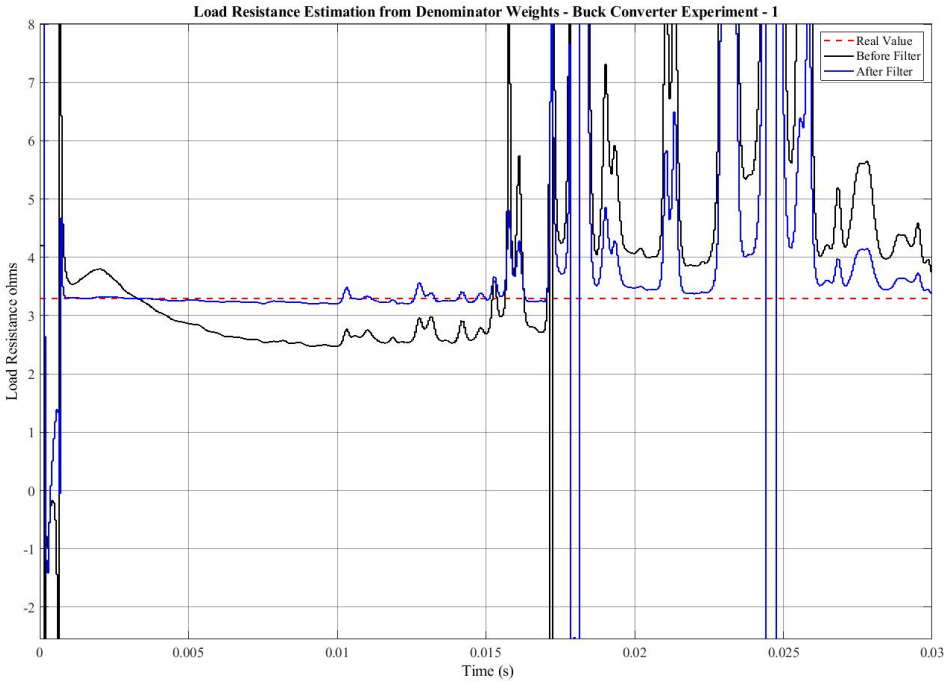

Figure 6.13 Load Resistance Estimation from Denominator Weights - Buck Converter Experiment – 1

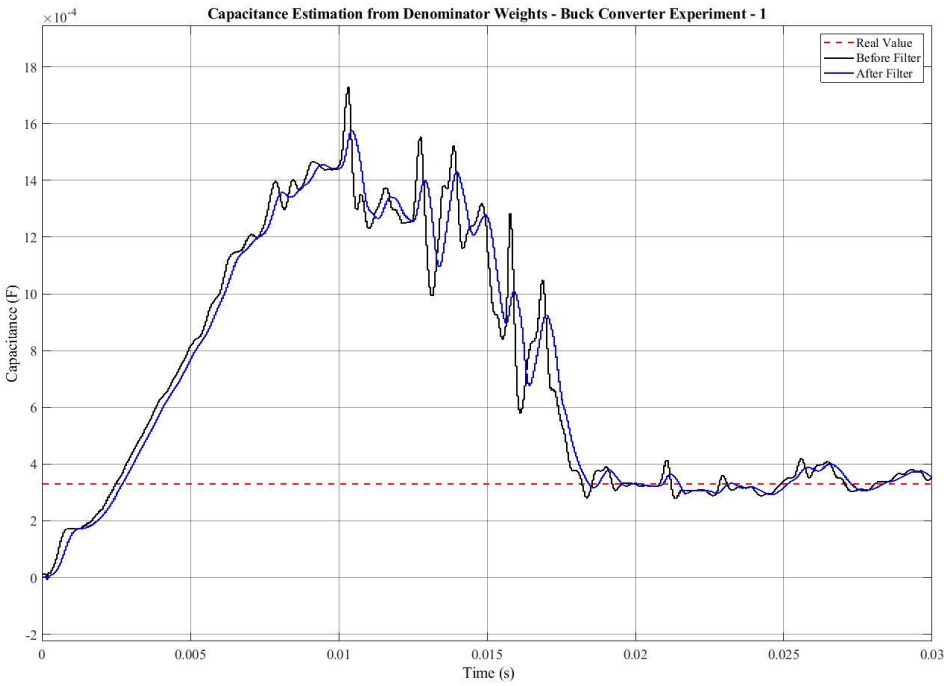

Figure 6.14 Capacitance Estimation from Denominator Weights - Buck Converter Experiment - 1

Results shown in Figures 6.13 and 6.14 have indicated a big oscillation. A four-tap moving average filter has been added to process the estimation results. The black line is the original estimation result, and the blue line is the processed estimation result after the filter. Figure 6.13 presents an accurate estimation result until 0.015 s where a big oscillation was observed. However, in Figure 6.14, a big oscillation at the beginning of the period was observed, but this ended with a relatively stable estimation result in the last 0.015 s. If just observing from the stable period of each estimation, the load resistance estimation error is within ±10%, and the capacitance estimation error is within ±20%. However, the average value of each estimation seems to be at the dashed lines of real value. Referring back to the simulation results, load resistance estimation from denominator weights also had more oscillations, as previously shown in Figure 4.14. In the practical result in Figure 6.13, the oscillation becomes even larger. It can be concluded that it is possible to estimate system parameters from the parametric estimation results by the TEOS modelling method, especially from numerator weights, but due to some practical causes (i.e. noise, manufacturing or soldering defects, components tolerance), the estimation results are not as accurate as those in the simulation test. In addition, the response of load resistance estimation from the denominator weights should be further improved.

6.3.2 Boost SMPC Experimental Test

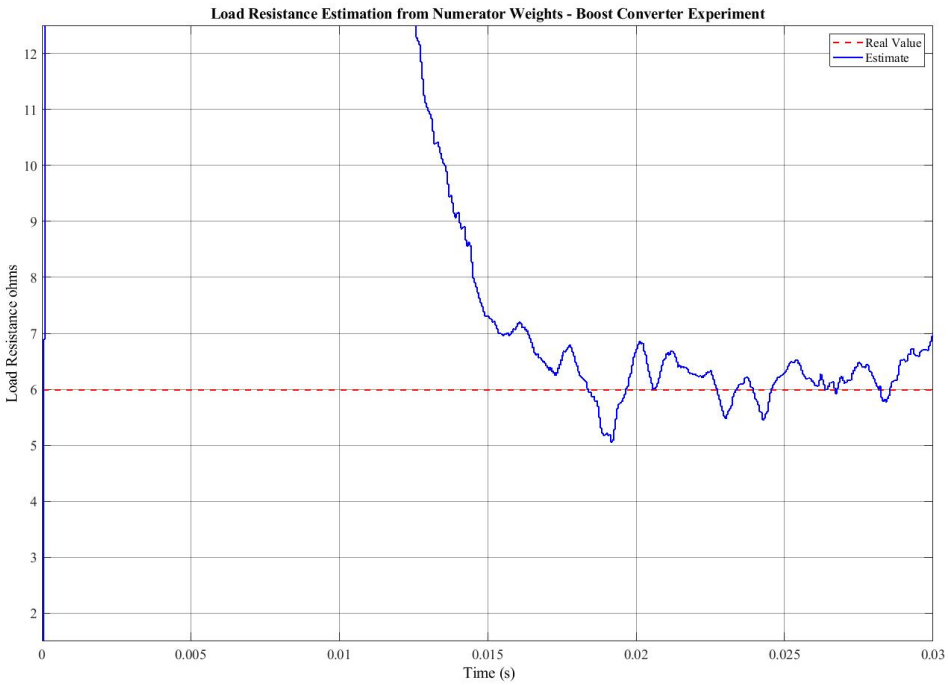

Figure 6.15 Load Resistance Estimation from Numerator Weights - Boost Converter Experiment – 1

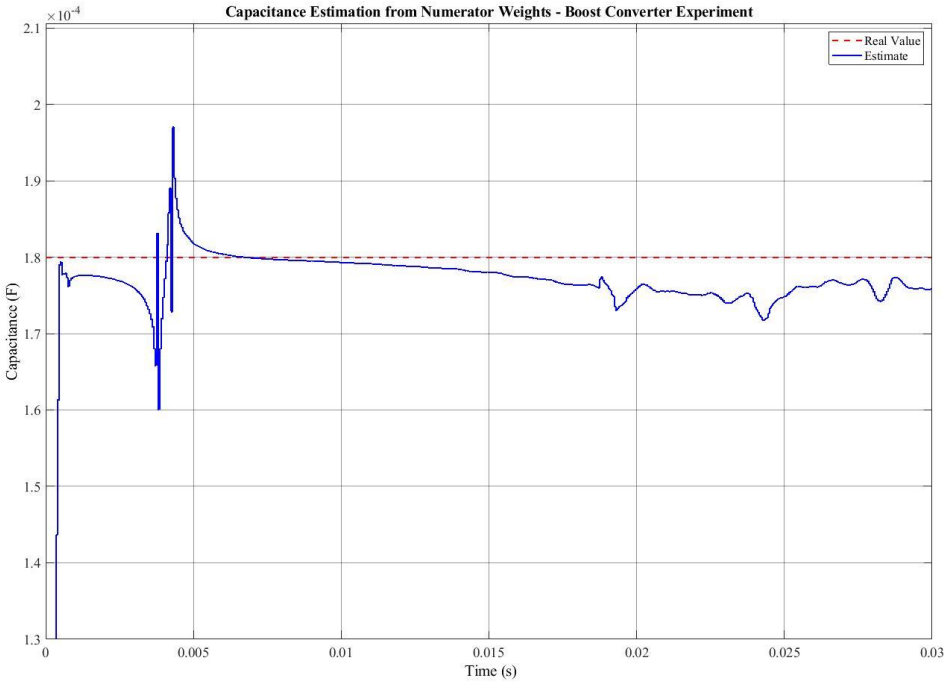

Figure 6.16 Capacitance Estimation from Numerator Weights – Boost Converter Experiment – 1

All the experimental results for the boost converter have been filtered by the four-tap moving average filter. Firstly, the system parameters are estimated from the numerator weights of TEOS model as shown in Figures 6.15 and 6.16. In Figure 6.15, the estimation error is within ±15%, and the capacitance estimation error in Figure 6.16 is within 6%, which is a good level of accuracy for the practical experiment. The two estimation results from the numerator weights have answered the question in the previous section, that the numerator weights parametric estimation results can accurately describe the system characteristics.

Figures 6.17 and 6.18 shows the system parameters estimation from the denominator weights of the boost converter. The load resistance estimation in Figure 6.17 tends to be stable between 0.015 s and 0.025 s, with an error in the limits of ±15%, but ends with a big oscillation for the last 0.005 s. However, for the capacitance estimation, it took about 0.017 s to reach the correct value, and then starts to oscillate a lot around the real value for the last 0.013 s. From the two results, although they have several oscillations, it can still be observed that the system parameters estimation tends to give an accurate results from the relationships we derived from the TEOS model. Until now, the TEOS model has proven to be able to help parametric estimation of both the minimum-phase buck converter and, especially, the non-minimum phase boost converter. Based on the simulation results and the experimental results in this chapter,

the TEOS model also has a great possibility for addressing the parametric estimation problem for the other non-minimum phase converters.

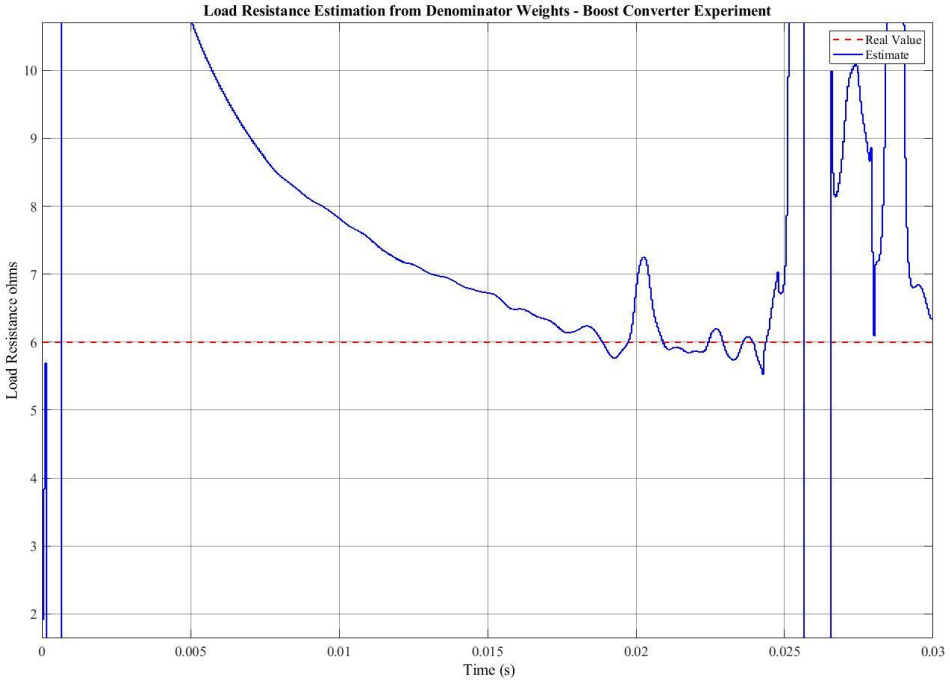

Figure 6.17 Load Resistance Estimation from Denominator Weights - Boost Converter Experiment - 1

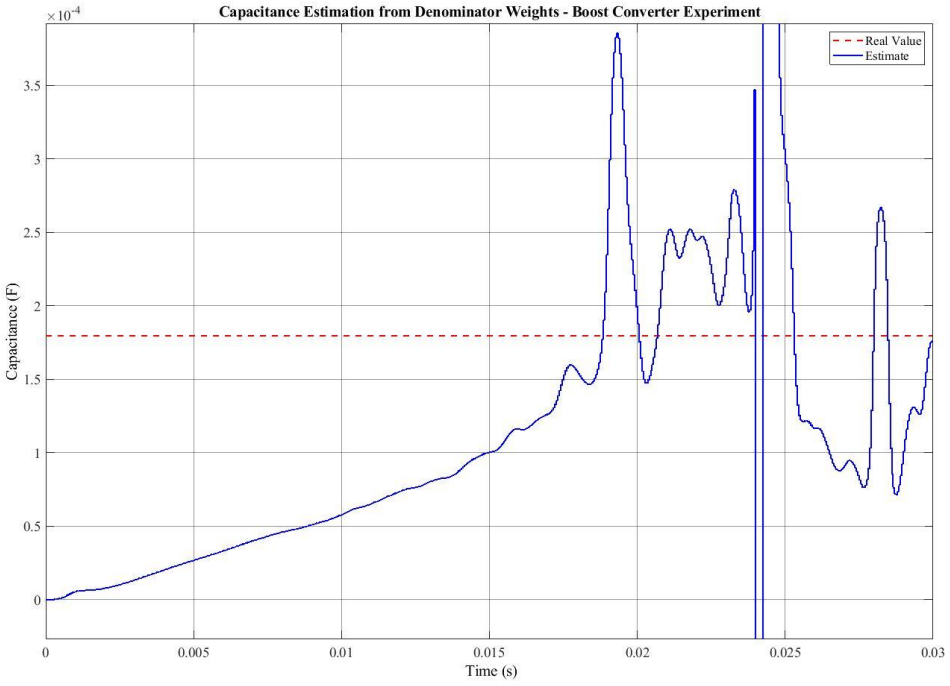

Figure 6.18 Capacitance Estimation from Denominator Weights - Boost Converter Experiment - 1

6.3 Chapter Summary

In this chapter, all the important experimental results are presented. In Appendix D and E, another set of estimation results, which used a sampled set of 600 input and output data are presented. Seven points can be concluded from the two sets of experimental results as follows:

1. Using different sampling points during a switching instant will have a slight influence on the dynamic response of the system, which will consequently have an effect on the parametric estimation performances.
2. Both models can work well on the buck converter with their specific sampling mechanism.
3. The numerator weights of the averaged model do not fit to the parametric estimation results of the boost converter. However, the TEOS model weights fit more to the estimation results compared to the averaged model.
4. The TEOS model works well, not only for the parametric estimation but also for the system parameter (load resistance and capacitance) estimations. Due to some practical reasons, such as noise, manufacturing or soldering defects, components tolerance etc., the experimental results are not as accurate as in the simulation test.
5. The parametric estimation results, and especially the system parameters estimation results from the numerator weights of the boost converter, have verified the validity of the TEOS model as a solution to the application of boost converter SI. In addition, it has shown a great possibility for the TEOS model to realise parametric estimation of other non-minimum phase converters.
6. Compared to the simulation results in Chapter 4, the experimental results showed more external interference, especially for the system parameters estimation from the denominator weights of the boost converter. Therefore, for other practical applications, more consideration should be paid to an anti-interferences design.
7. The experimental results have shown that both models, with their specific sampling mechanism, will have a good level of accuracy in the application of SIs, which could benefit the applications of adaptive controller design.

In summary, this chapter is the key chapter in this thesis including all the experimental results which can be used to verify the proposed solution in the practical situation. The experimental results have proven that the proposed TEOS model is a solution to the existing non-minimum phase converter SI problem. This can specifically improve the estimation accuracy about 20% when estimating the numerator weights of the mathematical discrete transfer function. This is very likely to also work on other non-minimum phase converters as it has been tested with buck-boost converter by simulation. In addition, the experimental results also verify the possibility of system parameters estimation from the TEOS model, which will be a novel method for system parameters estimation in the literature and also possibly benefit the area of fault detection and system components monitoring. These are the two main achievement arising from this research.

CHAPTER 7 CONCLUSIONS AND FUTURE WORK

Conclusions

Parametric estimation technique is essential for a variety of SMPCs applications. Its function is to estimate an accurate model of a system, which can further help adaptive controller to determine controller gains or help fault detection to monitor the system parameters without breaking a device. However, parametric estimation of non-minimum phase converters is not working well especially for estimating the numerator weights of a mathematical model. This research has analysed the reasons behind the problem and then proposed a solution to address this existing problem.

The causes to the problem have been analysed, and finally found that non-minimum phase converters have a RHP-zero in its continuous transfer function, which can be treated as a delay term. This RHP-zero which reflects in the circuit operation is that the output voltage will have an initial drop during a step increase of duty-cycle, which is a wrong response direction. In addition, if analysing it from frequency response, it can be found that there is no specific relationship between magnitude response and frequency response for a non-minimum phase system, thus, it can be tricky for parametric estimation technique to estimate an accurate model from the responses of a system.

There are several possible ways to resolve this problem. When analysing the output voltage response of a boost converter, a phenomenon has been found that when sampling during switch off-time with trailing edge PWM, the RHP-zero effect can be ignored as much as possible as shown in the figure 2.7. Consequently, this can be a very possible fit to the parametric estimation technique of a non-minimum phase converter system. Then we have modelled the off-time sampling line as shown in the figure 2.7 by small signal equations, and transformed it into a discrete form, namely TEOS model. Then it has been tested in simulation on a boost converter and a buck-boost converter. From the simulation results in the chapter 4, it is obvious that the TEOS model is a best-fit for the parametric estimation of the non-minimum phase converters, in estimating all the four parameters including the numerator weights. And the accuracy of estimating the numerator weights has improved about 20% than the commonly used state-space averaged model. Then this model has also been tested on a classic minimum phase converter, a buck converter. And the results in the section 4.4.1 also showed a good estimation result. All the simulation tests are within 1.5% estimation error. Finally, the proposed method has been tested in the practical experiment in the chapter 6. The experimental results in the

chapter 6 have shown that in the practical experiment, there are more oscillations. But the average value of oscillations and the trends are much more fit to the TEOS model. And also with the help of the correct system parameters estimation test results, it can be shown that TEOS model is accurate to describe the dynamics response of a system either on a minimum phase converter and a non-minimum phase converter.

Another big contribution of this research proposes a new system parameters monitoring approach which cannot be found in the literature review. Based on the analysis of the TEOS model, it can be found that system parameters can be extracted from the model. And with the help of parametric estimation, it is also possible to estimate the system parameters. However, the final TEOS model is very complicated. In section 2.5, the TEOS model has been simplified to a maximum degree to provide a simple way to estimate the system parameters without sacrificing much estimation accuracy. Due to the structure of the mathematical transfer function, system parameters can be estimated from either numerator weights or denominator weights. Then the simplified TEOS model has been tested in both simulation and practical experiments. In the simulation results shown in the section 4.5, it can be found that TEOS model is totally functional in describing the relationships between the transfer function weights and system parameters. However, for the estimation from transfer function denominator weights, it has much more oscillations compared to the estimation from numerator weights. And this issue also appears in the practical experimental results shown in the section 6.3. A proper filter is necessary if using the proposed approach and estimating the system parameters from denominator weights. But in general, TEOS model is able to be a novel technique for monitoring the system parameters.

In addition, the existing modelling methods and system identification methodology for SMPC are introduced in the chapter 2 and chapter 3. And due to its robustness and popularity of RLS adaptive algorithm, RLS is adopted for the following parametric estimation and system parameters estimation tests. The experimental platform is also presented in the chapter 5. The DSP settings and the designed boost converter board are presented as well.

In summary, TEOS model is verified to be a solution to the existing parametric estimation problem of non-minimum phase converters by both simulation and practical experimental results. And it can also provide a novel way for system parameters monitoring just by mathematical relationships without breaking a device.

Future work

From this research, there are several works which are worth trying in the future which are listed as below.

(1) The proposed solution method in this research is based on the modelling method. There are also several other possible ways to address this problem, which can be the improvement of adaptive algorithm, or the combination with a proper control scheme to give an accurate parametric estimation result of non-minimum phase converters.

(2) The simulation results are on-line estimation, which have presented a very nice set of estimation results with less estimation error and a stable response. However, in the practical experiment, on-line estimation is also worth trying which might give a much better result compared to the off-line estimation. Especially for the system parameters estimation results in figure 6.17 and figure 6.18, there are more oscillations at the end of the estimation. This might be fixed if using on-line estimation.

(3) In the chapter 2, two ways has been provided for estimating the system parameters which are either from numerator weights or denominator weights. System parameters relationships from both numerator weights and denominator weights was also obtained, which can possibly give a more accurate system parameters estimation result.

(4) In the practical estimation results, some un-ignorable noises have been observed. The simulation results have also shown that the system parameters estimation by TEOS model is sensitive to the noise signal. Thus, a better converter board design with filters and less components tolerance is also a good attempt in the future work.

(5) With the help of the proposed system parameters estimation approach, it is worth trying to design a novel sensorless fault detection scheme.

(6) As parametric estimation is also a key tool for the adaptive control system. Further attempts can also be done to design an adaptive controller for a non-minimum phase converter with the correct parametric estimation results by TEOS model.

APPENDIX A SELECTED COMPONENTS READINGS

The specifications of the MOSFET for boost converter design is shown in table A.1.

V_{DS}	**40**	**V**
$R_{DS(on),\ max}$	**1.4**	**mΩ**
I_D	**100**	**A**
Q_{OSS}	**54**	**nC**
Q_g *(0V… 10V)*	**61**	**nC**

Table A.1 MOSFET Product Summary

The specifications of the MOSFET Driver for boost converter design is shown in table A.2.

		MIN	MAX	UNIT
Supply voltage	VDD	–0.3	20	V
OUTA, OUTB voltage	DC	–0.3	VDD + 0.3	
	Repetitive pulse < 200 ns(3)	–2	VDD + 0.3	
Output continuous source/sink current	I_{OUT_DC}		0.3	A
Output pulsed source/sink current (0.5 µs)	I_{OUT_pulsed}		5	
INA, INB, INA+, INA–, INB+, INB–, ENA, ENB voltage(4)		–0.3	20	V
Operating virtual junction temperature, T_J		–40	150	°C
Lead temperature	Soldering, 10 s		300	
	Reflow		260	
Storage temperature, T_{stg}		–65	150	°C

Table A.2 MOSFET Driver Product Summary

The specifications of the Instrumentation Amplifier for boost converter design is shown in table A.3.

Specified from −55°C to 125°C	**0.9 µV/°C maximum input offset voltage drift** **5 ppm/°C maximum gain drift (G = 1)**
Low power	**2.3 mA maximum supply current**
Low noise	**3.2 nV/√Hz maximum input voltage noise at 1 kHz** **200 fA/√Hz current noise at 1 kHz**
Excellent ac specifications	**2 MHz bandwidth (G = 100)** **0.6 µs settling time to 0.001% (G = 10)** **80 dB minimum CMRR at 20 kHz (G = 1)**
High precision DC performance	**84 dB CMRR minimum (G = 1)** **2 nA maximum input bias current**

Table A.3 Instrumentation Amplifier Features

Appendix A Selected Components Readings

Table A.4 shows all the components selected for the boost converter design.

Components	Part Number	Package
MOSFET Driver	UCC27525	PSD(S-PWSON-N8) WSON(8)
Power MOSFET	BSC014N04LS	PG-TDSON-8FL
Instrumentation Amplifier	AD8421-EP	RM-8
Current Sensor	ACS756KCA-050B-PFF-T	Sketch
Linear Voltage Regulator 1	LP3990MF-3.3/NOPB	SOT-23
Linear Voltage Regulator 2	UA78M05IDCY	SOT-223-3
2Ω, ±1%, 50W Ohmite 850 Series Aluminium Resistor	N/A	Panel Mount
5Ω, ±1%, 50W Ohmite 850 Series Aluminium Resistor	N/A	Panel Mount
1Ω, ±1%, 50W Ohmite 850 Series Aluminium Resistor	N/A	Panel Mount
5kΩ Resistor	CRCW08055K00FKTA	0805 [2012 Metric]
10kΩ Resistor	RR0816P-103-B-T5	0603 [1608 Metric]
15kΩ Resistor	CPF0805B15KE1	0805 [2012 Metric]
20kΩ Resistor	ERA8AEB203V	1206 [3216 Metric]
Wired-To-Board Connector	MOLEX 172064-0006	Sketch
Wired-To-Board Terminal Block	MULTICOMP MA522-500M02	Sketch
Schottky Diode	SD101A SB00018/D8	DO-35
180µF Capacitor	A767MU187M1VLAE028	Radial Can
10µF Capacitor	50SVPF10M	Radial Can

1µF Capacitor X7R	C0805C105J3RACTU	0805 [2012 Metric]
0.33µF Capacitor X7R	C1608X7R1H334K080AC	0603 [1608 Metric]
100Pf Capacitor C0G/NP0	0603N101J500CT	0603 [1608 Metric]
10pF Capacitor C0G/NP0	C0603C100J5GACTU	0603 [1608 Metric]
4.7Pf Capacitor C0G/NP0	MCMT18N4R7C100CT	0603 [1608 Metric]

Table A.4 Selected Components for PCB Design

APPENDIX B SIMULINK BLOCK SETTINGS

The block diagram in Simulink is shown in figure B.1.

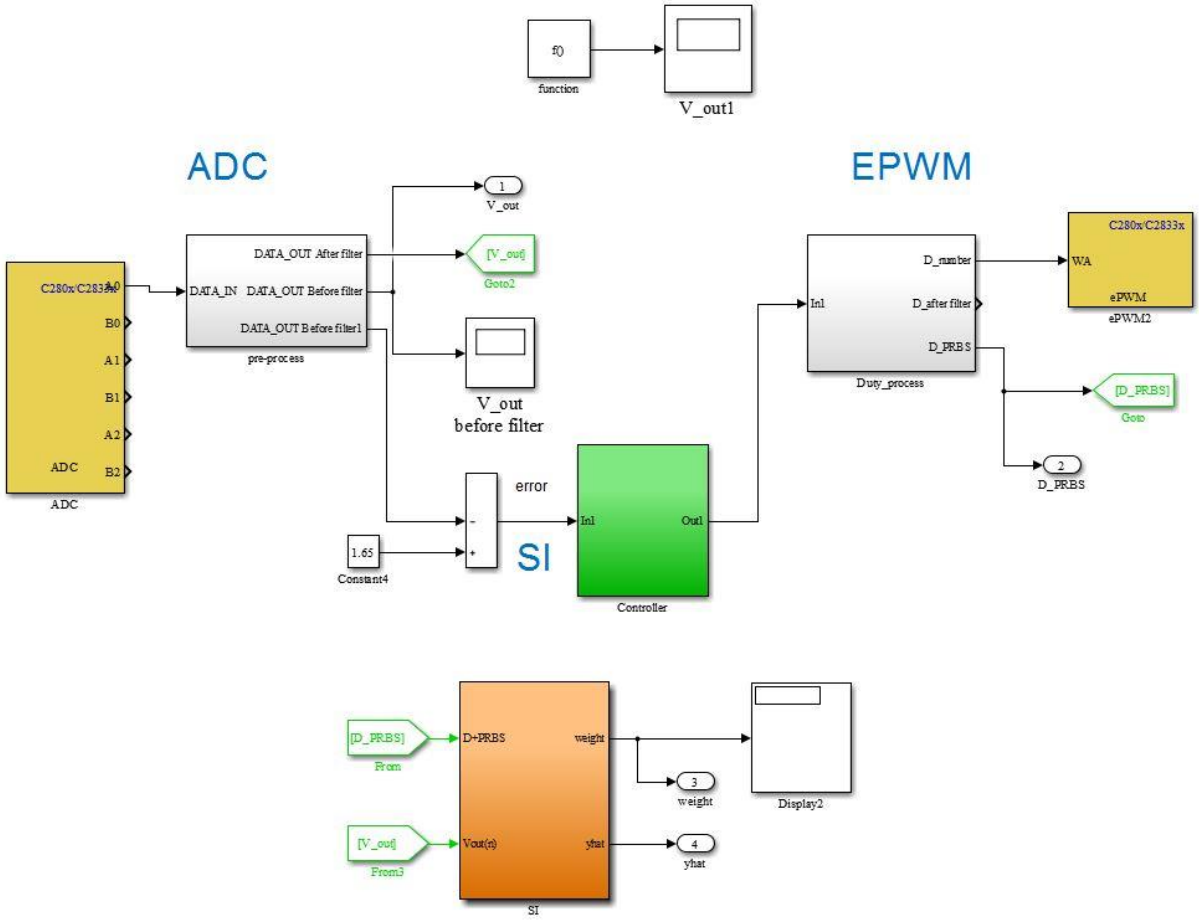

Figure B.1 Simulink Block Diagram

Figure B.2 shows what's inside the Duty-process block for generating the input data to the ePWM block.

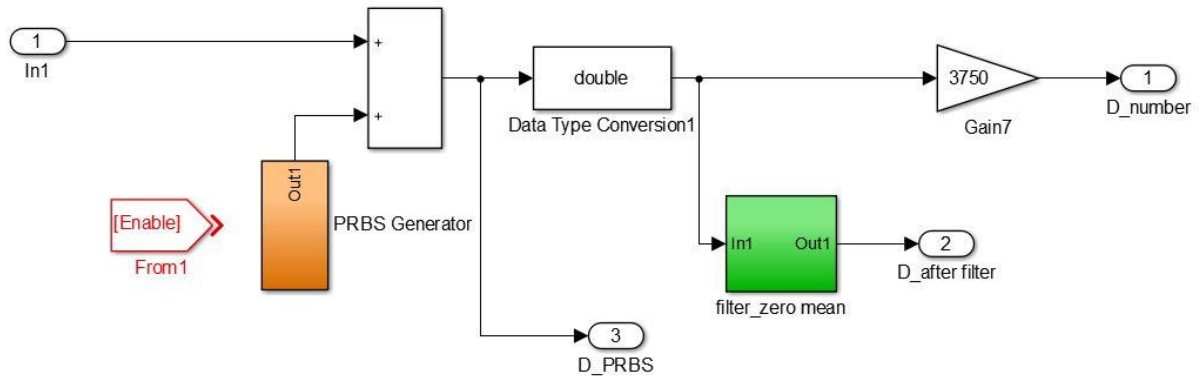

Figure B.2 Duty-process Block of EPWM

Figure B.3 shows what's inside the Pre-process block to process the data coming out of the ADC block.

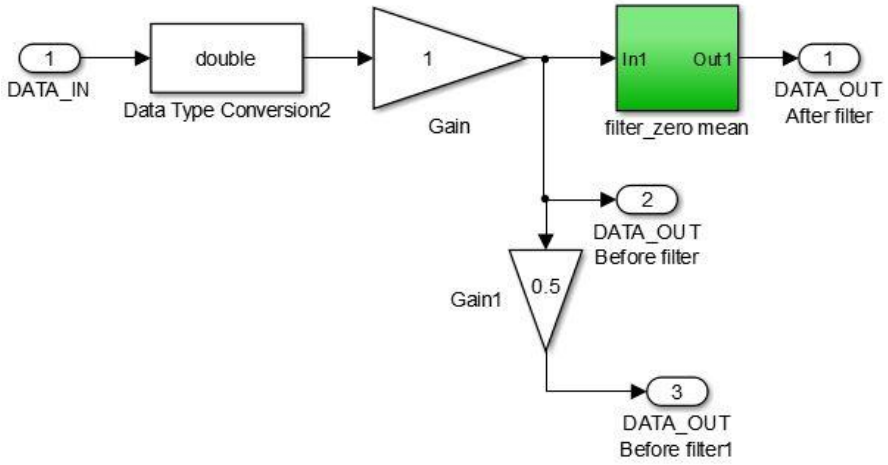

Figure B.3 Pre-process Block of ADC

Figure B.4 shows the deadband settings of ePWM2 block.

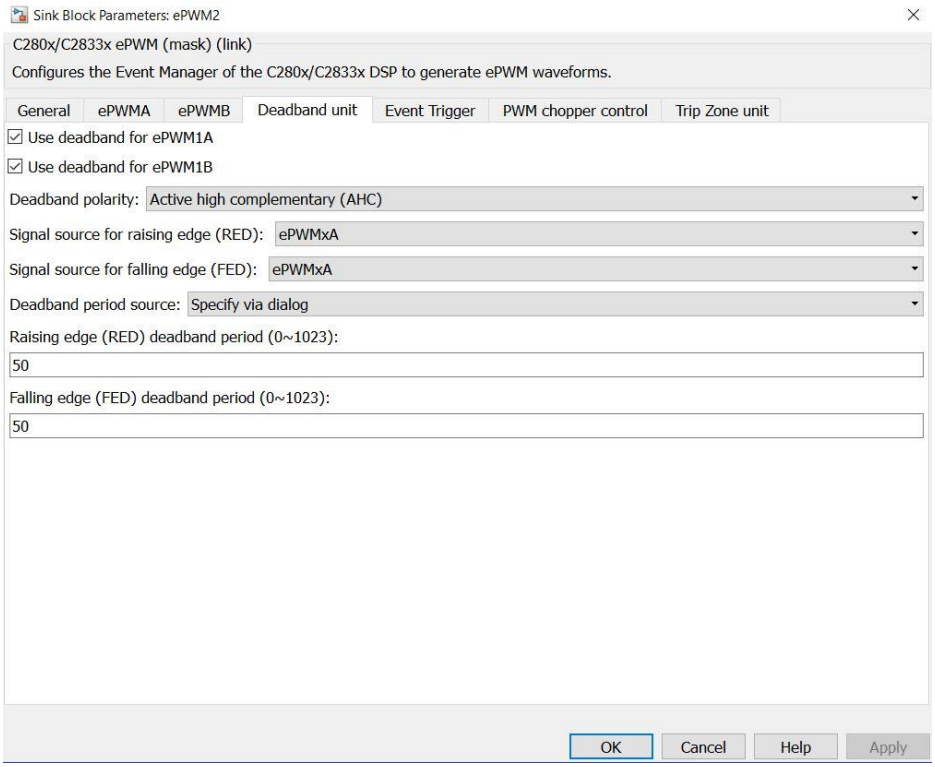

Figure B.4 Deadband Setting

APPENDIX C TEST BOARDS

Figure C.1 shows the regulator test PCB design.

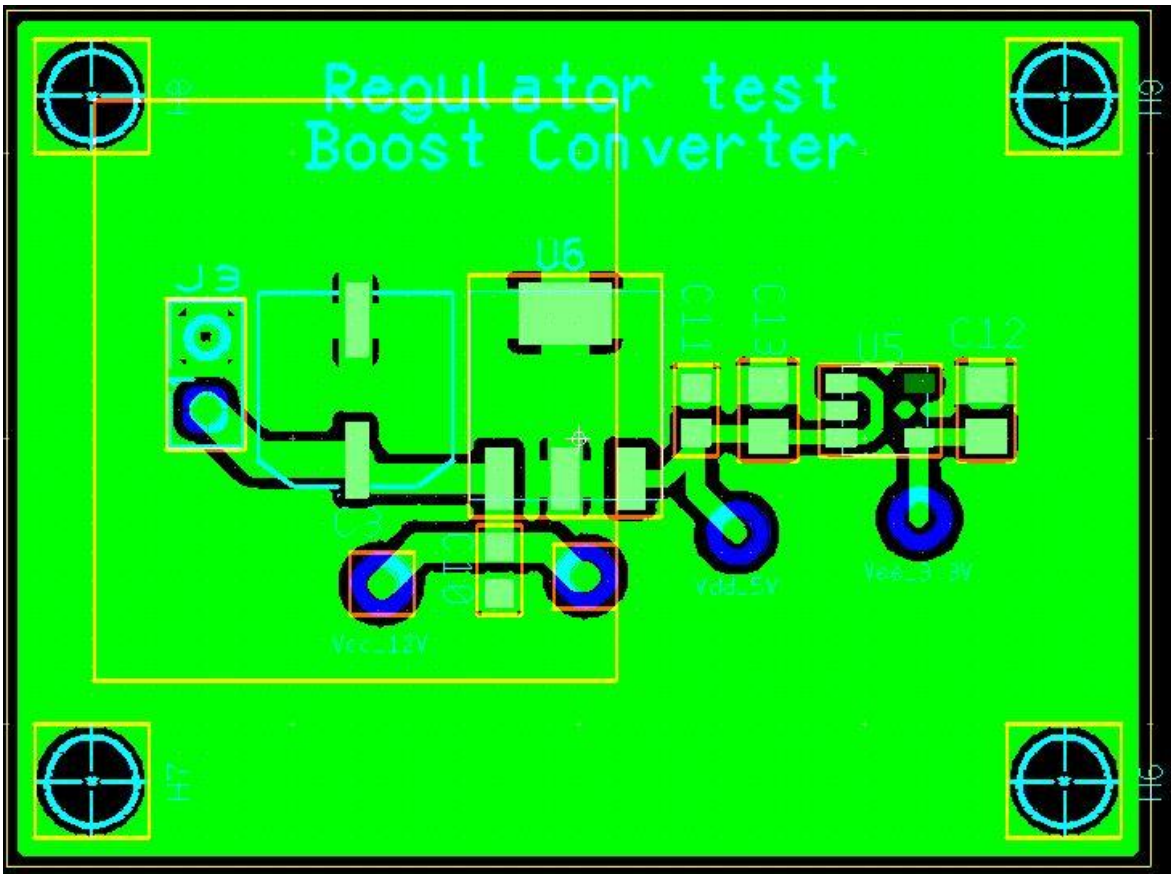

Figure C.1 Regulator Test Board

Figure C.2 shows the MOSFET Driver test PCB design.

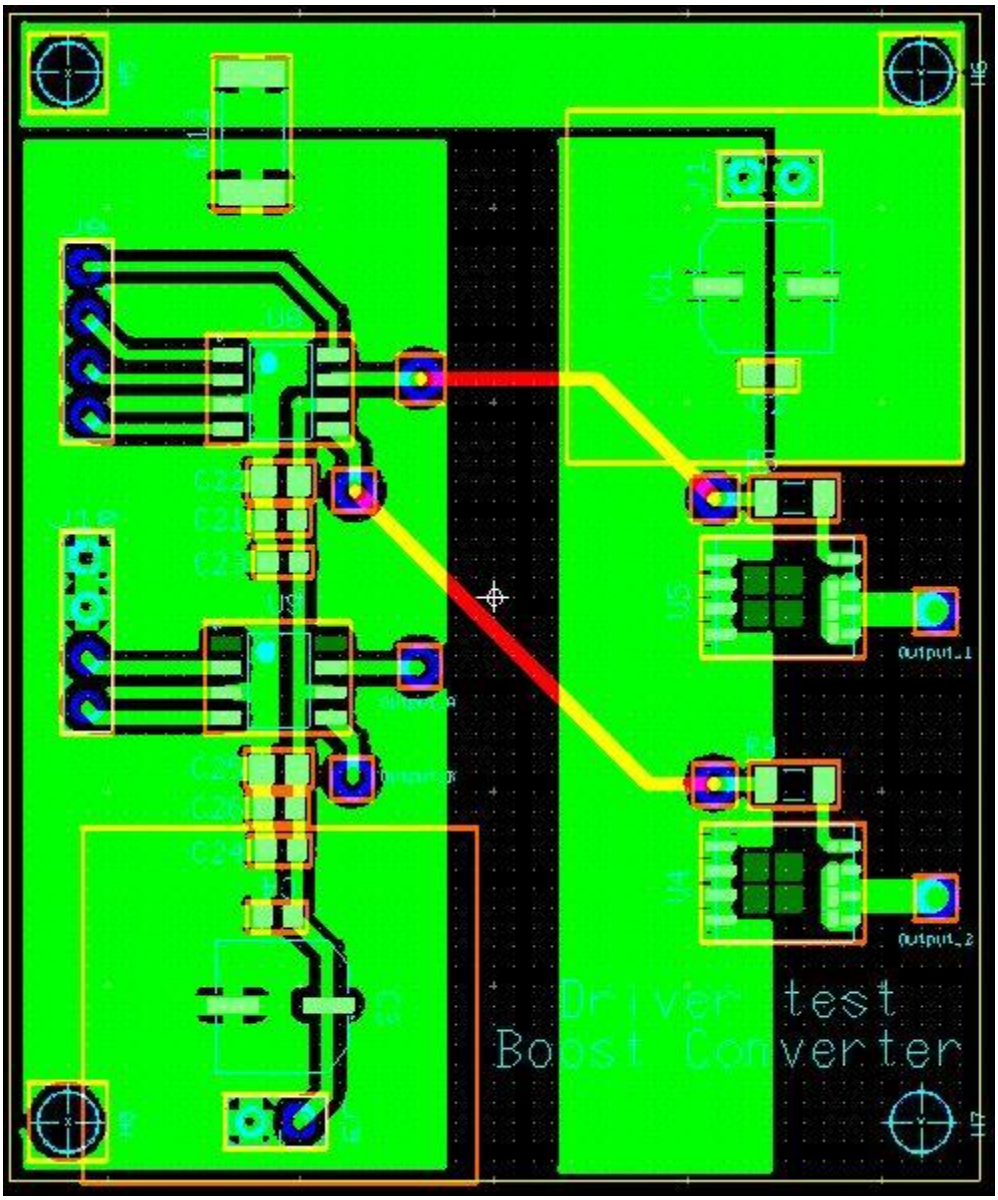

Figure C.2 MOSFET Driver Test Board

Figure C.3 shows the sensor test PCB design.

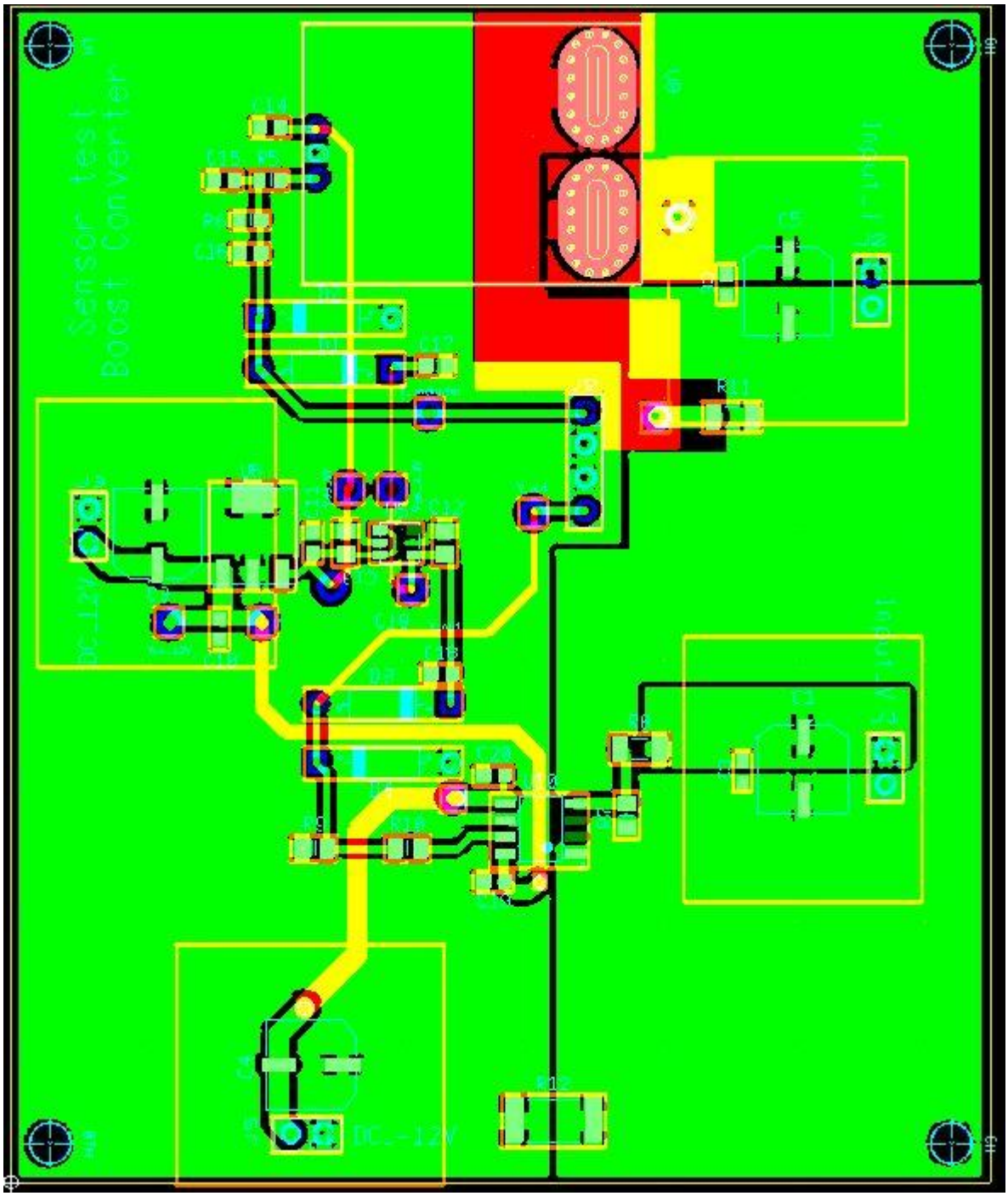

Figure C.3 Sensor Test Board

APPENDIX D SECOND SET EXPERIMENTAL RESULTS FOR BUCK CONVERTER

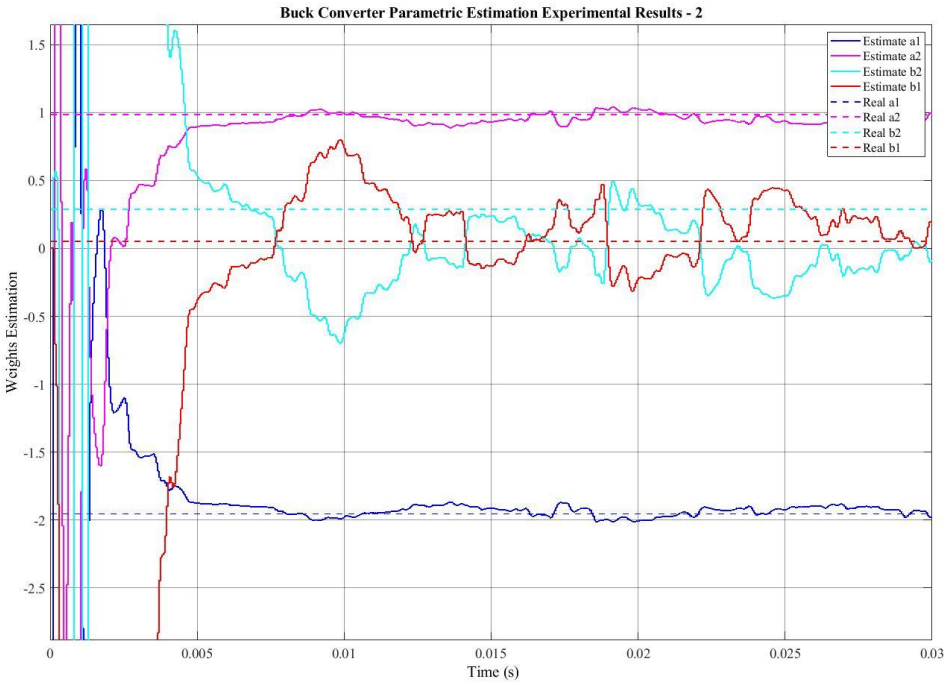

Figure D.1 Buck Converter Parametric Estimation Results – 2

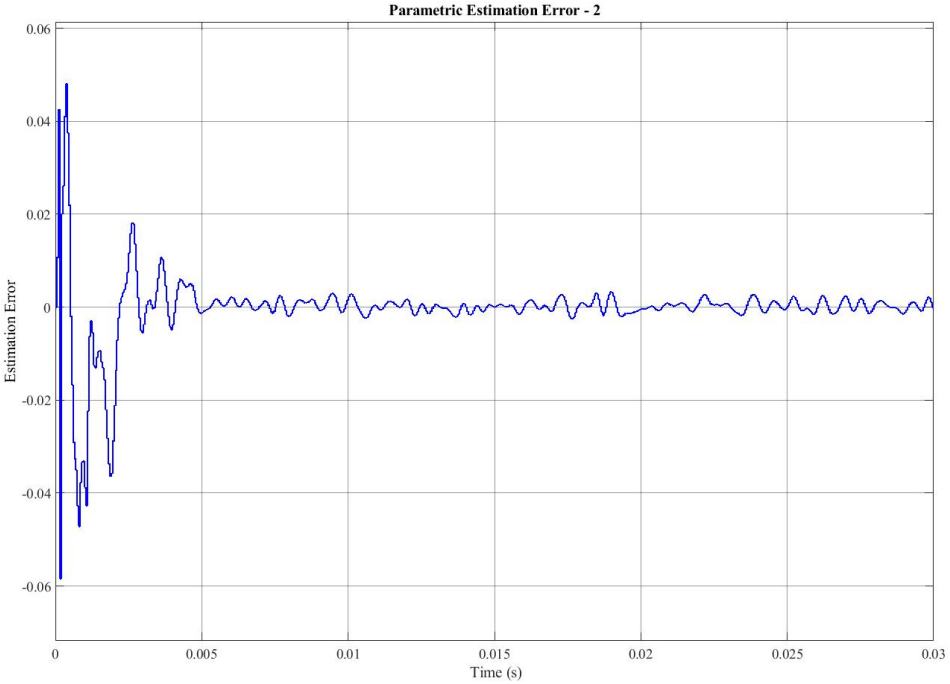

Figure D.2 Buck Parametric Estimation Error - 2

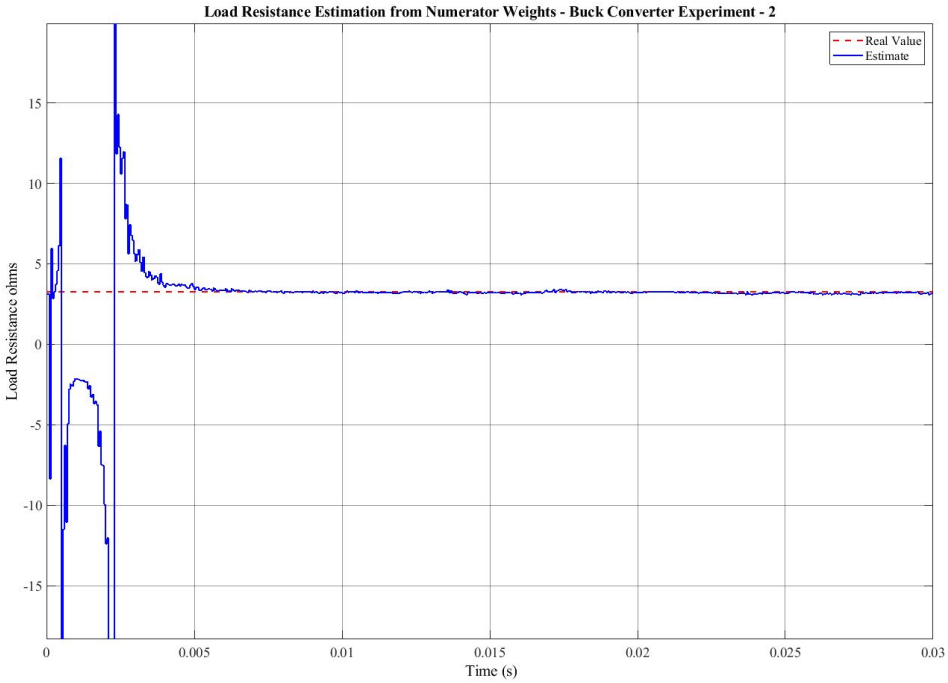

Figure D.3 Load Resistance Estimation from Numerator Weights – Buck Converter Experiment – 2

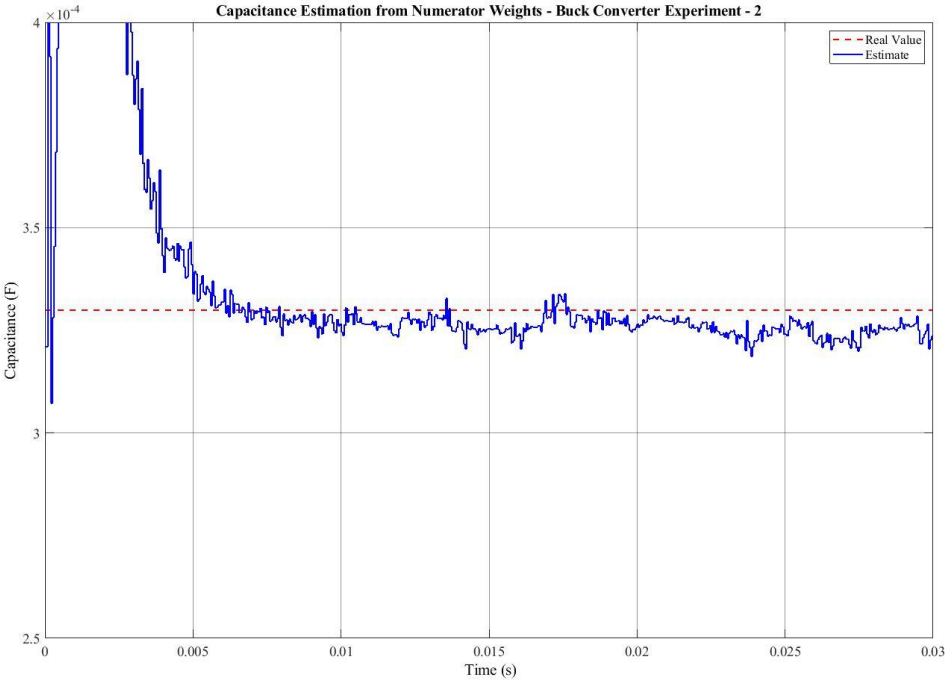

Figure D.4 Capacitance Estimation from Numerator Weights – Buck Converter Experiment 2

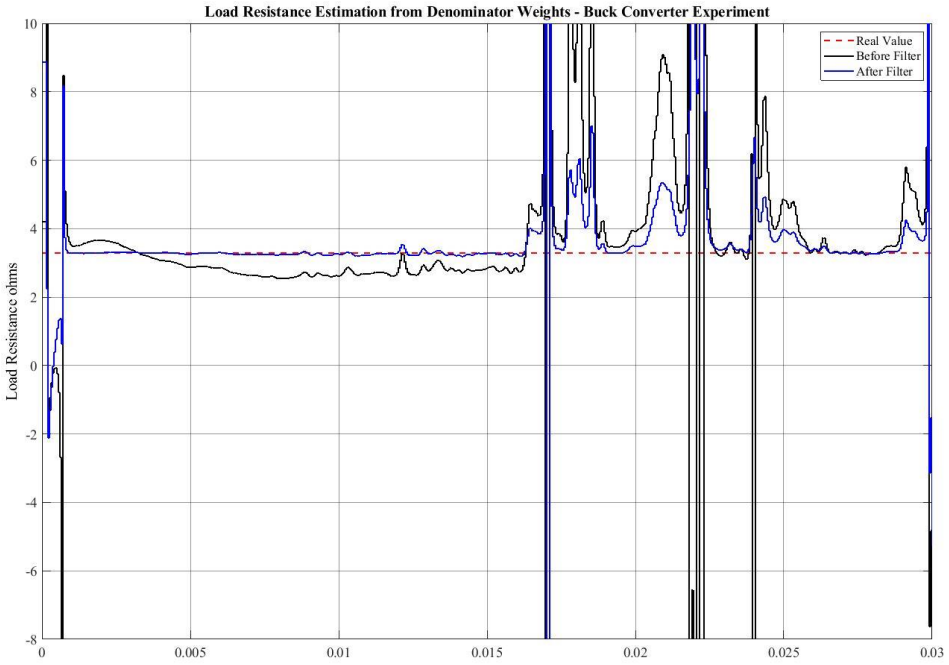

Figure D.5 Load Resistance Estimation from Denominator Weights – Buck Converter Experiment

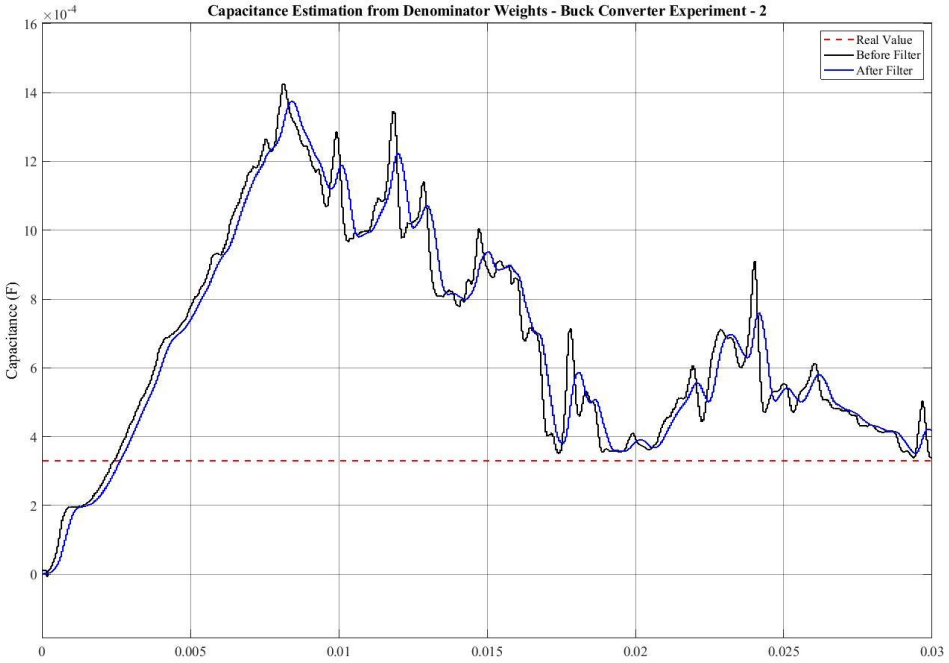

Figure D.6 Capacitance Estimation from Denominator Weights - Buck Converter Experiment

APPENDIX E SECOND SET EXERIMENTAL RESULTS FOR BOOST CONVERTER

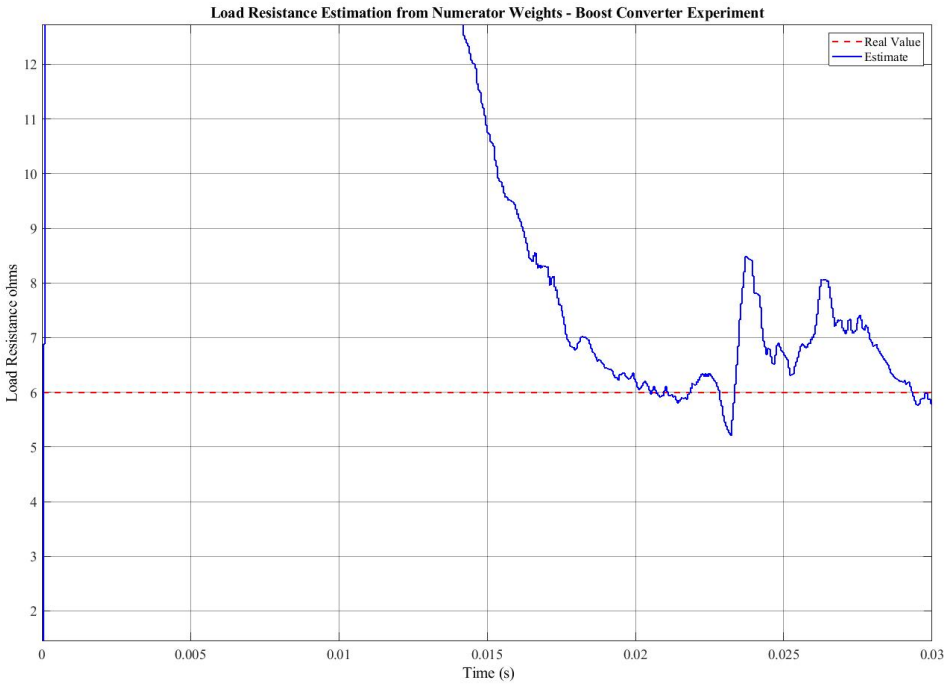

Figure E.1 Load Resistance from Numerator Weights - Boost Converter Experiment – 2

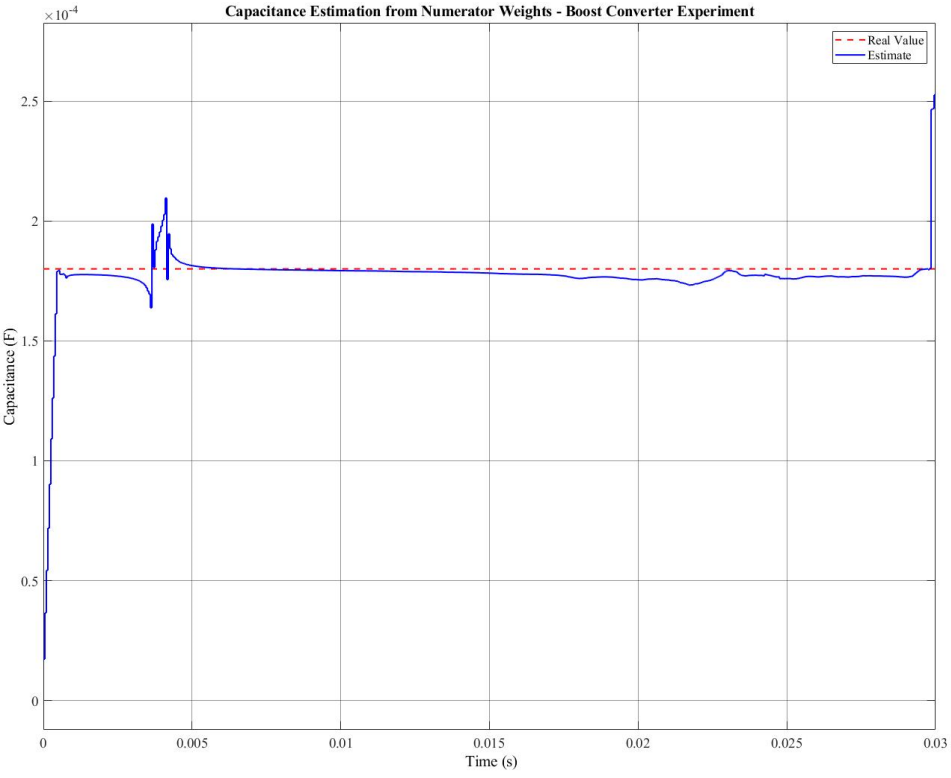

Figure E.2 Capacitance Estimation from Numerator Weights - Boost Converter Experiment - 2

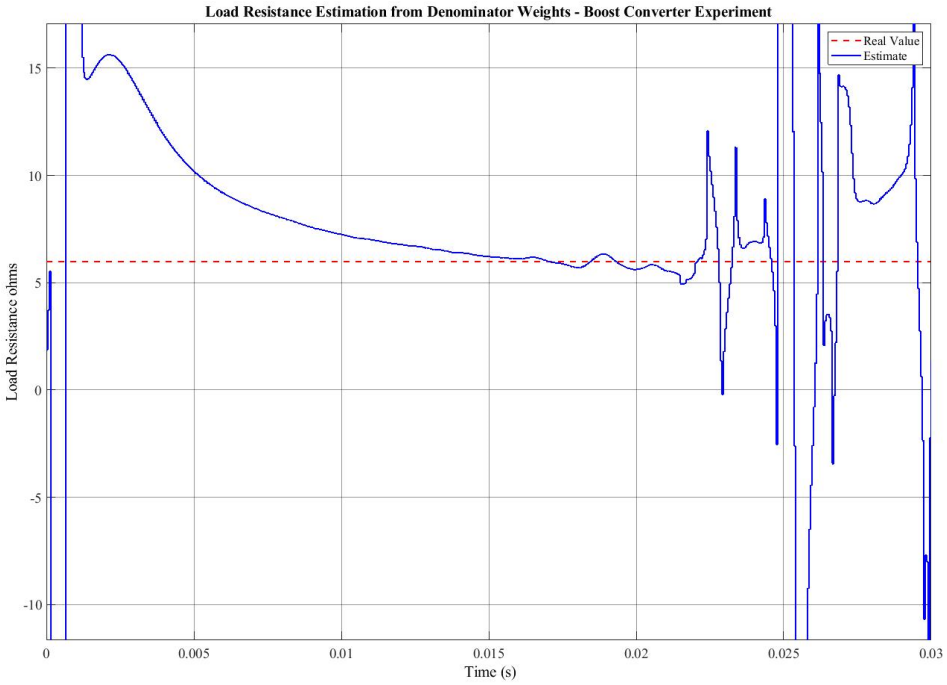

Figure E.3 Load Resistance Estimation from Denominator Weights - Boost Converter Experiment – 2

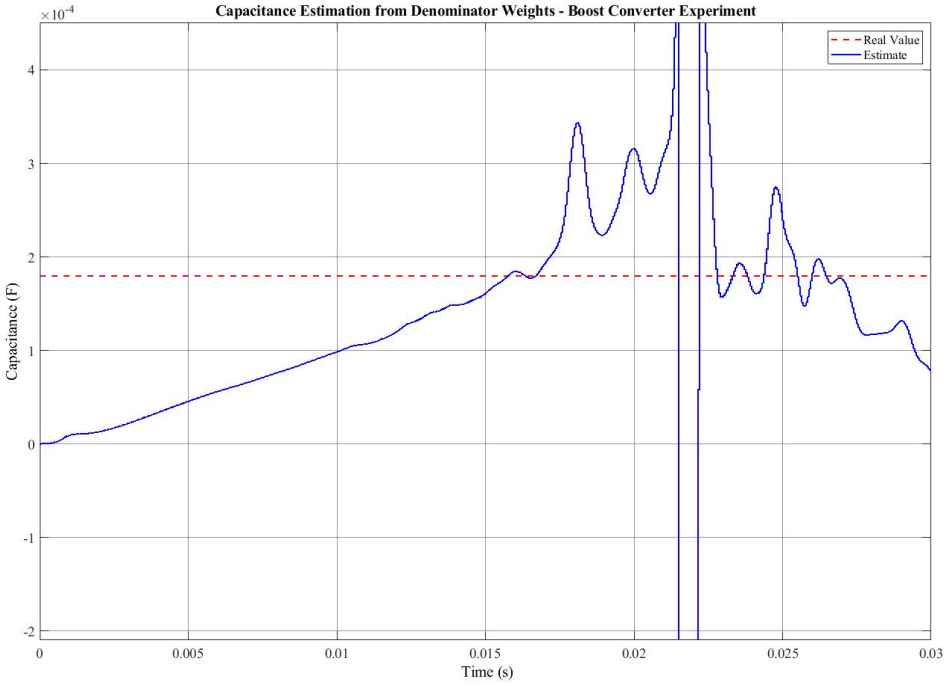

Figure E.4 Capacitance Estimation from Denominator Weights – Boost Converter Experiment – 2

REFERENCES

[1] A. El Aroudi, D. Giaouris, H. H.-C. Iu, and I. A. Hiskens, "A review on stability analysis methods for switching mode power converters," *IEEE Journal on Emerging and Selected Topics in Circuits and Systems,* vol. 5, no. 3, pp. 302-315, 2015.

[2] M. Forouzesh, Y. P. Siwakoti, S. A. Gorji, F. Blaabjerg, and B. Lehman, "Step-Up DC–DC Converters: A Comprehensive Review of Voltage-Boosting Techniques, Topologies, and Applications," *IEEE Transactions on Power Electronics,* vol. 32, no. 12, pp. 9143-9178, 2017.

[3] J. Poon, P. Jain, C. Spanos, S. K. Panda, and S. R. Sanders, "Fault prognosis for power electronics systems using adaptive parameter identification," *IEEE Transactions on Industry Applications,* vol. 53, no. 3, pp. 2862-2870, 2017.

[4] C. Wang, M. Armstrong, and S. Gadoue, "System identification and adaptive control of a DC-DC converter using a current balancing ON/OFF control technique for optimal transient performance," in *Power Electronics and Applications (EPE'15 ECCE-Europe), 2015 17th European Conference on*, 2015, pp. 1-10: IEEE.

[5] R. Li, M. Armstrong, S. Gadoue, and C. Wang, "On-line parameter estimation of non-minimum phase switch mode power DC-DC boost converters," 2016.

[6] S. Padhee, U. C. Pati, and K. Mahapatra, "Modelling switched mode DC-DC converter using system identification techniques: A review," in *Electrical, Electronics and Computer Science (SCEECS), 2016 IEEE Students' Conference on*, 2016, pp. 1-6: IEEE.

[7] M. Cacciato, G. Nobile, G. Scarcella, and G. Scelba, "Real-time model-based estimation of SOC and SOH for energy storage systems," *IEEE Transactions on Power Electronics,* vol. 32, no. 1, pp. 794-803, 2017.

[8] Z. Bubnicki, *Modern control theory*. Springer Science & Business Media, 2005.

[9] L. A. Zadeh, "From circuit theory to system theory," *Proceedings of the IRE,* vol. 50, no. 5, pp. 856-865, 1962.

[10] P. Eykhoff, *Trends and progress in system identification: IFAC Series for Graduates, Research Workers & Practising Engineers*. Elsevier, 2014.

[11] L. Ljung, "Convergence analysis of parametric identification methods," *IEEE transactions on automatic control*, vol. 23, no. 5, pp. 770-783, 1978.

[12] B. Miao, R. Zane, and D. Maksimovic, "Automated digital controller design for switching converters," in *IEEE Power Electronics Specialists Conference*, 2005, vol. 36, p. 2729.

[13] D. M. Sable, B. H. Cho, and R. B. Ridley, "Use of leading-edge modulation to transform boost and flyback converters into minimum-phase-zero systems," *Power Electronics, IEEE Transactions on*, vol. 6, no. 4, pp. 704-711, 1991.

[14] R. Bellman and R. Kalaba, "DYNAMIC PROGRAMMING AND ADAPTIVE PROCESSES--1: MATHEMATICAL FOUNDATION," RAND CORP SANTA MONICA CA1959.

[15] J. E. Bertram, "Control by stochastic adjustment," *Transactions of the American Institute of Electrical Engineers, Part II: Applications and Industry*, vol. 78, no. 6, pp. 485-491, 1960.

[16] D. D. Donalson and C. Leondes, "A Model Referenced Parameter Tracking Technique for Adaptive Control Systems I-The Principle of Adaptation," *IEEE Transactions on Applications and Industry*, vol. 82, no. 68, pp. 241-252, 1963.

[17] A. White, "Analysis and design of model-reference adaptive control systems," in *Proceedings of the Institution of Electrical Engineers*, 1966, vol. 113, no. 1, pp. 175-184: IET.

[18] R. Dressler, "An approach to model-referenced adaptive control systems," *IEEE Transactions on Automatic Control*, vol. 12, no. 1, pp. 75-80, 1967.

[19] C. Wells, "An approximation of the Kalman filter equations," *IEEE Transactions on Automatic Control*, vol. 13, no. 4, pp. 445-445, 1968.

[20] R. B. Shipley and D. Coleman, "A new direct matrix inversion method," *Transactions of the American Institute of Electrical Engineers, Part I: Communication and Electronics*, vol. 78, no. 5, pp. 568-572, 1959.

[21] V. Bobál, J. Böhm, J. Fessl, and J. Machácek, *Digital Self-tuning Controllers: Algorithms, Implementation and Applications*. Springer Science & Business Media, 2006.

[22] K. J. Aström, "Theory and applications of adaptive control," *IFAC Proceedings Volumes,* vol. 14, no. 2, pp. 737-748, 1981.

[23] H. Jianguo, G. Junchao, and Z. Qian, "On-line real time realization and application of adaptive fuzzy inference neural network," *Journal of Systems Engineering and Electronics,* vol. 11, no. 1, pp. 67-74, 2000.

[24] B. K. Bose, "Fuzzy logic and neural networks in power electronics and drives," *IEEE Industry applications magazine,* vol. 6, no. 3, pp. 57-63, 2000.

[25] Y. Tang and L. Xu, "Fuzzy logic application for intelligent control of a variable speed drive," *IEEE Transactions on Energy Conversion,* vol. 9, no. 4, pp. 679-685, 1994.

[26] K. J. Åström and B. Wittenmark, *Adaptive control*. Courier Corporation, 2013.

[27] I. D. Landau, Y. D. Landau, and G. Zito, *Digital control systems: design, identification and implementation*. Springer Science & Business Media, 2006.

[28] D. G. Shaw, S. W. Cichanowski, and A. Yializis, "A changing capacitor technology-failure mechanisms and design innovations," *IEEE Transactions on Electrical Insulation,* no. 5, pp. 399-413, 1981.

[29] H. Wang *et al.*, "Transitioning to physics-of-failure as a reliability driver in power electronics," *IEEE Journal of Emerging and Selected Topics in Power Electronics,* vol. 2, no. 1, pp. 97-114, 2014.

[30] S. Yang, D. Xiang, A. Bryant, P. Mawby, L. Ran, and P. Tavner, "Condition monitoring for device reliability in power electronic converters: A review," *IEEE Transactions on Power Electronics,* vol. 25, no. 11, pp. 2734-2752, 2010.

[31] A. Tanwani, A. D. Domínguez-García, and D. Liberzon, "An inversion-based approach to fault detection and isolation in switching electrical networks," *IEEE Transactions on Control Systems Technology,* vol. 19, no. 5, pp. 1059-1074, 2011.

[32] N. Wang, "Research and Realization of Control for Boost Converter," MSc, Xi'an University of Technology (XUT), 2008.

[33] X. Tian, "Design-for-reliability and implementation on power converters," in *Reliability and Maintainability Symposium, 2005. Proceedings. Annual*, 2005, pp. 89-95: IEEE.

[34] Y. Wu, Y. Wang, Y. Jiang, and Q. Sun, "Multiple parametric faults diagnosis for power electronic circuits based on hybrid bond graph and genetic algorithm," *Measurement*, vol. 92, pp. 365-381, 2016.

[35] M. Catelani *et al.*, "MLMVNN for parameter fault detection in PWM DC-DC converters and its applications for buck DC-DC converter," in *Environment and Electrical Engineering (EEEIC), 2016 IEEE 16th International Conference on*, 2016, pp. 1-6: IEEE.

[36] R. E. H. Thabet and H. Chafouk, "Fault detection and isolation methodology using interval predictors with application to DC-DC Buck converters," in *Control and Fault-Tolerant Systems (SysTol), 2016 3rd Conference on*, 2016, pp. 548-553: IEEE.

[37] A. Izadian and P. Khayyer, "Application of Kalman filters in model-based fault diagnosis of a DC-DC boost converter," in *IECON 2010-36th Annual Conference on IEEE Industrial Electronics Society*, 2010, pp. 369-372: IEEE.

[38] S. Yang, A. Bryant, P. Mawby, D. Xiang, L. Ran, and P. Tavner, "An industry-based survey of reliability in power electronic converters," *IEEE transactions on Industry Applications*, vol. 47, no. 3, pp. 1441-1451, 2011.

[39] R. Yahyaoui, A. Gaillard, A. De Bernardinis, and D. Hissel, "Signal processing-based switch fault detection methods for multi-phase interleaved boost converter."

[40] R. Yahyaoui, A. De Bernardinis, A. Gaillard, and D. Hissel, "Switch short-circuit fault detection algorithm based on drain-to-source voltage monitoring for a fault tolerant DC/DC converter," in *Industrial Electronics Society, IECON 2016-42nd Annual Conference of the IEEE*, 2016, pp. 2212-2217: IEEE.

[41] J. L. Soon and D. D.-C. Lu, "A simple open-circuit fault detection method for a fault-tolerant dc/dc converter," in *Power Electronics and Drive Systems (PEDS), 2015 IEEE 11th International Conference on*, 2015, pp. 98-103: IEEE.

[42] Z. Miao *et al.*, "A self-powered ultra-fast DC solid state circuit breaker using a normally-on SiC JFET," in *Applied Power Electronics Conference and Exposition (APEC), 2015 IEEE*, 2015, pp. 767-773: IEEE.

[43] E. Jamshidpour, P. Poure, and S. Saadate, "Photovoltaic systems reliability improvement by real-time FPGA-based switch failure diagnosis and fault-tolerant DC–DC converter," *IEEE Transactions on Industrial Electronics*, vol. 62, no. 11, pp. 7247-7255, 2015.

[44] T. Park and T. Kim, "Novel fault tolerant power conversion system for hybrid electric vehicles," in *Vehicle Power and Propulsion Conference (VPPC), 2011 IEEE*, 2011, pp. 1-6: IEEE.

[45] S. Ouni *et al.*, "A fast and simple method to detect short circuit fault in cascaded H-bridge multilevel inverter," in *Industrial Technology (ICIT), 2015 IEEE International Conference on*, 2015, pp. 866-871: IEEE.

[46] H.-K. Cho, S.-S. Kwak, and S.-H. Lee, "Fault diagnosis algorithm based on switching function for boost converters," *International Journal of Electronics*, vol. 102, no. 7, pp. 1229-1243, 2015.

[47] E. Ribeiro, A. J. M. Cardoso, and C. Boccaletti, "Open-circuit fault diagnosis in interleaved DC–DC converters," *IEEE transactions on power electronics*, vol. 29, no. 6, pp. 3091-3102, 2014.

[48] P. Krein and R. Bass, "Geometric formulation, classification and methods for power electronic systems," in *Power Electronics Specialists Conference, 1990. PESC'90 Record., 21st Annual IEEE*, 1990, pp. 499-505: IEEE.

[49] J. M. Burdio and A. Martínez, "A unified discrete-time state-space model for switching converters," *IEEE Transactions on Power Electronics*, vol. 10, no. 6, pp. 694-707, 1995.

[50] S. Hui and C. Christopoulos, "Modeling non-linear power electronic circuits with the transmission-line modeling technique," *IEEE transactions on power electronics,* vol. 10, no. 1, pp. 48-54, 1995.

[51] R. D. Middlebrook and S. Ćuk, "A general unified approach to modelling switching-converter power stages," *International Journal of Electronics Theoretical and Experimental,* vol. 42, no. 6, pp. 521-550, 1977.

[52] B. Lehman and R. M. Bass, "Extensions of averaging theory for power electronic systems," *IEEE Transactions on Power Electronics,* vol. 11, no. 4, pp. 542-553, 1996.

[53] R. W. Erickson and D. Maksimovic, *Fundamentals of power electronics*. Springer Science & Business Media, 2001.

[54] M. M. Peretz and S. Ben-Yaakov, "Time domain identification of PWM converters for digital controllers design," in *Power Electronics Specialists Conference, 2007. PESC 2007. IEEE*, 2007, pp. 809-813: IEEE.

[55] M. M. Peretz and S. Ben-Yaakov, "Time-domain identification of pulse-width modulated converters," *IET Power Electronics,* vol. 5, no. 2, pp. 166-172, 2012.

[56] D. Maksimovic and R. Zane, "Small-signal discrete-time modeling of digitally controlled PWM converters," *Power Electronics, IEEE Transactions on,* vol. 22, no. 6, pp. 2552-2556, 2007.

[57] V. Yousefzadeh, M. Shirazi, and D. Maksimovic, "Minimum phase response in digitally controlled boost and flyback converters," in *Applied Power Electronics Conference, APEC 2007-Twenty Second Annual IEEE,* 2007, pp. 865-870: IEEE.

[58] A. J. Forsyth and S. V. Mollov, "Modelling and control of DC-DC converters," *Power engineering journal,* vol. 12, no. 5, pp. 229-236, 1998.

[59] L. Guo, J. Y. Hung, and R. M. Nelms, "Evaluation of DSP-based PID and fuzzy controllers for DC–DC converters," *Industrial Electronics, IEEE Transactions on,* vol. 56, no. 6, pp. 2237-2248, 2009.

[60] J.-T. Su, D.-M. Liu, C.-W. Liu, and C.-W. Hung, "An adaptive control method for two-phase DC/DC converter," in *Power Electronics and Drive Systems, 2009. PEDS 2009. International Conference on,* 2009, pp. 288-293: IEEE.

[61] S. Abe, M. Ogawa, T. Zaitsu, S. Obata, M. Shoyama, and T. Ninomiya, "Power-stage frequency response cancellation of DC-DC converter with digital control," in *Power Electronics Electrical Drives Automation and Motion (SPEEDAM), 2010 International Symposium on*, 2010, pp. 44-49: IEEE.

[62] M. M. Peretz and S. Ben-Yaakov, "Time-domain design of digital compensators for PWM DC-DC converters," *Power Electronics, IEEE Transactions on*, vol. 27, no. 1, pp. 284-293, 2012.

[63] D. Maksimovic and R. Zane, "Small-signal discrete-time modeling of digitally controlled PWM converters," *IEEE transactions on power electronics*, vol. 22, no. 6, pp. 2552-2556, 2007.

[64] M. Veerachary, "Robust digital voltage-mode controller for synchronous soft-switching boost converter," in *Power Electronics and Drive Systems (PEDS), 2011 IEEE Ninth International Conference on*, 2011, pp. 1131-1136: IEEE.

[65] A. Hajizadeh, A. H. Shahirinia, N. Namjoo, and C. Y. David, "Self-tuning indirect adaptive control of non-inverting buck–boost converter," *IET Power Electronics*, vol. 8, no. 11, pp. 2299-2306, 2015.

[66] I. D. Landau and G. Zito, *Digital control systems: design, identification and implementation*. Springer Science & Business Media, 2007.

[67] A. R. Brown and R. Middlebrook, "Sampled-data modeling of switching regulators," in *1981 IEEE power electronics specialists conference*, 1981, pp. 349-369: IEEE.

[68] V. Rajasekaran, J. Sun, and B. S. Heck, "Bilinear discrete-time modeling for enhanced stability prediction and digital control design," *IEEE Transactions on Power Electronics*, vol. 18, no. 1, pp. 381-389, 2003.

[69] M. R. Modabbernia, F. Kohani, R. Fouladi, and S. S. Nejati, "The State Space Average Model of Buck-Boost Switching Regulator Including all of The System Uncertainties," *International Journal on Computer Science and Engineering (IJCSE)*, vol. 5, no. 2, pp. 120-132, 2013.

[70] K. Ireland and M. Rosen, *A classical introduction to modern number theory*. Springer Science & Business Media, 2013.

[71] G. P. Rao and H. Unbehauen, "Identification of continuous-time systems," in *Control Theory and Applications, IEE Proceedings-*, 2006, vol. 153, pp. 185-220: IET.

[72] N. Kong *et al.*, "Automated system identification of digitally-controlled multi-phase DC-DC converters," in *Applied Power Electronics Conference and Exposition, 2009. APEC 2009. Twenty-Fourth Annual IEEE*, 2009, pp. 259-263: IEEE.

[73] R. Isermann, "Process fault detection based on modeling and estimation methods—A survey," *automatica*, vol. 20, no. 4, pp. 387-404, 1984.

[74] V. Venkatasubramanian, R. Rengaswamy, S. N. Kavuri, and K. Yin, "A review of process fault detection and diagnosis: Part III: Process history based methods," *Computers & chemical engineering*, vol. 27, no. 3, pp. 327-346, 2003.

[75] J. Poon, P. Jain, I. C. Konstantakopoulos, C. Spanos, S. K. Panda, and S. R. Sanders, "Model-based fault detection and identification for switching power converters," *IEEE Transactions on Power Electronics*, vol. 32, no. 2, pp. 1419-1430, 2017.

[76] J.-Y. Choi, B. H. Cho, H. F. VanLandingham, H.-s. Mok, and J.-H. Song, "System identification of power converters based on a black-box approach," *IEEE Transactions on Circuits and Systems I: Fundamental Theory and Applications*, vol. 45, no. 11, pp. 1148-1158, 1998.

[77] V. Valdivia, A. Barrado, A. LÁzaro, P. Zumel, C. Raga, and C. FernÁndez, "Simple modeling and identification procedures for “black-box” behavioral modeling of power converters based on transient response analysis," *IEEE Transactions on Power Electronics*, vol. 24, no. 12, pp. 2776-2790, 2009.

[78] R. Pintelon and J. Schoukens, *System identification: a frequency domain approach*. John Wiley & Sons, 2012.

[79] M. Moonen, B. De Moor, L. Vandenberghe, and J. Vandewalle, "On-and off-line identification of linear state-space models," *International Journal of Control*, vol. 49, no. 1, pp. 219-232, 1989.

[80] M. M. F. S. Algreer, "Microprocessor based signal processing techniques for system identification and adaptive control of DC-DC converters," 2012.

[81] G. F. Franklin, J. D. Powell, and M. L. Workman, *Digital control of dynamic systems*. Addison-wesley Menlo Park, CA, 1998.

[82] B. Johansson and M. Lenells, "Possibilities of obtaining small-signal models of DC-to-DC power converters by means of system identification," in *Telecommunications Energy Conference, 2000. INTELEC. Twenty-second International*, 2000, pp. 65-75: IEEE.

[83] A. Barkley and E. Santi, "Improved online identification of a DC–DC converter and its control loop gain using cross-correlation methods," *Power Electronics, IEEE Transactions on*, vol. 24, no. 8, pp. 2021-2031, 2009.

[84] B. Miao, R. Zane, and D. Maksimovic, "System identification of power converters with digital control through cross-correlation methods," *Power Electronics, IEEE Transactions on*, vol. 20, no. 5, pp. 1093-1099, 2005.

[85] A. H. Sayed, *Fundamentals of adaptive filtering*. John Wiley & Sons, 2003.

[86] H. Unbehauen and G. P. Rao, "A review of identification in continuous-time systems," *Annual reviews in Control*, vol. 22, pp. 145-171, 1998.

[87] Y. V. Zakharov, G. P. White, and J. Liu, "Low-complexity RLS algorithms using dichotomous coordinate descent iterations," *Signal Processing, IEEE Transactions on*, vol. 56, no. 7, pp. 3150-3161, 2008.

[88] L. Loron and G. Laliberte, "Application of the extended Kalman filter to parameters estimation of induction motors," in *Power Electronics and Applications, 1993., Fifth European Conference on*, 1993, pp. 85-90: IET.

[89] C. Wang, M. Armstrong, S. Gadoue, and P. Missailidis, "System identification of a DC-DC converter system using a Fast Affine Projection algorithm," 2014.

[90] Y.-F. Liu and P. C. Sen, "Digital control of switching power converters," in *Control Applications, 2005. CCA 2005. Proceedings of 2005 IEEE Conference on*, 2005, pp. 635-640: IEEE.

[91] J. Morroni, R. Zane, and D. Maksimovic, "An online stability margin monitor for digitally controlled switched-mode power supplies," *Power Electronics, IEEE Transactions on*, vol. 24, no. 11, pp. 2639-2648, 2009.

[92] S. S. Haykin, *Adaptive filter theory*. Pearson Education India, 2007.

[93] J. Liu, Y. V. Zakharov, and B. Weaver, "Architecture and FPGA design of dichotomous coordinate descent algorithms," *Circuits and Systems I: Regular Papers, IEEE Transactions on,* vol. 56, no. 11, pp. 2425-2438, 2009.

[94] G. H. Golub and C. F. Van Loan, *Matrix computations*. JHU Press, 2012.

[95] Y. V. Zakharov, G. P. White, and J. Liu, "Low-complexity RLS algorithms using dichotomous coordinate descent iterations," *IEEE Transactions on Signal Processing,* vol. 56, no. 7, pp. 3150-3161, 2008.

[96] J. E. Mooney, Z. Ding, and L. S. Riggs, "Robust target identification in white Gaussian noise for ultra wide-band radar systems," *IEEE Transactions on Antennas and Propagation,* vol. 46, no. 12, pp. 1817-1823, 1998.

[97] P. L. dos Santos, J. A. Ramos, and J. L. M. de Carvalho, "Identification of bilinear systems with white noise inputs: An iterative deterministic-stochastic subspace approach," *IEEE Transactions on Control Systems Technology,* vol. 17, no. 5, pp. 1145-1153, 2009.

[98] C. Carangui, P. Delgado, M. Carpio, and D. P. Chacón-Troya, "Experimental identification of the transfer function model of a scale VTOL system by PRBS signals under ground effect," in *Automatica (ICA-ACCA), IEEE International Conference on*, 2016, pp. 1-5: IEEE.

[99] B. Safarinejadian, N. Kianpour, and M. Asad, "A novel identification method for fractional-order wiener systems with PRBS input," in *Control, Instrumentation, and Automation (ICCIA), 2016 4th International Conference on*, 2016, pp. 290-295: IEEE.

[100] A. V. Peterchev and S. R. Sanders, "Quantization resolution and limit cycling in digitally controlled PWM converters," in *Power Electronics Specialists Conference, 2001. PESC. 2001 IEEE 32nd Annual*, 2001, vol. 2, pp. 465-471: IEEE.

[101] A. Prodic, D. Maksimovic, and R. W. Erickson, "Design and implementation of a digital PWM controller for a high-frequency switching DC-DC power converter," in *Industrial Electronics Society, 2001. IECON'01. The 27th Annual Conference of the IEEE*, 2001, vol. 2, pp. 893-898: IEEE.

[102] H. Xu, X. Wen, and L. Kong, "DSP-based digitally controlled bi-directional DC-DC converter," in *Industrial Electronics Society, 2004. IECON 2004. 30th Annual Conference of IEEE*, 2004, vol. 1, pp. 800-804: IEEE.

[103] P. Meshram and R. G. Kanojiya, "Tuning of PID controller using Ziegler-Nichols method for speed control of DC motor," in *IEEE-international conference on advances in engineering, science and management (ICAESM-2012)*, 2012, pp. 117-122: IEEE.

[104] S. Kapat and P. T. Krein, "Improved time optimal control of a buck converter based on capacitor current," *Power Electronics, IEEE Transactions on*, vol. 27, no. 3, pp. 1444-1454, 2012.

[105] A. Soukup, "Enabling Greener Embedded Control Systems with Floating-Point DSCs," *TI White Paper*, 2008.